# Investigation of crystallization dynamics in phase-change material using the Master rate equation at ultrafast heating rates

**Submitted by Azzam Salahuddin Younus Aladool to the University of Exeter**

**as a thesis for the degree of**

**Doctor of Philosophy in Mathematics**

**In August 2017**



I certify that all material in this thesis which is not my own work has been identified and that no material has previously been submitted and approved for the award of a degree by this or any other University.

Signature: ……..

# Abstract

Phase-change materials are widely used in non-volatile computer memories, and in arithmetic and logic processing applications. Phase-change based devices are also required to operate at different and high heating rates in response to electrical or optical excitations to achieve the required read-write rates. Crystallization is a fundamental and complex process involved in the phase transition operation in phase-change materials. It is sensitive to the nature of the phase-change material, its thermodynamic and kinetic parameters, geometric and interface effects, and thermal history. Thus, crystallization is the time limiting process in phase-change technologies. This work is concerned with theoretically understanding the crystallization dynamics of the $Ge_2Sb_2Te_5$ (GST) phase-change material under different heating regimes and at the micro-structure level of the material to reduce crystallization times and increase the operating speed of phase-change devices and memories.

A review and comparison of crystallization models was carried out to distinguish the more physically realistic Master rate equation method's ability to naturally trace both the nucleation and growth processes during crystallization, through the attachment and detachment of monomers to calculate the distribution of nano-cluster size distributions necessary to achieve the aims of this research. Full mathematical derivations and numerical implementation details of both the original discrete form of the Master rate equation and its approximate form were provided. Error analysis and computational experiments illustrated the limitations of the approximate form of the rate equation, and its detrimental sensitivity to the model parameters to justify the use of the discrete rate equation throughout this work.

The crystallization rate is a strong function of the material's viscosity, and hence the physically realistic Mauro−Yue−Ellison−Gupta−Allan (MYEGA) model of the temperature dependence of viscosity was implemented in the Master rate equation. Crystallization simulations were carried out under ramped annealing conditions with heating rates from 50 K/s to 40,000 K/s to study the role of the viscosity model parameters (including the fragility index, glass transition temperature, and infinite temperature viscosity) on the crystallization dynamics. Those simulations showed, for high and low heating rates, the influence of the increasing fragility index on reducing the cluster nucleation time and increasing the crystallization speeds. Moreover, the increase of the glass transition temperature made a corresponding shift in crystallization temperature towards higher values. Furthermore, at low heating rates, infinite temperature viscosity parameter (i.e. extrapolated value of viscosity at temperature = $\infty$) has negligible effect on the crystallization dynamics while, at higher heating rates, smaller values of infinite temperature viscosity parameter increase the crystallization rate and final crystalline volume.

Due to the relatively low computational cost of the Master rate equation method (compared to atomistic level computations), an iterative numerical algorithm was developed to fit Kissinger plots simulated with the Master rate equation system to experimental Kissinger plots from ultrafast calorimetry measurements. The simulations and analysis revealed the strong coupling between the glass transition temperature and fragility index, and highlighted the often ignored role of the dependence of the glass transition temperature on heating rate for the accurate estimation of the fragility index from analysis of experimental measurements. The extracted fragility indices in this work were lower than published values, highlighting the limitations of existing methods of extracting the viscosity parameters (using oversimplified analytical models with disparity in model parameters), and the importance of

using detailed crystallization models for analysis of experimental measurements. Moreover, and for the first time, the variation of glass transition temperature with heating rate for GST was extracted from Kissinger measurements, in agreement with the values reported in the literature.

The influence of the preparation conditions of amorphous GST on the crystallization dynamics was theoretically investigated using the Master rate equation by systematically implementing initial distributions of cluster sizes resulting from different thermal treatments such as melt-quenching and pre-annealing, and theoretical Gaussian initial cluster size distributions. Simulations of ramped pre-annealing to temperatures much lower than the crystallization temperature showed distributions of nano-clusters sizes of 2 - 8 nm in agreement with recently published high-resolution transmission electron microscopy measurements. Furthermore, the simulations explicitly showed the marked decrease in crystallization temperature (and therefore increase in crystallization speed) when there is predominately a narrow distribution of smaller crystalline clusters embedded in the initial amorphous phase.

# Table of Contents

# List of Figures

# List of Tables

# Acknowledgments

First and foremost, I thank the Almighty Allah who surrounded me with blessings and provided me the strength and patience to complete this thesis.

A very special appreciation and gratitude go to my supervisor, **Dr Mustafa Aziz**, for his patience, encouragement and invaluable support throughout this work, without his wise and unlimited guidance the success of this work would have been impossible. This appreciation extends to **Prof Peter Ashwin,** my second supervisor, whose support and knowledge throughout the course of this thesis made it possible. I am forever indebted to them for converting my mistakes into lessons, pressure into productivity and skills into strengths.

I also would like to express my deepest gratitude to my beloved parents, brothers and sisters who provided unconditional love and care during the long period of this work. Sincere and warm thanks to my wife, Atyaf, who stood firmly by my side despite the fact that she couldn't join me in Exeter, she has been a true and great supporter during the best and worst times and she has been instrumental in instilling confidence.

Completing this work would have been more difficult without the support of my friends (too many to mention here, but you know who you are!), here in Exeter, in my country, and in other parts of the world.

Last but not least, I also would like to thank the academic and technical staff of Exeter University for their support. A special thanks to the staff of Mosul University, the university where I am employed, for nominating me to this PhD scholarship, which is provided by the Ministry of Higher Education of Iraq scholarship, the completion of this thesis would not have been possible without their supports.

Yours Sincerely

# CHAPTER 1: Introduction and motivation

## 1.1 Motivation for advanced memory technology

The global demand for data storage is currently increasing faster than ever. Computing technology has become an integral part of daily life, involved in how we communicate with each other, entertain ourselves and how we perform our jobs. With this increased presence of computing technology and the increasing reliance upon data for computers to perform tasks, especially where media storage is concerned, the need to store that data in a more reliable and compact way has become vital to progression in this field.

Data storage and memory technologies in general can be categorized into non-volatile and volatile memories. Volatile memories require a constant power supply and/or periodic refreshing to retain stored information. On the other hand, non-volatile memories are able to retain stored information without the requirement for a constant power supply or periodic refreshing.

Turning our attention first to volatile memories, the two most common of these memories in use today are Static Random Access Memory (SRAM) and Dynamic Random Access Memory (DRAM). These technologies have operation speeds as fast as a few nanoseconds, and hence are typically embedded within the Central Processing Unit (CPU) as Level 1 (L1) and Level 2 (L2) cache memories, and are used to carry out primary processing operations in computing systems [1][2]. Although SRAM and DRAM have been the workhorses of the memory hierarchy for a number of years, there are fundamental scaling limitations associated with these technologies, and according to the International Roadmap for Semiconductors

(ITRS) of 2013 it is unclear whether SRAM and DRAM cells will be scalable beyond 16 nm dimensions. Hence alternative memory technologies will be required for future computing systems [3].

In contrast to volatile memories, non-volatile memories such as Flash solid-state memories, Hard Disk Drives (HDD), and optical memories (the CD, DVD and Blu-Ray disk) have the ability to retain stored information even without a constant power supply and/or without periodic refreshing. These memories have also been in use for a number of years to complement volatile memories, and are used primarily for bulk storage in the data storage hierarchy. For example, storing application software, music files, image and video files to name a few [4][5]. However, these technologies also have fundamental scaling limitations, and similar to SRAM and DRAM, associated with the smallest possible size of the data baring unit and it is not clear whether these technologies will be able to scale down beyond sub-10 nm dimensions in the future [3]. Therefore, there is a strong desire to develop new emerging technologies for future electronic and computing systems that cannot only complement but also replace in some environments the above mentioned traditional data storage and memory technologies. One such technology is Phase-Change memories, including solid-state phase-change random access memories (PCRAM) and optical storage disk technology, which has demonstrated excellent performance features in comparison to, for example, volatile memories as shown in Table 1.1.

**Table 1.1 Relative comparison of memory technologies in terms of main characteristics** [6]

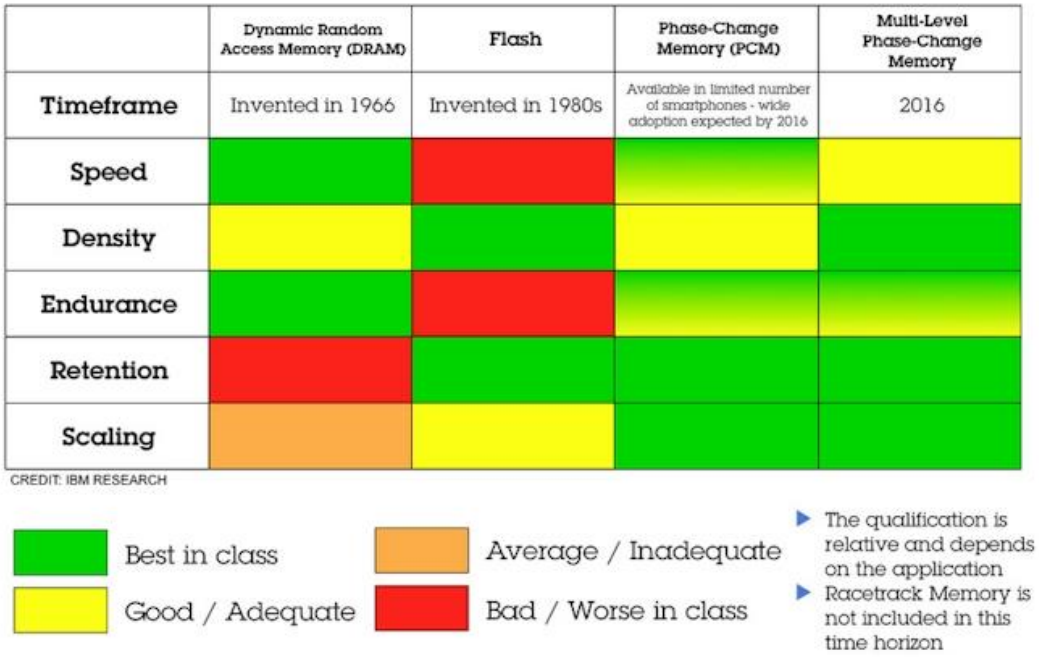


Phase-change memories are non-volatile and based on the reversible switching of chalcogenide (glass-like) phase-change materials between the high resistance amorphous phase (with low optical reflectivity) and the low resistance crystalline phase (with high optical reflectivity) using suitable electrical or optical pulses. The amorphous phase is typically a disordered phase (short-range atomic order) (see Figure 1.1 (d)) whereas the crystalline phase is an ordered phase (long-range atomic order) (see Figure 1.1 (c)). The distinctive contrast between the electrical resistivity and optical conductivity of the two phases and the ability to repeatedly switch between the two phases enable the storage of crystalline and amourphous as regions of different contrast in the phase-change material [7] (see Figure 1.1). In particular, this technology has demonstrated excellent scalability down to dimensions as small as single nanometre dimensions in PCRAM [8][9], ultra-fast switching speeds (picosecond to nanosecond range) [10], ultra-low power consumptions [8][9],

multilevel operation [11], good data retention (10 years at 110 $^{o}$C) [12], and excellent endurance (up to $10^{12}$ cycles) [12]. This makes PCRAM one of the leading contenders to complement or even replace other existing solid-state memory technologies in the future.

Thus it is recognised that phase-change materials have significant technological potential for memory and other device applications (such as neuromorphic computing[13], and functional optical absorbers and modulators [14]). Since the memory functionality and general device operation is based on the switching of phase-change materials, it is now important to discuss the characteristic and key features of these materials to understand the factors that influence the switching speed of phase-change memories and devices.

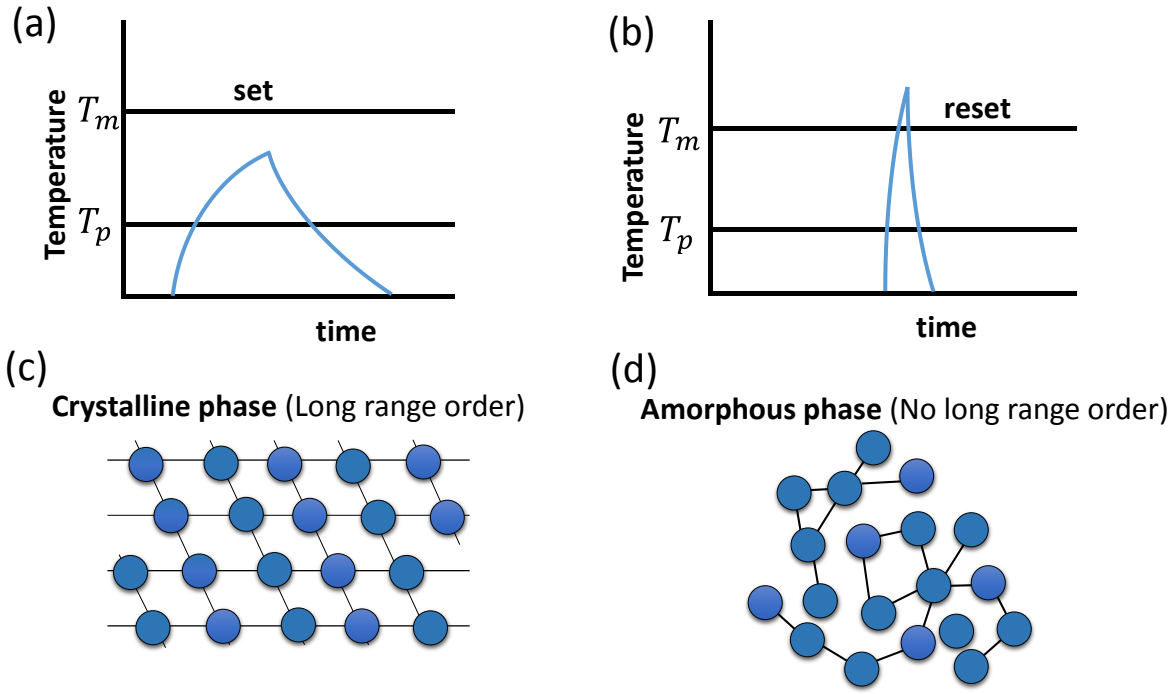


**Figure 1.1 This figure illustrates the processes of crystallization and amorphisation in phase-change materials. (a) Shows the crystallization process starting from the amorphous phase with the application of temperature profile that exceeded the crystallization temperature $T_p$ followed by slow cooling to form the ordered crystal structure (set) shown in (c). (b) Shows the amorphisation process starting with the crystalline phase and application of a temperature profile that exceeded the melting temperature $T_m$ followed by fast cooling to the disordered amorphous structure (reset) as shown in (d).**

## 1.2 Phase Change Materials

Some of the most promising materials for the development of the phase-change memory technology are chalcogenides formed from binary, ternary or quaternary alloys consisting of one or more element from Group 16 (VIA) of the periodic table, in particular Tellurium (see Figure 1.2 [15] ).

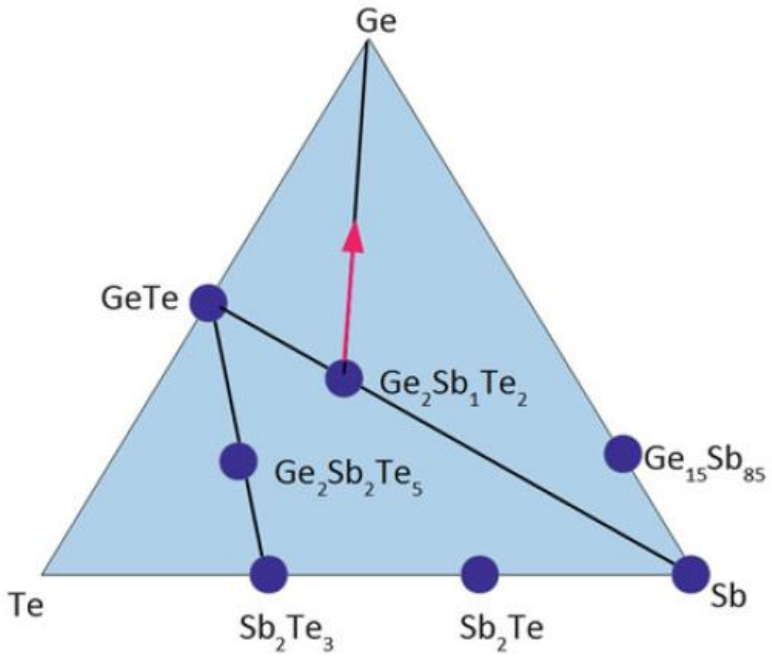


**Figure 1.2 Tertiary Ge-Sb-Te phase diagram with some popular phase change alloys highlighted. The red line arrow indicates the trend of adding Ge to $Ge_2Sb_1Te_5$ (Reprinted from** [16]**)**

Phase Change Materials were first discovered by Stanford Ovshinsky in the 1960s during his work on amorphous solids. It was in 1968 that Ovshinsky illustrated an electrical switching phenomena between amorphous and crystalline phases of Germanium (Ge)- Antimony (Sb) - Tellurium (Te) materials at short time scales (tens of nanoseconds) [15]. Since then phase change materials have been a topic of intense research for modern data storage and memory applications, and have been used as the active material for established technologies such as optical CDs, DVDs and BluRay disks [4]. The most commonly used phase change material over the years has been $Ge_2Sb_2Te_5$ (also referred to as simply GST) although other phase

change materials such as AgInSbTe (AIST), GeSb, GeTe and GaLaS have also been used frequently in research on phase change materials [7].

## 1.3 The phase transition process

The phase transition process causes structural changes in phase-change materials and is typically thermally driven, either by directly heating the material through a heating stage, electrically through Joule heating (by application of voltage differences) or through absorption of optical energy (supplied by a focused laser beam for example). Starting in the amorphous phase, application of temperatures near to or greater than a characteristic temperature called the crystallization temperature, $T_p$, and lower than the melting temperature of the material, $T_m$, leads to the formation of ordered nano-crystals in the amorphous material. Continued annealing leads to growth of the crystalline clusters until the heated region is fully crystalline (see Figure 1.1 (a) and (c)). The heated material or region remain in the crystalline phase after removal of the heat source.

Reverting back (from the crystalline phase) to the amorphous phase requires application of temperatures higher than the melting point of the material, $T_m$, followed by fast cooling and quenching to the disordered amorphous phase as shown by Figure 1.1 (b) and (d) fast cooling rates in the tens of Kelvins per nanosecond are needed to re-amorphise phase-change materials [17], and this can be achieved through careful design of the thicknesses and thermal properties of the thermal layers adjacent to the phase-change active layer in practical structures, to remove the heat quickly from the heated region [18].

Both crystallization and (re) amorphisation are transient processes with time scales determined by the amplitude and time profile of the heat source, the material thermal history, and by the material composition and thermodynamic properties. For example, the typical time duration of phase-change material's amorphous phase to remain stable without crystallization is 10 years [19], while crystallization using fast optical or voltage pulses can occur over tens and hundreds of nanoseconds [15].

(Re) amorphisation of the melted phase-change material can happen quickly over time scales of few nanoseconds [20]. Crystallization of the amorphous phase, on the other hand, is the more complex and time limiting process in phase-change materials and is thus the subject of past and present theoretical and experimental investigations in the phase-change community and the focus of this research programme and thesis.

The crystallization mechanism in amorphous phase-change materials are reviewed next to provide insight into the factors that influence the crystallization speed in phase-change materials, and leading to the description of the kinetic properties of phase-change materials that characterise their switching speed.

## 1.4 Crystal Nucleation and Growth

Formation of crystal nuclei (nucleation) and their growth are two mechanisms required for the crystallization to occur according to the classical nucleation theory [21]. Nucleation typically takes place either in any region of the old amorphous phase (known as homogeneous nucleation) or when a new phase contacts with the old phase at interfaces and

impurities (which is known as heterogeneous nucleation) (see section 2.2). The driving force for crystallization (nucleation and growth) is the difference in free energy (W(r) see Figure 1.3 ) of the amorphous and the crystalline phases.

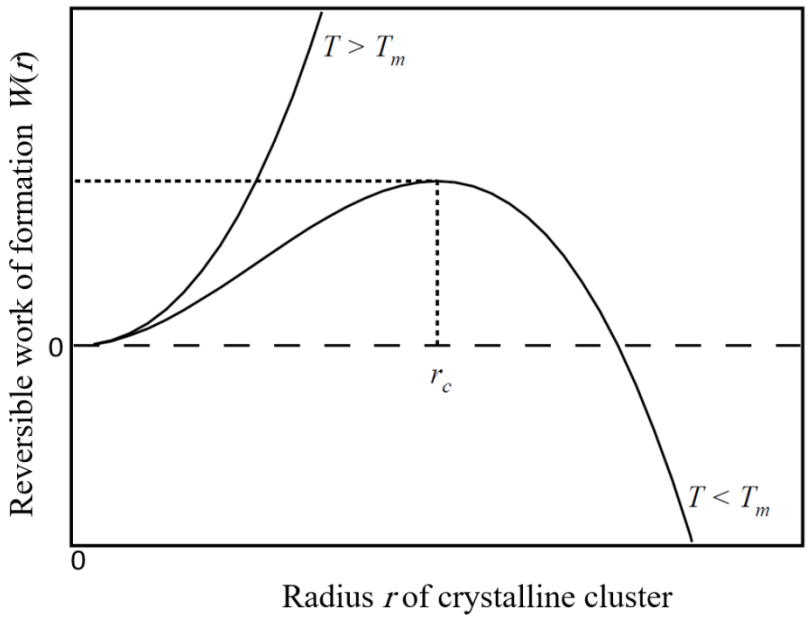


**Figure 1.3 Reversible work (free energy change) $W(r)$ for the formation of crystalline clusters of radius r in the parent phase.**

Figure 1.3 displays the evolution of $W(r)$ as a function of both temperature and the radius of the cluster. The quantity $r_c$ is the critical radius. A cluster of radius $r_c$ is called a critical cluster and $W(r_c)$ the critical work for cluster formation. For $T > T_m$, $W(r) > 0$ for any radius $r$, hence, the clusters spontaneously decay. For $T < T_m$, $W(r)$ increases for $r < r_c$, resulting in clusters of size smaller than the critical size which are energetically not favourable and spontaneously decay, while clusters would grow for $r > r_c$ as a result of gaining free energy. In other words, in the early stages free energy treatment, nucleation is the creation of post-critical clusters of size $r > r_c$. However, after being nucleated, the attachment and detachment of molecules to and from the cluster make clusters above the critical size to grow to a macroscopic size, and consequently, the material is crystallized.

As described above, crystallization normally takes place through the formation of crystal nuclei and their subsequent growth. However, different materials are dominated by different mechanisms. For example, $Ge_4Sb_1Te_5$ and $Ge_2Sb_2Te_5$ are nucleation dominated while crystallization can proceed largely by growth in AIST phase-change material (see Figure 1.4).

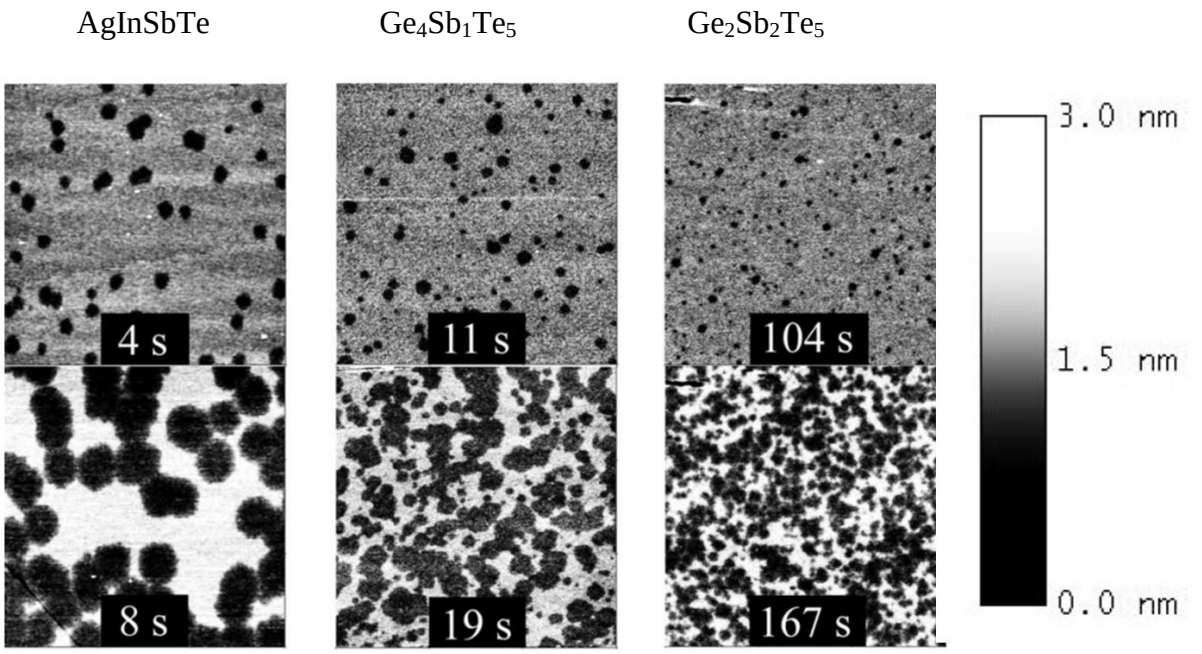


**Figure 1.4 AIST and two Ge-Sb-Te phase-change materials after thermal annealing at 185 $^0$C for (AIST), 180 $^0$C for ($Ge_4Sb_1Te_5$), and 145 $^0$C ($Ge_2Sb_2Te_5$). The dark areas are crystalline, the bright areas amorphous. Heating the material for different durations, for AgInSbTe after 4s a small number of nuclei of dark spots appear, and grow to form crystals after 8s (grouth dominated). For $Ge_4Sb_1Te_5$ and $Ge_2Sb_2Te_5$ after 11s and 104s respectively a large number of spot dark appear, and continously grow to the varied sizes, and still formation of new nuclei after 19s for $Ge_4Sb_1Te_5$ and 167s for $Ge_2Sb_2Te_5$ (nucleation dominated) (After** [22] [23]**).**

## 1.5 Crystallization Kinetics

As indicated previously the crystallization process is the time limiting process in phase-change materials, which has implications on the switching speed and data rates of phase-change based technologies. Hence characterisation of both the crystallization speed and stability of the amorphous phase, or crystallization kinetics, is important for understanding

the crystallization mechanism at high heating rates and increasing the writing/erasure speeds (and therefore data rates) in phase-change memories and related technologies.

A number of parameters affect the crystallization speed in phase-change materials including the material composition, the thermodynamic parameters of the material and viscosity, material thickness, presence and type of adjacent layers and interfaces, concentration of impurities and defects, dominant crystallization mechanism, pre-annealing and initial state of the amorphous material, and magnitude and rate of the heating source.

To infer the effect of these parameters and characterise the crystallization kinetics in phase-change materials, a number of parameter have been identified and measured experimentally including the crystallization temperature, the activation energy of the phase transition process, and the viscosity dependence on temperature of the phase-change material. These parameters will be briefly described next outlining their role in the crystallization process, and illustrating the disparity in their measured values and hence limited understanding of crystallization dynamics at the high heating rates expected in practical phase-change technologies.

### 1.5.1 Crystallization temperature and activation energy

The crystallization temperature, $T_p$, and activation energy, $E$, are typical quantities for evaluating the crystallization kinetics of phase-change materials. The crystallization temperature is a characteristic temperature at which the atomic mobility becomes sufficient for crystallization to proceed (where the crystallization rate is maximum) (see Figure 1.5).

For practical applications, the crystallization temperature is required to be sufficiently larger than room temperature (300 K) to ensure stability of the amorphous phase over the expected operating temperatures, while enabling crystallization to occur using practical (and not excessive) applied powers and temperatures. The crystallization temperature is heating rate dependent, and can be measured using differential scanning calorimetry (DSC) where the energy released/absorbed during ramped thermal annealing of a phase-change sample (normally a powder) is measured at different heating rates, $\phi$. The crystallization temperature at a given heating rate is then determined at the peak of the of measured energy curve with temperature. Alternatively the crystallization temperature can be estimated from sheet resistance measurements of phase-change film samples annealed at different heating rates, where the crystallization temperature is identified as the temperature where the change in sheet resistance with temperature is maximum [24]. Typical heating rates used in DSC and sheet resistance measurements go up to few tens of Kelvins per second, and measured values of $T_p$ for GST are in range ~ 403 K [25].

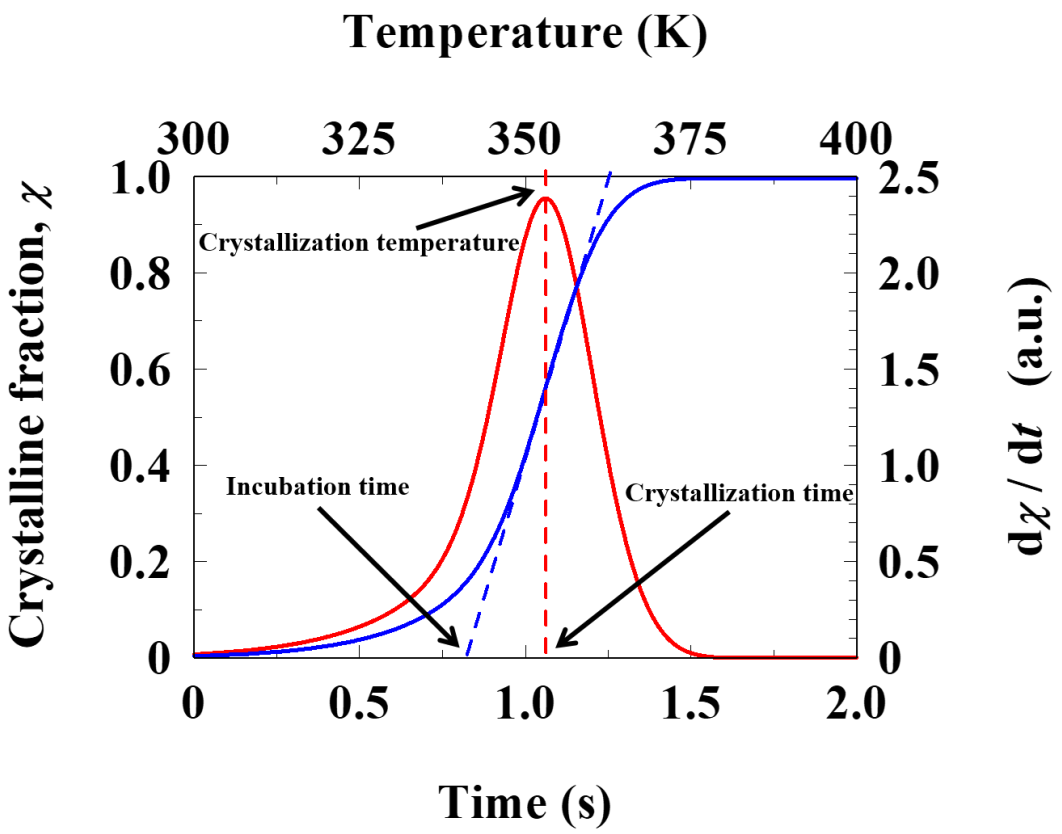


**Figure 1.5 Crystalline fraction (solid blue line, as a function of temperature and time) is an essential quantitative characteristic for phase-change processes, which can determine the amount of material that has already been crystallized. Differentiated crystalline fraction curve (dashed red line), indicates the crystallization temperature and crystallization time. Nucleation time (incubation time) is determined from the slop of the crystalline fraction (dashed blue line).**

Using the measured peak temperature, $T_p$, at each heating rate, $\phi$ (either from DSC or sheet resistance measurements) and plotting the natural logarithm $\ln(\phi/T_p^2)$ against $1/T_p$ produces the well-known Kissinger plot [26], with a typical straight line relationship (Arrhenius behaviour) whose slope is related to and can be used to determine the activation energy, $E$, of the underlying reaction. The activation energy is the minimum required energy for the molecules to be activated and hence for chemical transformation to occur [27]. In this case the reaction is crystallization from the initial amorphous phase, and where it is understood that measured $E$ includes the activation energies for both nucleation and growth. Recent studies however, measured the crystallization dynamics over a broad range of heating rates

(50K/s up to 40,000K/s) using ultrafast DSC measurements for GST [28] [29] and for other phase-change materials (such as GeSb [29] and AIST [30]). A non-Arrhenius behaviour was observed in the Kissinger plots for GST in these measurements which cannot be described with a single activation energy.

### 1.5.2 Material viscosity

The classical theory of nucleation indicates strong dependence of both the nucleation and growth rates of the material on the viscosity, $\eta$ [21]. Hence the viscosity of the material or in particular the viscosity dependence on temperature of the material has direct impact on the crystallization speed in phase-change materials. The viscosity describes the degree of mobility of the molecules in the material over increasing temperatures up to the melting point. Therefore, the viscosity characterises the fragility of a material or its susceptibility to structural relaxation over the temperature range from the characteristic glass transition temperature, $T_g$ (where $\log_{10}(\eta) = 12$) to the crystallization temperature. The degree of reduction in viscosity with thermal gradients near $T_g$ is referred to as the fragility index of the material [31] and reflects the material's ability for fast crystallization.

Direct measurements of the dependence of viscosity on temperature for phase-change alloys are scarce and over a limited temperature range [32]. An Arrenhius temperature dependence of viscosity was suggested to describe the measured behaviour, with one or more activation energies for viscous flow and low fragility index (indicating a strong glass behaviour) [32]. Indirectly, the dependence of viscosity on temperature was extracted from high resolution microscopy measurements of growth rates of crystal clusters, and invoking the inverse dependence of growth velocity on viscosity from classical nucleation theory [22]. More

recently, the viscosity dependence on temperature for phase-change alloys was estimated indirectly by fitting to Kissinger plots measured using DSC using the simplified bulk model for crystallization of Johnson-Mehl-Avrami-Kolomogrov (JMAK) [28][29]. This approach assumes growth dominated crystallization and yields the fitting parameters to an assumed mathematical description of the viscosity dependence on temperature. Using the direct and indirect approaches of estimating the temperature dependence of viscosity allowed the estimation of the fragility indices of phase-change alloys and therefore potential classification of their suitability for fast crystallization applications.

### 1.5.3 Initial material state

The phase transformation from the initial amorphous phase of the material often starts with the formation of nuclei, which then grows and is consequently crystallized. Controlling and increasing the crystallization speed during the writing and erasing stages is critically important for the development of high-speed, low-power phase-change memories.

Phase-change materials are expected to undergo repeated structural changes during phase transitions as part of their operation as memory elements (and other applications). In many cases they are also operated at elevated temperatures above room temperature, but less than the crystallization or melting temperatures of the material. These elevated temperatures and repeated structural transformations (such as melt-quenching) affect the initial amorphous state of the material before the next crystallization cycle. The effect of repeated structural changes was observed as drift in the resistance of phase-change memory elements in PCRAM [for example [33]]. Moreover, it was experimentally shown that laser pre-annealing of amorphous phase-change films at elevated temperatures lower than the crystallization

temperature leads to a reduction in the nucleation incubation time of the material and faster crystallization compared to crystallization using the as-deposited amorphous material [34]. Thus, the initial state of the amorphous phase (melt-quenched or pre-annealed) has an important impact on the crystallization dynamics and therefore the switching speed in phase-change material.

## 1.6 Motivation, aims and objectives of research

Phase-change materials are expected to be switched repeatedly using short voltage or (laser) optical pulses, with rise times and pulse widths in the tens and hundreds of nanoseconds. They thus experience high thermal gradients and complex temperature histories during their operation. To further understand the crystallization mechanism under these fast annealing regimes, recent research has focused on characterising crystallization dynamics at very high heating rates in the thousands and tens of thousands of Kelvins per second using ultrafast DSC [28] and sheet resistance measurements [24]. Moreover, high-resolution electron microscopy was recently employed to study the formation of nano-clusters and effects of initial cluster size distributions in amorphous phase-change material under cyclic heating at moderate temperatures (lower than the crystallization temperature) - expected in practical devices - on the crystallization dynamics and explain PCRAM device performance following repeated switching [35].

The reported ultrafast DSC measurements and sheet resistance measurements yielded Kissinger curves that cannot be described using a single activation energy. Attempted fittings to these Kissinger plots using bulk, growth dominated crystallization models (JMAK) and

assumed mathematical descriptions of the temperature dependence of viscosity yielded inconsistent values of the fragility indices [28] [29]. These results indicate the incomplete understanding of the crystallization dynamics and role of viscosity at very high heating rates. They also highlight the severe limitations of bulk crystallization models that assume growth dominated crystallization to model and analyse the complex crystallization dynamics in GST. The inconsistency and disparity in the estimated values of the kinetic parameters, in particular those related to viscosity in phase-change materials strongly point to the importance of the appropriate mathematical description of the viscosity dependence on temperature to practically reflect the structural changes in the material and to produce accurate estimations of the materials kinetic parameters.

The recent high resolution electron microscopy studies showed the formation of nano-clusters of different size under moderate temperature annealing, and used to explain the anamolus drift in resistance in PCRAM cells [25]. This indicates the importance of the initial size distribution and concentration of crystalline nano-clusters in the amorphous phase on the resulting crystallization dynamics in phase-change materials prior to annealing, which is not yet well understood. Atomistic level simulations are necessary to model such complex behaviour [36][37], however these are computationally expensive particularly when considering larger clusters and their interactions. They are thus not practical for device level modelling nor for analysis of experimental measurements.

To understand crystallization dynamics in phase-change materials subject to complex thermal histories and high thermal gradients, there is thus the need for a comprehensive transient mathematical model of crystallization that is able to describe both the nucleation and growth

processes, taking into account and following the formation and evolution of nano-clusters of different sizes in the material. This is while providing practical computational times to be used for the fitting and analyses of experimental measurements, and facilitating a robust platform for the integration of different models of the viscosity dependence on temperature and introduction of complex thermal histories. The objectives of this research programme are therefore:

- Carry out extensive literature search and review of crystallization models for phase-change materials; leading to
- The development and implementation of a rate-type computional model of crystallization that includes transient nucleation (homogenous and heterogenous) and growth, and capable of simulating cluster sizes up to hundreds of monomers,
- Evaluation of the discrete and continuous forms of this model against published numerical and experimental crystallization data,
- Review models of viscosity and adaptation of physically realistic models over a wide temperature range, and review of their parameters in the literature,
- Carry out a systematic study of the effects of the kinetic and viscosity parameters on the crystallization dynamics in the GST phase-change material at different heating rates using the rate-equation model,
- Develop an iterative fitting computational algorithm based on the rate-equation system for analysis of ultrafast DSC measurements and Kissinger plots, and extracting the important viscosity parameters, and
- Carry out systematic crystallization simulations at different heating rates for different initial cluster size distributions modelling as-deposited, melt-quenched, and pre-annealed amorphous material, and assuming hypothetical Gaussian size distributions with different cluster size means and variances.

## 1.7 Contribution to knowledge

The outcomes of this thesis have contributed to aspects related to phase-change material, specifically using the Master rate equation to investigate crystallization dynamics at ultrafast heating rates. This contribution can be summarised as follows:

- Implementation of Master rate equation computational model capable of modelling transient nucleation and growth, with cluster sizes up to hundreds of monomers. Continuous version of the fundamental discrete model was derived and error estimate analysed, illustrating the limitations of the approximate form of the Master rate equation.

- Implementation of the physically realistic Mauro−Yue−Ellison−Gupta−Allan (MYEGA) model [38] for the viscosity dependence of temperature in the Master rate equation and provided detailed understanding of the effect of the viscosity parameters on crystallization dynamics in GST [39].

- Development of iterative algorithm based on the Master rate equation for fitting to Kissinger plots leading to a new method for the extraction of viscosity parameters from measurements [39].

- Analysis of Kissinger plots at ultrafast heating rates using the developed algorithm highlighted the importance of the crystallization and viscosity models for the extraction of the correct viscosity parameters from DSC measurements [39].

- Analysis of the published ultrafast DSC measurements using the new fitting algorithm revealed the strong coupling between the glass transition temperature and viscosity

index in the analysis of Kissinger plots, and suggested a new approach for the evaluation of the glass transition temperature using the same algorithm [39].

- Systematic theoretical study of the initial cluster size distributions in the amorphous phase revealed the enhancement of crystallization dynamics with narrower distribution of small cluster sizes compared to larger clusters, for the same initial crystalline concentration (See Appendices, research paper (2)).

## 1.8 Thesis outline

In **chapter 1,** the project motivation is presented, and followed by a detailed introduction to phase change materials including their operation mechanisms and performance characteristics along with the crystallization kinetics.

In **chapter 2,** an overview of various phase change models such as the JMAK model, the classical nucleation, and growth theory, ab initio modelling, Master rate equation model, and the Gillespie Cellular Automata (GCA) approach are presented. This is followed by a review of these models leading to conclusions about their applicability in modelling phase change materials.

In **chapter 3**, mathematical review of Master rate equation is presented. Then, the continuous Master rate equation is derived from the original discrete form using Taylor expansion and the error truncation terms are analysed. The employability of the Master rate equation in phase-change modelling, and its numerical implementations are also included in this chapter.

In **chapter 4**, the effects of viscosity parameters on crystallization dynamics is investigated, to study the role of the physically realistic MYEGA viscosity parameters on the crystallization dynamics in $Ge_2Sb_2Te_5$ under ramped annealing conditions with heating rates ranged between 50 K/s and 40,000 K/s. This has been shown through carrying out various simulations of crystalline fraction as a function of temperature and time by determining the peak crystallization temperature $T_p$ from the peaks in the crystallization fraction at different heating rates.

In **chapter 5**, Kissinger curves corresponding to ultrafast DSC experiments are analysed. An iterative algorithm is developed providing more detailed fittings and alternative evaluations of the fragility indices and glass transition temperature using the MYEGA model by comparison to Kissinger plots published in literature.

In **chapter 6**, a theoretical investigation is carried out using the Master rate equation approach to further understand the resulting distribution of cluster sizes following pre-annealing and melt-quenching in as-deposited phase-change $Ge_2Sb_2Te_5$. Moreover, this approach is used to systematically investigate the effect of different assumed initial cluster size distributions and densities on the crystallization dynamics in phase-change material subject to low (50 K/s) and high (40,000 K/s) heating rates.

In **chapter 7,** the key findings of this thesis are summarized and the possible future work is discussed.

# CHAPTER 2: An overview of phase-change models

As indicated in the introduction chapter of this thesis, there is a need for a transient mathematical model of crystallization that enables the capture of the nucleation and growth processes in phase-change materials, follows the creation and evolution of nano-clusters and their size distributions, is flexible and robust to incorporate physically realistic models of viscosity and nucleation processes, and be computationally efficient to enable analysis of experimental kinetic measurements. Such a model and the related analysis will enable the fundamental and missing understanding of the crystallization dynamics in the GST phase-change material subject to very high heating rates and thermal conditions expected in practical devices and systems. This understanding will ultimately lead to the development of high switching speed phase-change based devices and systems.

The crystallization and amorphization processes in phase-change materials can be mathematically modelled by various approaches: Johnson-Mehl-Avrami-Kolmogorov (JMAK) theory, classic nucleation and growth theory, atomistic modelling, Master rate equation approaches, and the Gillespie Cellular Automata (GCA) method. In this chapter, a review of these approaches is presented and a description of the Master rate equation approach is introduced, which can model transient and non-equilibrium crystallization with low computational cost, and therefore it is considered in this work.

## 2.1 JMAK Theory

This is the most popular theory used to describe crystallization dynamics in phase-change material, due mainly to its simplicity in not treating nucleation and growth separately. In this

theory, a closed-form expression for the volume fraction of the transformed crystalline region was derived by Johnson-Mehl-Avrami-Kolomogrov (JMAK) and given by [40] [41][42] :

$$\chi(t) = 1 - \exp\left(-(k(T)t)^n\right) \tag{2.1}$$

where $\chi(t)$ is the volume fraction of crystallized material at time $t$, and $n$ is the Avrami coefficient which depends on the nature and dimensionality of the crystallization process. $k(T)$ is the crystallization rate which, for simplicity and including both nucleation and growth rates, can be written as:

$$k(T) = \upsilon \exp\left(-\frac{E}{\kappa_B T}\right) \tag{2.2}$$

where $\upsilon$ is the frequency factor, $E$ is understood as the total activation energy of crystallization (including nucleation and growth), $T$ is the absolute temperature, and $\kappa_B$ is the Boltzmann constant. The derivation of JMAK theory is based on the following assumptions, which are not always valid for a real system [32]:

- Nucleation occurs randomly and uniformly.
- Constant temperature (isothermal heating)
- Nucleation rate is time independent.
- The growth is cluster size independent.
- Growth is interface controlled.

In a real system, nucleation can take place on surfaces, at interfaces, and impurities; this type of nucleation is a process known as heterogeneous nucleation [43]. Moreover, the nucleation rate cannot be considered time independent for the entire crystallization process with temperature history [44]. JMAK cannot differentiate materials with identical amount of crystallization but different crystallite size distributions, and this is crucial to track the

dynamical crystallization progress of different annealing conditions. Therefore, a more physically realistic model should be used for modelling phase change material considering both time-dependent and cluster size simultaneously to describe transient crystallization.

## 2.2 Classical nucleation and growth theory

Nucleation and crystal growth theory was first developed by Gibbs, Volmer, Weber, Becker, Doring, Turnbull and Fisher and is known as the classical nucleation model [21]. The classical nucleation and crystal growth theory proposes that the crystallization of an initially amorphous phase-change material is described by the formation of small, unstable clusters of the crystalline phase inside the amorphous material. When these clusters reach a critical size where they subsequently become kinetically stable, they can grow rather than dissociate. These clusters form randomly either homogeneously in any region within the phase-change material or heterogeneously at surfaces, interfaces, and impurities. These two different nucleation processes (homogeneous and heterogeneous) have different time scales with the same temperature conditions, therefore affecting crystallization dynamics and must be considered in modelling crystallization in practical device structures [45].

In the classical nucleation theory, both the nucleation and growth processes are described using temperature dependent rate models to evaluate the probability of these thermally activated events. The steady-state homogeneous nucleation rate $R_{\text{hom}}$ can be determined via the expression [46] (for temperatures below the melting point):

$$R_{\text{hom}} = K_{\text{hom}} \exp\left(\frac{-E}{\kappa_B T}\right) \exp\left(\frac{-W(r_c)}{\kappa_B T}\right) \qquad \textbf{(2.3)}$$

with $K_{hom}$ being the attempt frequency, and $E$ the activation barrier for self-diffusion (for adding one more atom). The energy barrier $W(r_c)$ to form a nucleus of critical size is defined by:

$$W(r_c) = \frac{16\pi}{3} \frac{\sigma^3}{K_1^{\,2}} \tag{2.4}$$

where $K_1$ is the bulk free energy difference between the amorphous and the crystalline phase. $\sigma$ is specific surface energy. The total energy barrier for nucleation is therefore $E+ W(r_c)$.

To account for interface effects, equation (2.3) is modified to write the temperature dependent heterogeneous nucleation rate $R_{\text{het}}$ as [47]:

$$R_{het} = K_{het} \exp\left(\frac{-E}{k_B T}\right) \exp\left(\frac{-W(r_c)}{k_B T}\right) \varphi(\theta_w) \tag{2.5}$$

$K_{het}$ is another frequency pre-factor, and with the other parameters previously defined in Eq. (2.3). The expression $\varphi(\theta_w)$ in Eq. (2.5) is a function of contact angle (wetting angle $\theta_w$) and enables to distinguish between homogenous ($\theta_w \to \pi$) and heterogeneous ($\theta_w \to 0$) nucleation in the bulk and at interfaces, respectively. $\varphi(\theta_w)$ is determined using the spherical cap model (see Figure 2.1) and it can be described by [43]:

$$\varphi(\theta_w) = \frac{1}{4}(2 + \cos\theta_w)(1 - \cos\theta_w)^2 \tag{2.6}$$

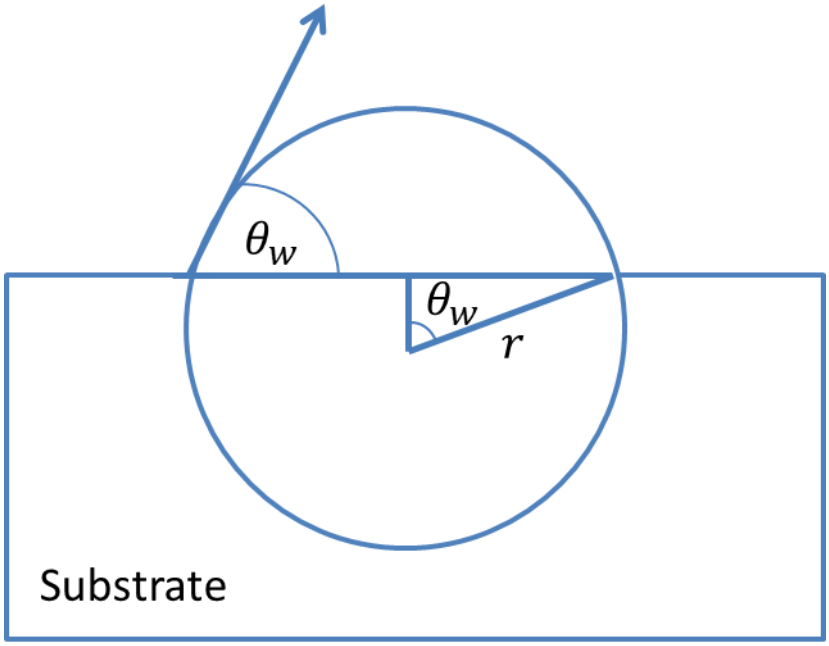


Figure 2.1 Spherical cap model for heterogeneous cluster formation. The exposed crystal cluster has the shape of a spherical cap, whose volume is $\varphi(\theta_w)\times\frac{4}{3}\pi r^3$.

As previously described in the nucleation process, when a cluster reaches a critical size where it is thermodynamically stable, then it is more likely to grow through the attachment of molecules rather than dissolution of the cluster. The growth velocity $V_g$ of a crystallite (cluster) was proposed by Meinders via the expression [48]

$$V_g = K_g \exp\left(\frac{-E_g}{\kappa_B T}\right)\left[1-\exp\left(\frac{-K_1}{\kappa_B T}\right)\right] \qquad \textbf{(2.7)}$$

with $K_g$ is a growth velocity pre-factor, $E_g$ is the activation energy for the diffusion of atoms from the amorphous to the crystalline phase, and other parameters as described in Eq. (2.3) and Eq. (2.4).

The cluster nucleation and growth rates can be estimated by means of the classic nucleation theory. The assumptions and limitations of classical nucleation model can be summarized as follows:

- Nuclei exceeding the critical size are assumed to grow rather than dissociate. However, dissociation process is possibly involved.
- Nucleation theory only deals with crystal clusters exceeding the critical size and therefore ignores transient subcritical cluster formation.
- Nucleation theory cannot model different cluster sizes and their interactions.

In addition to the above limitations, classical nucleation theory is based on steady-state crystallization and not able to model transient and non-equilibrium crystallization processes [32]. Therefore, an approach is required which can model nucleation and growth processes simultaneously by considering the attachment and detachment of molecules to describe transient crystallization and a distribution of clusters of different sizes. Such model is more physically realistic to model the operation of phase-change devices.

## 2.3 Ab initio modelling

*Ab initio* molecular dynamics, or first principles molecular dynamics, is a combination of Density Functional Theory (DFT) [49][50][51] electronic structure calculations and molecular dynamics (MD) [52] simulations. DFT is a quantum mechanical method that determines the electronic structure of many-body systems by arrangement, type, and number of atoms present. Molecular dynamics (MD) simulations are a sequence of static calculations described by the motion of interacting particles using Newtonian dynamics. These methods are crucial in characterizing the physical properties of materials. Thus it is possible to study the microscopic behaviour of phase-change material with temperature variation, by simulating the crystallization and amorphisation processes using the atomistic models. These simulations were successfully modelling the crystallization process in $Ge_2Sb_2Te_5$ [53] [36].

Although this approach can provide deep insight into the crystallization behaviour of phase-change materials, these simulations are too computationally expensive for device-level modelling or for analysis of experimental data at present and therefore they are not considered in this work.

## 2.4 The Master rate equation

Phase-change materials experience different thermal histories and gradients during their course of operation. Thus to accurately capture and simulate the crystallization dynamics in real systems a model is required which is capable of capturing the transient evolution of various cluster sizes, their interaction and growth, and the micro-scale initial state of the amorphous parent phase [32].

The Master rate equation approach was used by Kelton and Greer [54] to study the transient nucleation and growth process in the glasses under isothermal conditions. Kelton and Greer [54] discussed thoroughly the importance of taking transient nucleation behaviour into account when interpreting transformation kinetics, which leads to better understanding of glass formation. This technique was extended to non-isothermal conditions [55] [56] and for DSC measurement analysis [57]. Also its simple implementation of arbitrary initial cluster distributions was used to study the crystallization process in glasses [54].

Senkader and Wright [32] were the first to use the Master rate equation approach to model $Ge_2Sb_2Te_5$. This approach was also used for modelling both complete or partial crystallization and amorphization in $Ge_2Sb_2Te_5$, dependent on the duration and temperature used for annealing [58]. This model was also able to track the formation of initial clusters distribution

and crystallization temperature in as-deposited amorphous state of $Ge_2Sb_2Te_5$ in thin film [59].

The Master rate equation approach assumes that the smallest possible existing cluster size is a combination of two monomers. Furthermore, the clusters of different sizes can grow or dissociate by attachment or detachment of monomers. The appearance of a cluster of *n* GST molecules (monomers) results from a series of interactions between monomers. Cluster of *n* GST monomers can have possible interactions at time *t* that is given by

$$(n-1) \leftrightarrow (n) \leftrightarrow (n+1) \tag{2.8}$$

This mechanism is shown in Figure 2.2 and based on it the following equation is written for $n \geq 2$ ($n$=1 representing the amorphous phase)

$$\begin{aligned} \frac{dZ(n,t)}{dt} = {} & f(n-1,t)Z(n-1,t) + g(n+1,t)Z(n+1,t) \\ & - f(n,t)Z(n,t) - g(n,t)Z(n,t) \end{aligned} \tag{2.9}$$

where $t$ is the time, $f(n,t)$ and $g(n,t)$ are attachment and detachment rates, respectively, and $Z(n,t)$ be the cluster size distribution. The rates $f(n,t)$ and $g(n,t)$ control the speed of crystallization, which are functions of the temperature dependence of the viscosity, and hence, the simulations are sensitively characterized by the viscosity parameters. Consequently, this enables modelling a wide range of material behaviours more realistically. Moreover, this model is computationally less expensive in predicting cluster size distributions, as it does not take the spatial dependence of clusters into account. Also, the implementation of arbitrary initial cluster distributions can easily be applied. One of the current limitations of the Master rate equation is the inability to model spatial variations in crystalline fraction.

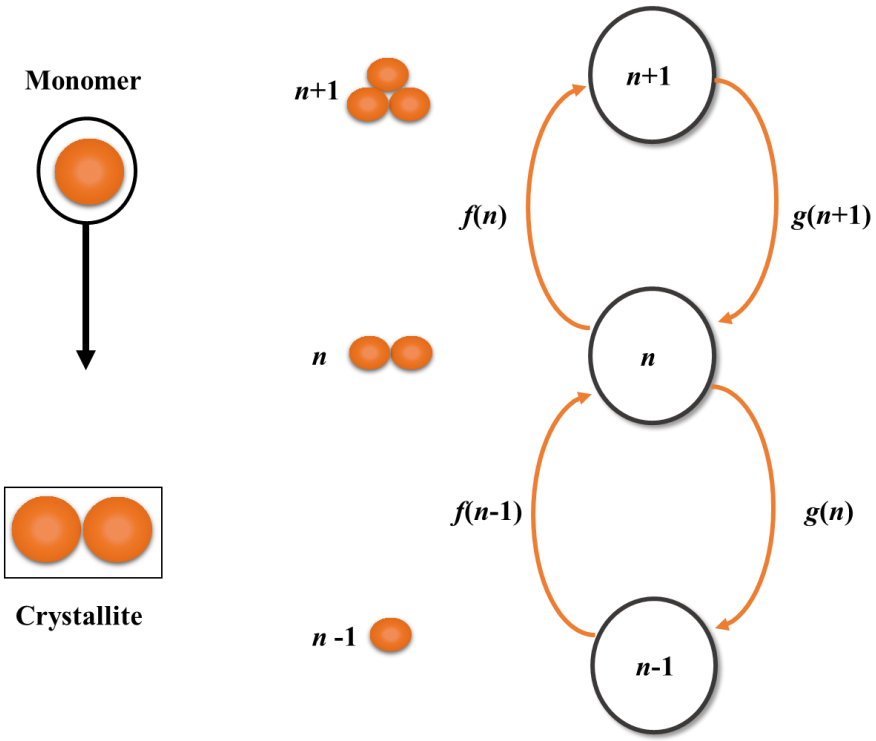


**Figure 2.2 Attachment and detachment of monomers, *f* is the attachment frequency and *g* is the detachment frequency.**

## 2.5 Gillespie Cellular Automata approach

The Gillespie Cellular Automata (GCA) approach has been previously described in detail by Ashwin et al [52]. It combines thermodynamic aspects of rate equation-based methods with elements from probabilistic cellular automata models. In short, this model considers a homogeneous, isotropic material in a square lattice where each site can be either amorphous or crystalline. For each point $(i,j)$ in the lattice, the state is described by two parameters: $(r_{ij})$ the phase of the $(i,j)$ site, and an orientation $(\Phi_{ij})$ (with two adjacent crystalline sites belonging to same crystallite (crystal grain) if they have the same orientation). The local changes that can occur are defined by three events, namely nucleation, growth and dissociation. Nucleation is where a single crystallite is formed by two originally amorphous sites, site $(i,j)$ and an adjacent site. Growth, on the other hand, is where an originally

amorphous site ($i$,$j$) becomes attached to an adjacent crystal. Finally, dissociation is where an originally crystalline site ($i$,$j$) detached from the crystal of which it is a part to become amorphous. For illustration of those three events see Figure 2.3. The rate at which each of these three events varies with temperature in a similar way to the Master rate equation in [32] as the bulk and the energy surface vary [60][9]. This model is particularly applicable for nano-scale device level modelling and studying the spatial dependence of nano-clusters in nano-structures. It would be computationally expensive if this model is applied for the analysis of experimental measurements of crystallization kinetics in phase-change materials, hence a less expensive model is required.

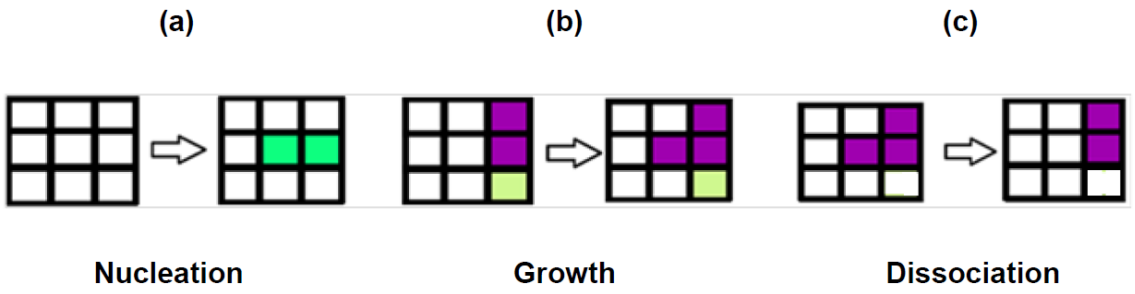


**Figure 2.3 Instantaneous events in the Gillespie cellular automata approach: (a) Nucleation, (b) Growth, and (c) Dissociation. Reprinted from** [61]**.**

## 2.6 Phase-change models review conclusions

The aim of this work is to study and understand the crystallization dynamics in the GST phase-change materials at very high annealing rates and different temperature histories through mathematical modelling. For such detailed study it is required to model both the nucleation and growth process and their rates, which control the crystallization dynamics, by following the formation and evolution of crystalline nano-clusters of different sizes in the

amorphous material. Moreover, the mathematical modelling approach needs to be flexible to model different materials with physically realistic descriptions of their properties such as viscosity dependence on temperature and able to simulate small and large cluster sizes up to hundreds and thousands of monomers. This is all while being robust by being able to follow the evolution of these cluster populations with different time scales subject to complex thermal histories and gradients, and providing practical computational times that enable application and analysis of experimental measurements of crystallization kinetics in phase-change materials.

The crystallization process has been modelled using different approaches in the literature, including the analytical and well-known JMAK model [40] [41][42]. This model considers nucleation as a random and uniform process at constant temperature and therefore isothermal annealing conditions. However, these assumptions may not be applicable in this work since crystallization in phase-change material, due to nucleation, is not random nor uniform [43]. Also, the nucleation rate in the JMAK model is assumed constant and time-independent for the entire crystallization process with temperature which is not the case for different cluster sizes [54].

Nucleation and growth are considered separately in the classical nucleation and growth model [21]. This model cannot provide information about the clusters sizes distribution, and it is not able to model transient and non-equilibrium crystallization.

At the fundamental level, ab initio atomic scale modelling, which employ Density Functional Theory [53], can be used to study the crystallization process and follow in great detail the time development of nano-clusters with temperature. Although this approach can provide deep insight into the crystallization behaviour of phase-change materials, at present these

simulations are too computationally expensive for device-level modelling or for experimental data analysis and will therefore not be considered in this work.

One attempt to bridge the gap between the large-scale, simplified analytical models (such as the JMAK approach), and the detailed, numerically expensive, atomistic models is the Master rate equation method. This method enables the simulation of the attachment and detachment of monomers in materials therefore enabling the transient modelling of nucleation and growth processes during crystallization, including the transient evolution of cluster sizes with temperature changes. Moreover, the attachment and detachment rates in this model, which control the speed of crystallization, are functions of the thermodynamic parameters and viscosity of the material, which can be specified, therefore, enabling the realistic modelling of a wide range of material behaviour. Another advantage of this model is the fast prediction of cluster size distributions compared to atomistic simulations or the Gillespie Celluar-Automata approach. This is particularly applicable here since this work is not concerned with nano-scale device level modelling or studying the spatial dependence of nano-clusters in nano-structures, but is more focused on studying crystallization dynamics in phase-change films or powders used in measurements of crystallization kinetics at very high heating rates (and includes provision for modelling heterogeneous effects). These advantages help to extract the parameters to describe the viscosity of GST and to compare to experimental data, and to investigate the effect of these parameters and initial cluster size distribution on crystallization dynamics. A detailed mathematical review of the Master rate equation model, its different forms, and implementation for modelling crystallization in the GST phase-change material will be presented in the next chapter.

# CHAPTER 3: A mathematical review of Master rate equation

The Master rate equation has, as described in preceding chapter, been used successfully for modelling crystallization in phase-change materials as it takes into account transient effects describing the creation and evolution of clusters and their size distributions through the attachment and detachment of monomers. This method enables tracking of the changes in the nano-clusters in the phase-change material subject to complex thermal histories and gradients, while providing practical computational times which particularly enabled the successful modelling and analysis of calorimetry measurements of crystallization to study and extract the important kinetic parameters for crystallization as will be described in later chapters of this thesis. In this chapter, a mathematical derivation of the discrete Master rate equation and its continuous form is presented along with their detailed implementation in modelling phase-change materials. A comparison between the fundamental discrete Master rate equation model and the continuous approximation is carried out, illustrating the truncation error in the continuous approximation and the subsequent limitations of this approximation on crystallization simulations.

## 3.1 Introduction

A more detailed description of the crystallization process can be achieved when the kinetics involved in this process is considered. This concept is based on a specific mechanism where clusters of different sizes can be changed when they grow and dissociate. Farkas, in (1927), as cited by D. Kashchiev in 2000 [43], was the first to consider the kinetic treatment in the cluster concept and applied the idea of the classical Szilard model for cluster formation. The Szilard model allows clusters to change their sizes by nearest-size transitions, i.e. it assumes

that the cluster formation is a consequence of successive attachments and/or detachments of single molecules (monomers) only [62]. The basic kinetic equation (general Master rate equation) is derived considering all possible changes in cluster size such as gaining and losing both monomer and cluster of different sizes. Based on this derivation, a simplified form of the general Master rate equation can be achieved easily. In this thesis, the considered simplified form (Master rate equation) represents the case of cluster growth and decay by gaining and losing monomers only (i.e. based on the Szilard model). The implementation of the Master rate equation in modelling phase-change material in both discrete and continuous form is also presented. The continuous and the discrete forms of the Master rate equation were evaluated and compared to investigate the effect of numerical solver parameters such as the upper limit of cluster size and cluster size sub-interval on the crystallization dynamics at low and high heating rates.

## 3.2 Mathematical formulation of the general Master rate equation

The crystallization process can be described using basic assumptions in the framework of the cluster approach. The following assumptions are necessary to allow a mathematical formalism to be developed (D. Kashchiev 1984 [63]):

1) Various sizes of clusters are existing in the old phase.

2) The cluster size can be transformed from size $n$ to size $m$ at time $t$ and at the time-dependent rate $f_{nm}(t)$ $(1/s)$ (where $n, m = 1, 2, ....$).

The first assumption is in line with the fact that the density of the old phase transforms non-uniformly into the density of the new phase. The second assumption guarantees the crystallization process occurs under time-dependent conditions. The kinetic description of

the crystallization process is mathematically developed based on these assumptions. The first assumption implies that the variable to be solved is the cluster size distribution. Using the second assumption, the general Master rate equation can be formulated based on the concept of cluster transformation, from *n*-sized into *m*-sized clusters. Due to the different shapes and sizes of the different clusters, a general rate equation description becomes mathematically complicated because the equations must take both shape and size of clusters into account. To simplify the mathematical analysis, uniformly-shaped clusters are assumed [43]. The assumption of uniform cluster shapes greatly reduces the complexity of the derivation of the general Master rate equation as the cluster size becomes the only variable to characterize the clusters. The evolution of the crystallization process can thus be described by the function $Z_n(t)$ which represents the cluster size distribution in the solution to the general Master rate equation [43].

The *n*-sized clusters can decrease or increase in size as shown in Figure 3.1. The change in cluster size may take place due to an attachment or detachment of other clusters of size (1,2,3,4…..*n*) to and from this *n*-sized cluster, considering the single monomer as a cluster of size ($n$ = 1). This change in cluster size is represented by the arrow in this figure, which starts from an *n*-sized cluster and increases to an *m*-sized cluster by the quantity $f_{nm}Z_n$ which represents the number of the size transitions from *n* to *m* per unit time and volume.

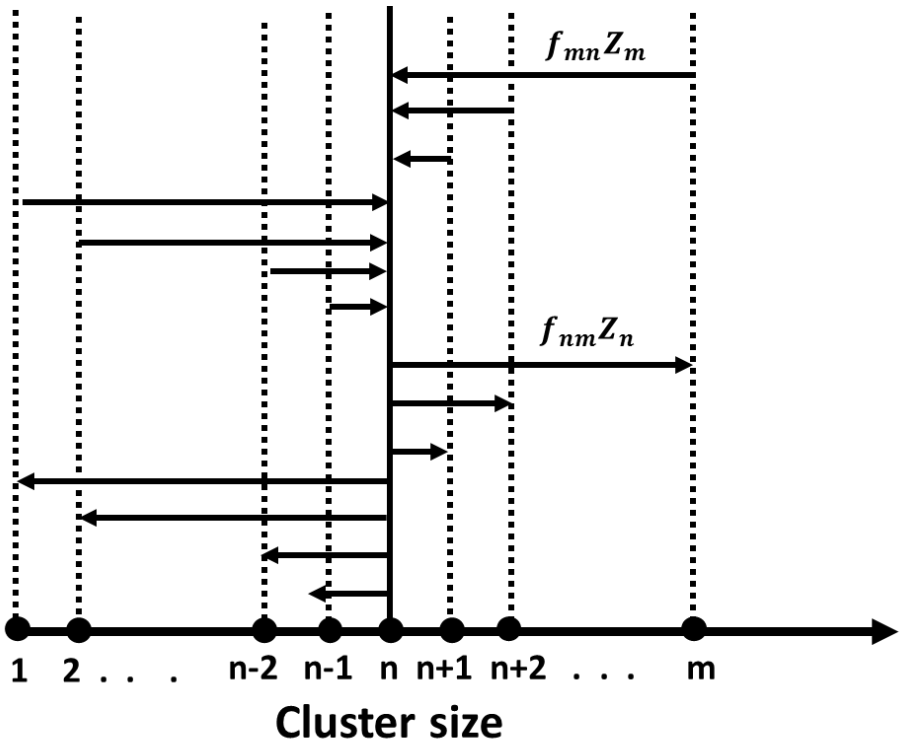


**Figure 3.1 The possible changes in the size of clusters are schematically presented, the number of cluster size *n* increases when the arrows leaving *n*-sized toward *m*-sized, and decreases when the arrows leaving *m*-sized toward *n*-sized.**

The cluster of size *n* changes to size *m*, and consequently, the concentration of clusters of size *n* will be diminished per unit time via the expression:

$$\sum_{m=1}^{M} f_{nm} Z_n(t), \tag{3.1}$$

where *M* is a number of molecules (monomers) in the old phase at time *t*. The reverse reaction, i.e. the transition from an *m*-sized cluster to an *n*-sized cluster, is denoted by the concentration $Z_m$ that is decreased by

$$\sum_{m=1}^{M} f_{mn} Z_m(t). \tag{3.2}$$

The rate of change of $Z_n(t)$ per unit time incorporating both the rates of increase and decrease of cluster sizes is represented by the derivative $dZ_n(t)/dt$, and leads to the derivation of the general Master rate equation from the difference between Eq. (3.1) and Eq. (3.2) [43]:

$$\frac{dZ_n(t)}{dt} = \sum_{m=1}^{M} ( f_{mn} Z_m(t) - f_{nm} Z_n(t)) \,. \tag{3.3}$$

The general Master rate equation (3.3) is a system of first-order ordinary differential equations (ODEs) that must be solved simultaneously for the different cluster size densities $Z_n(t)$, and for a closed system (i.e. $M$ = constant) for simplicity. The Master rate equation has a physically acceptable solution with the initial condition:

$$Z_n(t=0) = Z_i(n) \tag{3.4}$$

where $Z_i(n)$ is the initial cluster size distribution. The relationship between $M$ and $Z_n(t)$ is governed by mass conservation and is expressed as:

$$\sum_{n=1}^{M} n Z_n(t) = M / V \tag{3.5}$$

where $V$ is the volume of the system.

In Eq. (3.3), the number of monomers $n$ is assumed to be an integer leading to the discrete rate equation. For large systems, Zeldovich [43] considered $n$ as a continuous variable and written the continuous form of the rate equation for closed-systems as:

$$\frac{dZ(n,t)}{dt} = \int_{1}^{M} ( f(m,n) Z(m,t) - f(n,m) Z(n,t)) dm \tag{3.6}$$

for $n \in [1, M]$ with the same initial condition in Eq. (3.4), and mass conservation written as:

$$\int_{1}^{M} n Z(n,t) = M / V \tag{3.7}$$

Equation (3.3) is a system of ODEs while Eq. (3.6) is an integro-differential equation, which is the main difference between these equations.

The general Master rate equation (3.3) or Eq. (3.6) is significantly complicated to be solved either analytically or numerically as it considers all possible changes in cluster size such as gaining and losing both monomers and clusters of different sizes (see Figure 3.1). It can be simplified by considering gaining and losing single monomer only as described next [43].

### 3.2.1 The Master rate equation based on the Szilard model

A simplified form of the general Master rate equation can be derived, and so-called Master rate equation, which involves the attachment and detachment of single monomer only following the Szilard model [43]. The restricted assumption based on the Szilard model is that the size of the cluster is only changed by the nearest transition as shown in Figure 3.2. The forward transition is when the cluster size is changed from ($n$) to ($n$ + 1) and conversely, in the backward transition, when the cluster size is changed from ($n$ − 1) to ($n$). The general Master rate equation (3.3) is simplified by assuming that $f_{nm}(t) = 0$ for $|n - m| > 1$, and $f_{nm}(t) \neq 0$ for $|n - m| = 1$ to consider only the attachment and detachment of a single monomer from and to the old phase. Thus Eq. (3.3) now reduces to:

$$\frac{dZ(n,t)}{dt} = f(n-1,t)Z(n-1,t) + g(n+1,t)Z(n+1,t) - f(n,t)Z(n,t) - g(n,t)Z(n,t) \quad \textbf{(3.8)}$$

for $n$=1,2,…..,$M$. In (3.8) $f(n,t) = f_{n,n+1}(t)$ and $g(n,t) = f_{n,n-1}(t)$ are the attachment and detachment rates respectively [64]. Equation (3.8) is a discrete form of the Master rate

equation, which can also be written as a partial differential equation when $n$ is considered as a continuous variable (i.e. $n \in \mathbb{R}^+$).

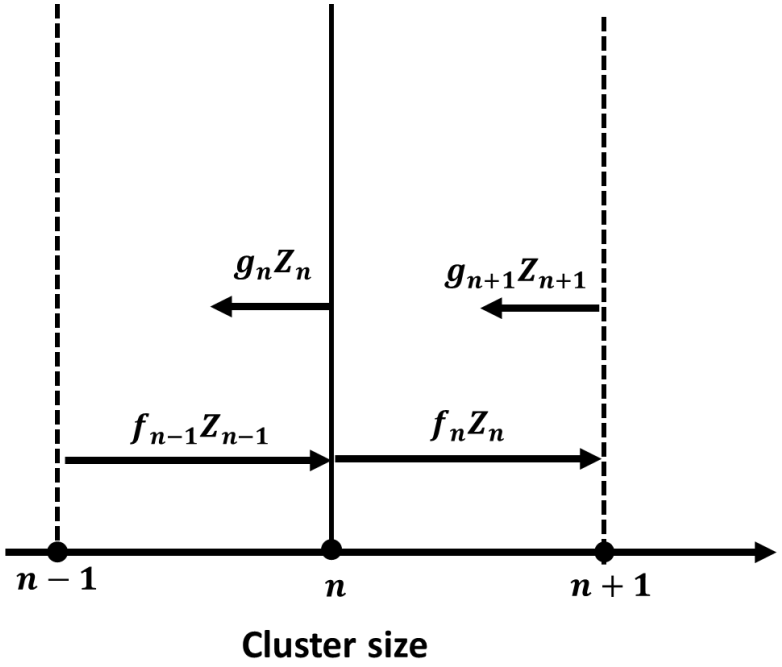


**Figure 3.2 Szilard model scheme of nucleation, where $g_n = g(n,t)$ and $f_n = f(n,t)$ are, respectively, the rates of attachment to and detachment from a cluster of size $n$ units (monomers). In this way cluster may grow or detach by gaining or losing only single monomer.**

Following the Tunitskii approach, as suggested by Kashchiev in 2000 [43], Eq. (3.8) can be transformed into a partial differential equation by approximating the quantities $f(n\text{-}1,t)Z(n\text{-}1,t)$ and $g(n+1,t)Z(n+1,t)$ using the truncated Taylor expansions up to second order around $n$ to yield:

$$f(n-1,t)Z(n-1,t) = f(n,t)Z(n,t) + \left[\frac{\partial}{\partial n}\left[f(n,t)Z(n,t)\right]\right]\left[(n-1)-n\right] + \left[\frac{\partial^2}{\partial n^2}\left[f(n,t)Z(n,t)\right]\right]\left[(n-1)-n\right]^2 \quad \textbf{(3.9)}$$

for $f(n\text{-}1, t)Z(n\text{-}1, t)$ and:

$$g(n+1,t)Z(n+1,t) = g(n,t)Z(n,t) + \left[\frac{\partial}{\partial n}\left[g(n,t)Z(n,t)\right]\right]\left[(n+1)-n\right] + \left[\frac{\partial^2}{\partial n^2}\left[g(n,t)Z(n,t)\right]\right]\left[(n+1)-n\right]^2 \quad \textbf{(3.10)}$$

for $g(n+1,t)Z(n+1,t)$. Then substituting Eq. (3.9) and Eq. (3.10) into Eq. (3.8) yields:

$$\frac{dZ(n,t)}{dt} = -\frac{\partial}{\partial n}\left(\left[f(n,t)-g(n,t)\right]Z(n,t) - \frac{1}{2}\frac{\partial}{\partial n}\left(\left[f(n,t)+g(n,t)\right]Z(n,t)\right)\right) \quad \textbf{(3.11)}$$

Equation (3.11) is the continuous form of the Master rate equation (3.8).

Both forms of the Master rate equation in (3.8) and (3.11) require knowledge of the attachment and detachment rates. However, finding the detachment frequency $g(n,t)$ is difficult since the process of when a molecule is detached from a cluster depends on the cluster properties rather than the new bulk phase, which is not known or understood in detail. Calculating $g(n, t)$ using an indirect process might be possible using knowledge of $f(n, t)$. The detachment frequency can be calculated from the reverse process of molecules attaching to the cluster following Zeldovich's approach. This approach for writing the detachment rate in terms of the attachment rate was generalised by Zeldovich [62] following the earlier work of Kashchiev [64] by writing the balance equation:

$$f(n,t)C(n,t) = g(n+1,t)C(n+1,t) \quad \textbf{(3.12)}$$

Equation (3.12) expresses the relationship between $f(n,t)$ and $g(n,t)$ and $C(n,t)$, and it is applicable to transient and steady-state cases [43]. $C(n,t)$ is a quasi-equilibrium cluster size distribution and it is physically defined in the section 3.4. The balance relation in Eq. (3.12)

can be applied to exclude the term $g(n,t)$ from Eq. (3.8) resulting in the modified (discrete) Master rate equation:

$$\frac{dZ(n,t)}{dt} = f(n-1,t)C(n-1,t)\left[\frac{Z(n-1,t)}{C(n-1,t)} - \frac{Z(n,t)}{C(n,t)}\right] - f(n,t)C(n,t)\left[\frac{Z(n,t)}{C(n,t)} - \frac{Z(n+1,t)}{C(n+1,t)}\right]. \quad \textbf{(3.13)}$$

For the continuous form, applying the truncated Taylor expansion gives

$$\frac{Z(n+1,t)}{C(n+1,t)} = \frac{Z(n,t)}{C(n,t)} + \left(\frac{\partial}{\partial n}\left[\frac{Z(n,t)}{C(n,t)}\right]\right)\left[(n+1)-n\right], \quad \textbf{(3.14)}$$

and this can then be used twice to approximate the first and second finite differences in the brackets in (3.13) resulting in the following partial derivatives:

$$-\frac{\partial}{\partial n}\left[\frac{Z(n-1,t)}{C(n-1,t)}\right] \text{ and } -\frac{\partial}{\partial n}\left[\frac{Z(n,t)}{C(n,t)}\right]. \quad \textbf{(3.15)}$$

Substituting Eq. (3.15) into Eq. (3.13) yields the modified continuous (PDE) form of the Master rate equation:

$$\frac{dZ(n,t)}{dt} = -f(n-1,t)C(n-1,t)\frac{\partial}{\partial n}\left[\frac{Z(n-1,t)}{C(n-1,t)}\right] + f(n,t)C(n,t)\frac{\partial}{\partial n}\left[\frac{Z(n,t)}{C(n,t)}\right] \quad \textbf{(3.16)}$$

A Taylor expansion can then be used to represent the new finite-difference term on the right-hand-side in Eq. (3.16) as before:

$$f(n-1,t)C(n-1,t)\frac{\partial}{\partial n}\left[\frac{Z(n-1,t)}{C(n-1,t)}\right] = f(n,t)C(n,t)\frac{\partial}{\partial n}\left[\frac{Z(n,t)}{C(n,t)}\right] + \frac{\partial}{\partial n}\left(f(n,t)C(n,t)\frac{\partial}{\partial n}\left[\frac{Z(n,t)}{C(n,t)}\right]\right)\left[(n-1)-n\right], \quad \textbf{(3.17)}$$

and substituting Eq. (3.17) into Eq. (3.16) to produce the simplified and continuous Master rate equation of

$$\frac{dZ(n,t)}{dt} = \frac{\partial}{\partial n}\left(f(n,t)C(n,t)\frac{\partial}{\partial n}\left[\frac{Z(n,t)}{C(n,t)}\right]\right). \quad \textbf{(3.18)}$$

The continuous Master rate equation of Eq. (3.18) is a continuous form of the Master rate equation of Eq. (3.8), where $f(n,t)$ is the attachment frequency of the $n$-sized cluster and $C(n,t)$ is the quasi-equilibrium cluster size distribution. In the next section, the implementation of both forms of the Master rate equation for modelling crystallization in phase-change materials is presented.

## 3.3 Cluster formation thermodynamics

The mechanism of attachment and detachment of monomers in the classical nucleation theory [43], depends on the required work for cluster formation. The work for cluster formation, denoted by $W(n,T)$, is the sum of a surface-free energy and a bulk-free energy at temperature $T$

$$W(n,T) = -K_1(T)n + K_2 n^{2/3}, \tag{3.19}$$

where $n$ is the number of monomers, $K_1$ is the difference in the bulk free energy between the old and new phases, which may be calculated from [65]:

$$K_1 = \sigma_0 \Delta H_f \left( \frac{T_m - T}{T_m} \right) \left[ \frac{7T}{T_m + 6T} \right], \tag{3.20}$$

where $\sigma_0$ is the volume of a monomer, $T_m$ is the melting temperature of the phase-change material, and $\Delta H_f$ is the enthalpy of fusion at the melting point. The difference in the surface energy between the two phases can be described by the interfacial energy coefficient $K_2$ which may be written as [43]:

$$K_2 = \left[ \varphi(\theta_w) \right]^{2/3} a\sigma, \tag{3.21}$$

where $a = (36\pi\sigma_0^2)^{1/3}$ is the surface area for spheres, $\sigma$ the interfacial energy, and $\varphi(\theta_w)$ (defined in Eq. (2.6)) is the caps geometrical factor to model the effects of heterogeneous nucleation with wetting angle $\theta_w$ [43] (see Figure 2.1):

It can be seen from Eq. (3.20) that the sign of $K_1$ changes at $T = T_m$, and below the melting temperature $K_1 > 0$ indicating a maximum whose position is determined from solving

$$\frac{\partial W(n,T)}{\partial n} = 0 \tag{3.22}$$

for the critical size $n^*$ yielding

$$n^* = \frac{8}{27}\left(\frac{K_1}{K_2}\right)^3 . \qquad \textbf{(3.23)}$$

This is the critical size when the cluster is likely to continue to grow rather than dissociate. The cluster formation thermodynamics described in this section will be providing the driving force for crystallization in the Master rate equation.

## 3.4 The discrete Master rate equation approach

The set of equations (3.8) can be solved by determining the attachment and detachment rates. The attachment rate is determined following [43] as:

$$f(n,t,T) = Z_m \hat{f} n^{2/3} \exp\left(\frac{W(n,T) - W(n+1,T)}{k_B T}\right), \qquad \textbf{(3.24)}$$

$\hat{f}$ is defined in Eq. (3.30).

The detachment rate may be expressed in terms of the attachment rate following Zeldovich as indicated in Eq. (3.13), repeated here for convenience [62][64]:

$$f(n,t,T)C(n,T) = g(n+1,t,T)C(n+1,T) \qquad \textbf{(3.25)}$$

for $n$ = 1, 2, ... where $C(n,T)$ is the quasi-equilibrium cluster size distribution, which can be expressed thermodynamically as [43]

$$C(n,T) = \exp(-W(n,T)/k_B T). \qquad \textbf{(3.26)}$$

Hence the detachment rate can be written as [43]:

$$g(n,t,T) = f(n-1,t,T)\frac{C(n-1,T)}{C(n,T)}. \quad \textbf{(3.27)}$$

In Eq. (3.24) $k_B$ is the Boltzmann's constant, and $Z_m$ is the density of the remaining amorphous monomers, which is computed from:

$$Z_m = Z_0 - \sum_{n=2}^{n_{\max}} nZ(n,t), \quad \textbf{(3.28)}$$

where $Z_0$ is total monomer density of the starting (amorphous) phase. Thus, the volume fraction of crystallized material $\chi$ can be computed from Eq. (3.28) using:

$$\chi = \sum_{n=2}^{n_{\max}} nZ(n,t)/Z_0 \quad \textbf{(3.29)}$$

It is noted that the detachment rate in Eq. (3.27) should be independent of the amount of free monomers $Z_m$ (i.e. remove $Z_m$ from the attachment rate $f$ in Eq. (3.27)) [58]. In Eq. (3.24) and Eq. (3.27) $\hat{f}$ is given by:

$$\hat{f} = \frac{c\sigma_0^{2/3}(1-\cos\theta_w)}{2d_0\varphi(\theta_w)^{2/3}}D, \quad \textbf{(3.30)}$$

where $d_0$ is the diameter of a monomer, $c = (36\pi)^{1/3}$ is the shape factor for heterogeneous nucleation, and $D$ is the diffusion coefficient, which may be described by the Stokes-Einstein equation:

$$D = \frac{k_\beta T}{3\pi\lambda\eta(T)} \tag{3.31}$$

In Eq. (3.31), $\lambda$ is the jump distance which is taken to be equal the interatomic distance in GST (2.99Å) [66], and $\eta(T)$ is the temperature-dependent viscosity. This indicates that both the attachment and detachment rates in Eq. (3.8) are strongly dependent on the functional dependence of viscosity on temperature, and therefore influencing the crystallization dynamics in phase-change material. Modelling the viscosity dependence on temperature and corresponding crystallization dynamics in phase-change materials is addressed in the next chapter of this thesis.

### 3.4.1 Numerical implementation of the discrete Master rate equation

The system of coupled equations in (3.8) was solved numerically for the cluster size distribution $Z(n,t)$ using the *ode15s* solver in Matlab, with absolute and relative tolerances of $10^{-10}$ (to provide convergence to a stable and accurate solution with practical computation times). This adaptive time solver is appropriate where the solution component changes slowly, with regions of very sharp changes [67]. This solver is suitable for stiff systems, such as the one being solved in this thesis, as the crystallization simulations can have large gradient for the rate of crystallization volume fraction. The solution tracks the formation and destruction of clusters of size $n \geq 2$ ($n = 1$ representing the amorphous phase) with temperature history. The initial starting phase in all simulations was the amorphous phase with initial cluster size distribution $Z(n,0) \rightarrow 0$ ($10^{-11}$ clusters/m$^3$ used here in the numerical

implementation). Starting from room temperature $T_0$ = 300 K, the numerical simulations were performed with any prescribed mathematical function for the heat source. For the ramped heating simulations, the temperature increase was given by

$$T = T_0 + \phi t \,, \tag{3.32}$$

where $\phi$ is the constant heating rate and $t$ is the time. The maximum number of equations solved in Eq. (3.8) in this chapter (upper limit of cluster size) varied up to 1000. Different maximum cluster sizes from 40 up to 1000 were used in crystallization simulations at heating rates up to 40,000 K/s to study the effect of the maximum cluster size on the stability and accuracy of the numerical solutions. The simulations showed particularly negligible changes in the transient response of the crystallization curves and in the corresponding peak crystallization temperatures with increasing cluster size (important in this work for accurate fitting to experimental Kissinger plots described later). The only noticeable difference was a 16% maximum increase in the steady-state crystalline volume fraction happening only at the highest heating rate as the maximum cluster size was increased from 40 to 1000 monomers. These simulations confirmed, for these anneals, the validity of using a maximum cluster size of 40 which is larger than the maximum critical cluster size for the temperature range used in the simulations, and enabling quick computational times and fitting to experimental measurements.

The following describes a few crystallization simulations at a constant heating rate to illustrate the range of important outputs available from the solution of the Master rate equation. This includes the transient evolution of the crystalline volume fraction of the material, $\chi$, which is an essential quantitative characteristic for phase-change processes and determines the amount of material that has been crystallized in the initial amorphous phase.

This is computed from the cumulative contribution of the various cluster size populations as indicated in Eq. (3.29). Hence the micro details of these clusters are also an output from this model providing the time evolution of the different cluster size populations which are important to characterise both the nucleation and growth dynamics during crystallization. Ramped annealing conditions are used in the simulations as they reflect the transient heat source expected in parctical phase-change devices and systems. Heterogeneity of nucleation is assumed and accounted for using the spherical cap model, which allows representing the surface interaction of phase-change material and its substrates by the so called wetting angle [43]. The thermodynamic and materials parameters used in the simulations as listed in Table 3.2 with the exception of of $\sigma$ =0.1 J/m$^2$, $\theta_w$ = 94$^0$ [32]. The MYEGA model [38] was used to show that discrete model is capable of producing very good agreement with experimental data, with parameters $T_g$ = 418 K, $m$ = 90, to be discussed in more detail in the next chapter of this thesis.

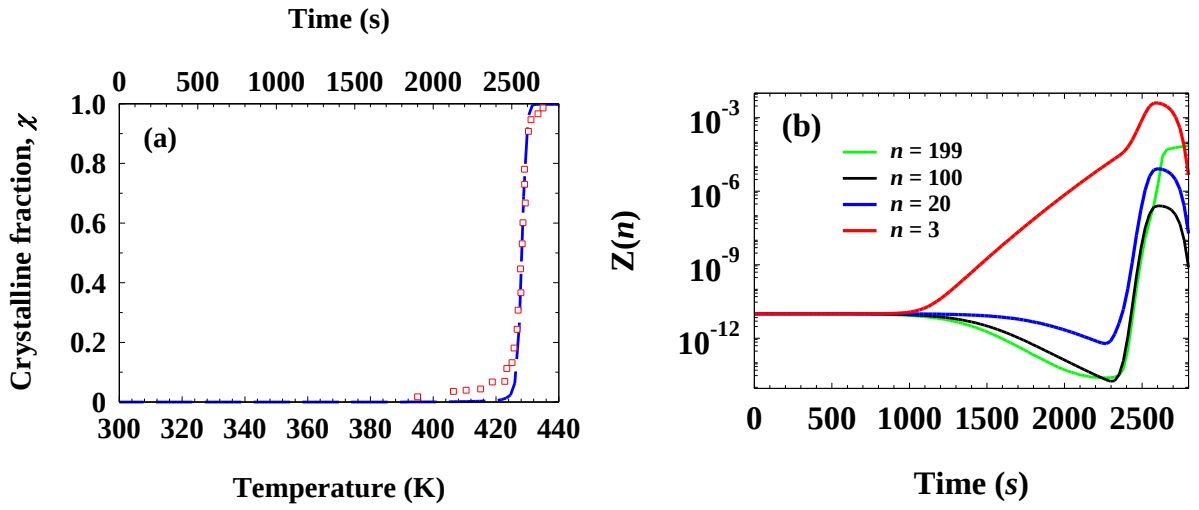


**Figure 3.3(a) Calculated crystalline volume fraction as a function of temperature during ramped anneals at 0.05K/s heating rate for $Ge_2Sb_2Te_5$. Red squares show the experimental data** [68]**, and the blue line represent the model simulation. (b) Corresponding non-uniform transient nucleation of different cluster sizes. Maximum cluster size used was 200 monomers.**

Figure 3.3(a) shows the calculated crystalline volume fraction for an initially amorphous material heated from room temperature using ramped annealing at a slow heating rate of 0.05 K/s. The onset of the rising part of the crystallization curve can be used to estimate the incubation time for the material, and determine the crystallization temperature at which the rate of crystallization is maximum. Figure 3.3(a) also illustrates the good agreement between the simulated crystallization curve and experimental measurements on GST using optical measurements, indicating the ability of this modelling approach in predicting real material behaviour. The corresponding time evolution of clusters of different sizes calculated using the Master rate equation is illustrated in Figure 3.3(b). In this figure smaller clusters form at the early stages of crystallization, which then subsequently contribute to the growth of larger clusters until the full volume is crystallized at the end of the simulation time.

For further clarification of the cluster formation it is even more important to present the cluster size distribution as a function of cluster size at different instant of time. Figure 3.4 (a) shows cluster size distribution at different instances of time. This figure illustrates the formation of small clusters from the attachment of monomers at an early stage in (1 - 2450 second) and over time the clusters grow to larger sizes. Cluster size becomes redistributed where larger clusters gaining more monomers and smaller cluster decay. Ultimately, the distribution in the system is settled to the steady state distribution shown by black line in Figure 3.4 (a). Figure 3.4 (b) and (c) are graphic illustrations of a random distribution of the cluster sizes in the simulation space corresponding to the curves in Figure 3.4 (a).

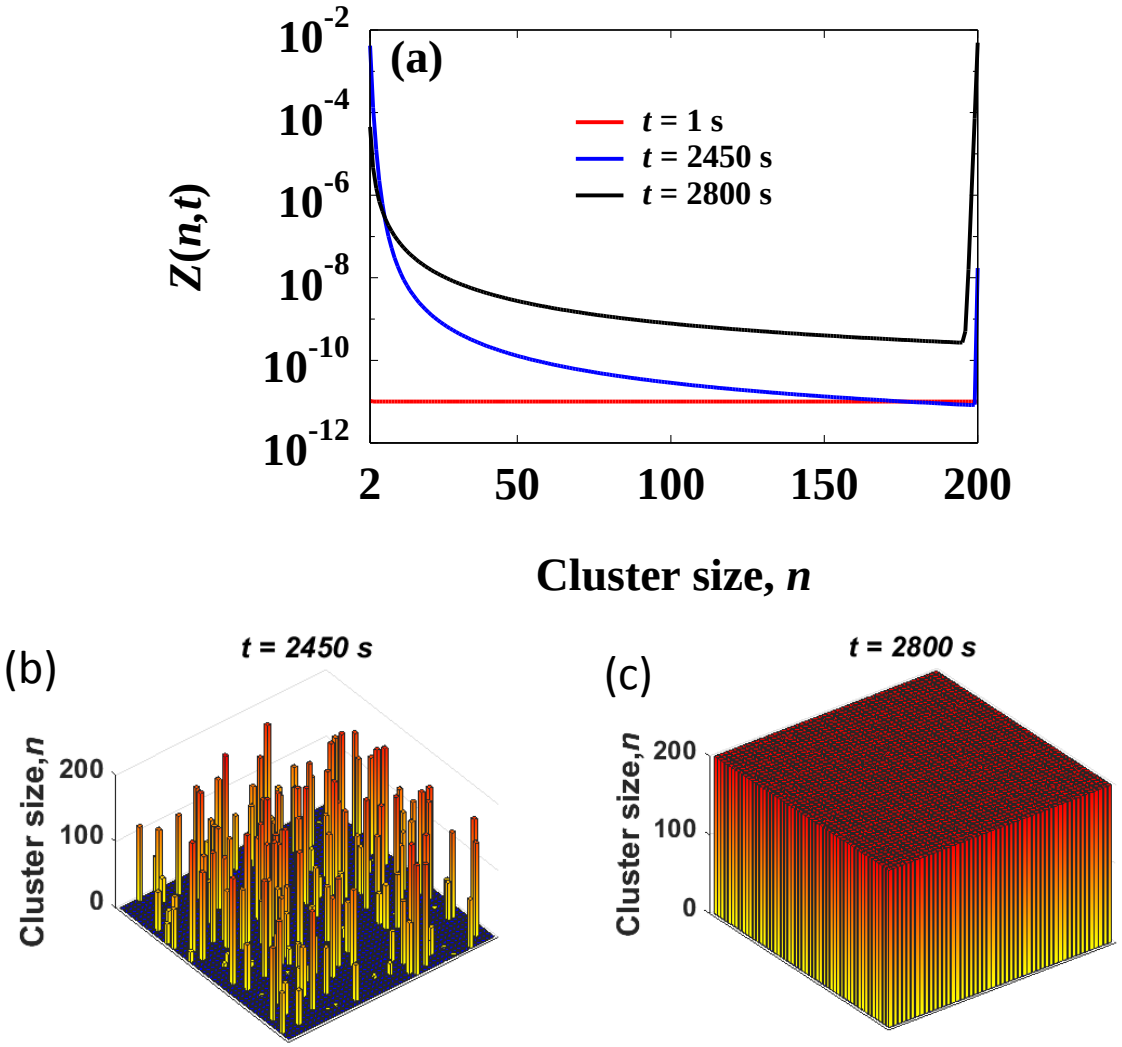


**Figure 3.4 Cluster size distribution at three instances of time calculated from the numerical solution of the discrete Master rate equation for ramped annealing at a constant heating rate of 0.05 K/s. The three-dimensional plots in (b) and (c) have been converted from the vector one-dimensional plots in (a) to a two-dimensional, arbitrary space of cluster size height matrix for better visualisation.**

## 3.5 Continuous Master rate equation

The continuous Master rate equation is first applied for modelling phase-change in $Ge_2Sb_2Te_5$ by Blyuss et al [69]. This model produces a continuous distribution of clusters of size $n \geq 2$

from solution of the truncated Master rate equation. While solving the discrete Master rate equation requires the solution of a large number of coupled ODEs (for the different cluster sizes), the continuous approximation solves a single partial differential equation (PDE) with independent variables *n* and *t*. However, the continuous Master rate equation is an approximation in itself as results of the Taylor truncation as indicated in section 3.5.2.1 and the subsequent limitations of this approximation can affect the crystallization simulations (see Section 3.5.2.2).

The continuous Master rate equation for cluster size evolution is expressed by [43]:

$$\frac{dZ(n,t)}{dt} = \frac{\partial}{\partial n}\left( f(n,T,Z_m)C(n,T)\frac{\partial}{\partial n}\left[\frac{Z(n,t)}{C(n,T)}\right]\right), \qquad \textbf{(3.33)}$$

for $n \geq 2$, which is derived from Eq. (3.8) using truncated Taylor expansion following the work by Zeldovich [62], where $f(n, T, Z_m)$ is the attachment frequency of the *n*-sized cluster and is dependent on the concentration of available monomers $Z_m$. Moreover, $C(n,T)$ is the quasi-equilibrium cluster size distribution [43][69] defined in Eq. (3.26).

The amount of crystallized material can be calculated by integrating the size distribution function. $Z_m$ is determined under consideration of mass conservation by:

$$Z_m = Z_0 - \int_2^\infty nZ(n,t)dn, \qquad \textbf{(3.34)}$$

where $Z_0$ is total monomer density of the starting (amorphous) phase.

The boundary conditions in Eq. (3.33) for large *n* is dictated by the bounded total cluster density:

$$\lim_{n\to\infty} Z(n) \to 0, \tag{3.35}$$

while at $n = 2$ the boundary condition can be written as [69]:

$$\begin{aligned} &- f(2,T,Z_m)\frac{\partial}{\partial n}Z(n,t)\Big|_{n=2} + \\ &\left[f(1,T,Z)F_1(T) + f(2,T,Z_m)F_2(T)\right]Z(2,t) \\ &= f(1,T,Z_m) \end{aligned} \tag{3.36}$$

where $F_1 \equiv \dfrac{C(1,T)}{C(2,T)}$ and $F_2 \equiv \dfrac{\partial}{\partial n}\ln C(n,T)$.

### 3.5.1 Numerical implementation of the continuous form of the Master rate equation

The system (3.33) - (3.35) was solved numerically for the cluster size distribution $Z(n,t)$ using the *NAG routine d03ps* in Matlab following Blyuss et. al. [69]. This routine uses a backward difference approximation for convection-diffusion equations with adaptive remeshing: this is particularly suitable for this system due to the exponential behaviour of the cluster size distribution at small clusters ($n$=2) and the larger cluster ($n_{max}$). In a similar manner to the original and discrete Master rate equation, the solution to the continuous version tracks the formation and destruction of clusters of size $n \geq 2$ ($n$ = 1 representing the amorphous phase) with temperature history. The simulations were carried out on a finite interval [2, $L$] where $L$ is the maximum cluster size, and this interval is divided up into 100. $\Delta L$=100 was chosen because it provided convergence of the solution within reasonable simulation time. An adaptive time stepping algorithm is used in this solver, with absolute and relative tolerances of $10^{-10}$ (similar to the discrete solver). The initial starting phase in all simulations was the

amorphous phase with initial cluster size distribution $Z(n,0) \rightarrow 0$ ($10^{-11}$ clusters/$m^3$ used here). Starting from room temperature $T_0$ = 300 K, the numerical simulations were performed at particular heating rates $\phi$ according to Eq. (3.32). The maximum number of equations solved in Eq. (3.33) (upper limit of cluster size) is $L$ = 40 [69].

Few simulations are produced here from solution of the continuous Master PDE representing the dynamics of crystallization and cluster size distributions. The values of the material parameters used in this section were the same parameters used by Blyuss et. al. in [69]. The simulations were carried out by annealing the GST phase-change material using ramped annealing at a rate of 0.05 K/s starting from room temperature (300 K). Figure 3.5 (a) shows the calculated crystalline volume fraction with good agreement to the experimental data in [68] measured at the same heating rate. Cluster size distribution at different instances of time is shown in Figure 3.5 (b) which illustrates the formation of small clusters from the attachment of monomers at an early stage in (1 - 2450 second) and over time the clusters grow to larger sizes. A redistribution of cluster sizes occur with larger clusters gaining more monomers, while smaller clusters decay. Ultimately, the distribution in the system is settled to the steady state distribution shown by black line in Figure 3.5 (b).

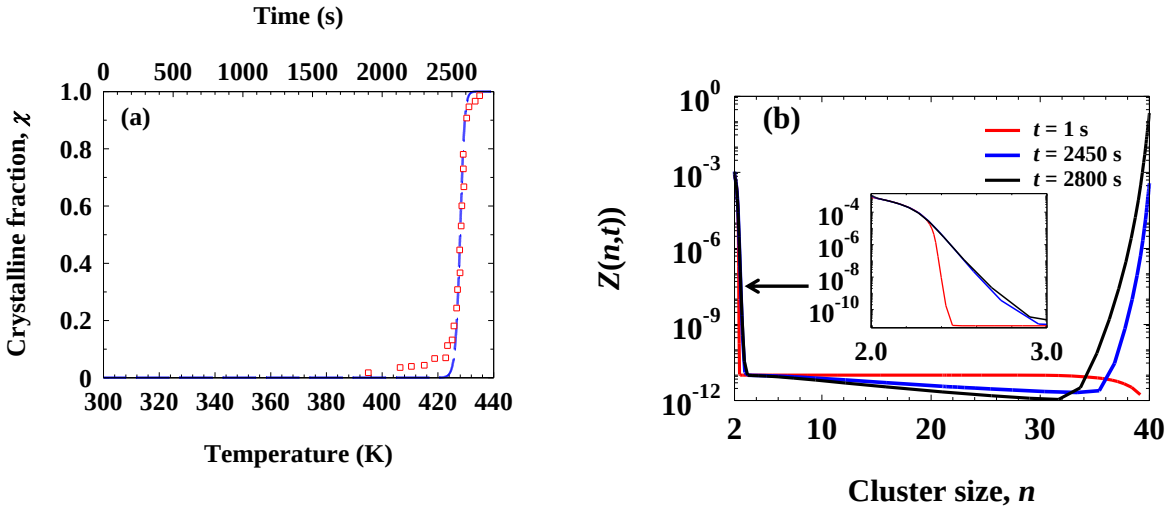


**Figure 3.5 (a) Calculated crystalline volume fraction as a function of temperature during ramped anneals at 0.05K/s heating rate for $Ge_2Sb_2Te_5$. Red squares show the experimental data** [68]**, and the blue line represent the model simulation. (b) Cluster size distribution at three instances of time. Maximum cluster size used was 40 monomers. Simulation parameter values are taken from Ref.** [69] **and are summarized in Table 3.1.**

**Table 3.1 Thermodynamic and material parameters used for the numerical simulations** [69]**.**

| Parameter | Value | unit |
|---|---|---|
| Volume of a monomer $\sigma_0$ | $2.9 \times 10^{-28}$ | $m^3$ |
| Enthalpy of fusion $\Delta H_f$ | $6.18 \times 10^8$ | $J/m^3$ |
| Melting temperature $T_m$ | 889 | K |
| Specific surface energy $\sigma$ | 0.1 | $J/m^2$ |
| Wetting angle $\theta_w$ | 94 | deg |
| Activation energyture $E_a$ | 2.0 | eV |
| Prefactor $K_\eta$ | $5.82 \times 10^{-12}$ | (Pa s) |

### 3.5.2 Truncation error of the derivation of continuous approach

The phase change process is described by means of the discrete and continuous Master rate equation approaches that completely determine the evolution of the cluster size distribution. The main aspects of this section is to investigate the errors involved in the approximate continuous form of the Master rate equation, in comparison to the fundamental discrete form, to better understand the limitations and applicability of the continuous form of the Master rate equation for modelling crystallization dynamics. As previously indicated, the main advantage of continuous approach is that it solves a single PDE for the transient cluster density [70] thus providing quick computational times in comparison to the discrete approach, which solves a large system of coupled ODEs for each cluster size thus requiring additional computational burden. However, the continuous approach is an approximation itself, from the truncation of the Taylor expansion used in the process of converting the discrete form of the Master equation to the continuous form [71]. In this section, two methods will be used to investigate the error involved in this approximation. The first method follows the mathematical derivation of the continuous form of the rate equation to investigate the resulting truncation error. The second way of investigation is via a number of numerical experiments using the continuous Master rate equation simulating the crystalline volume fraction, using different simulation parameters such as the maximum cluster size maximum cluster sizes, and study their effects on the calculated crystallization curves at different heating rates.

#### 3.5.2.1 Mathematical derivation of the truncation error

Starting with the mathematical investigation, the error term induced from the continuous approach of the Master rate equation is derived next. As mentioned in Section 3.4 and

following the generalizing approach of Zeldivich [62] and Kashchiev [64], the detachment frequency can be eliminated from the Master rate equation Eq. (3.8) by using Eq. (3.12). Thus the discrete Master rate equation including $C(n,t)$ instead of the detachment frequency $g(n-1,t)$ can be written as:

$$\frac{dZ(n,t)}{dt} = f(n-1,t)C(n-1,t)\left[\frac{Z(n-1,t)}{C(n-1,t)} - \frac{Z(n,t)}{C(n,t)}\right] - f(n,t)C(n,t)\left[\frac{Z(n,t)}{C(n,t)} - \frac{Z(n+1,t)}{C(n+1,t)}\right] \quad \textbf{(3.37)}$$

where $n = 1,2,3,\ldots,M$ and $M$ is the overall number of molecules in the sample at time $t$. According to Taylor's theorem with Lagrange form for the remainder, and under a suitable regularity assumption, the first order forward and backward differencing approximation of a given function $f(x)$ can be expressed, respectively, as [72]:

$$f(x-h) = f(x) - hf'(x) + \frac{h^2}{2} f''(\xi_1) \quad \textbf{(3.38)}$$

$$f(x+h) = f(x) + hf'(x) + \frac{h^2}{2} f''(\xi_2) \quad \textbf{(3.39)}$$

where $h > 0$, for some $\xi_1 \in (x-h, x)$ and $\xi_2 \in (x, x+h)$. The continuous form of the discrete Master equation in (3.37) can be derived using the forward and backword differencing forms Eq. (3.38) and Eq. (3.39) as follows:

1. Consider $n$ as a continuous variable and assume that $\tilde{Z}(n,t)$ is a second order differentiable extension of the solution $Z$ of Eq. (3.37) to the continuous domain $n \in R^+$

such that $\widetilde{Z}(n,t) = Z(n,t)$ for all $n \in N^{+}$. From Eq. (3.38) the right-hand side of Eq. (3.37) can be written as:

$$\begin{aligned} & f(n-1,t)C(n-1,t)\left[\frac{Z(n-1,t)}{C(n-1,t)} - \frac{Z(n,t)}{C(n,t)}\right] \\ & \quad - f(n,t)C(n,t)\left[\frac{Z(n,t)}{C(n,t)} - \frac{Z(n+1,t)}{C(n+1,t)}\right] \\ & \quad = -\frac{\partial}{\partial n}\left[ f(n,t)C(n,t)\left[\frac{Z(n,t)}{C(n,t)} - \frac{Z(n+1,t)}{C(n+1,t)}\right]\right] \\ & \quad + \frac{1}{2}\frac{\partial^2}{\partial \hat{n}_1^{\,2}}\left[ f(\hat{n}_1,t)C(\hat{n}_1,t)\left[\frac{Z(\hat{n}_1,t)}{C(\hat{n}_1,t)} - \frac{Z(\hat{n}_1+1,t)}{C(\hat{n}_1+1,t)}\right]\right]_{\hat{n}_1=\xi_1(n)} \end{aligned} \tag{3.40}$$

for some $\xi_1 \in (n\text{-}1, n)$. Since the values $\xi_1$ vary depending on the continuous variable $n$ in the range $(n\text{-}1,n)$, and due to the regularity of the functions $f(n,t)$ and $C(n,t)$ in addition to the solution $\widetilde{Z}$, therefore it is reasonable to consider $\xi_1$ as a differentiable function in the continuous variable $n$ (i.e. $\xi_1 \in \xi_1(n) \in (n\text{-}1,n)$), which allows to employ the chain rule to calculate the derivatives in the variable $n$ on the right-hand side of Eq. (3.40).

2. Following the same argument, from equation Eq. (3.39) we can write:

$$\frac{\widetilde{Z}(n+1,t)}{C(n+1,t)} - \frac{\widetilde{Z}(n,t)}{C(n,t)} = \left(\frac{\partial}{\partial n}\left[\frac{\widetilde{Z}(n,t)}{C(n,t)}\right]\right) + \frac{1}{2}\left(\frac{\partial^2}{\partial \hat{n}_2^{\,2}}\left[\frac{\widetilde{Z}(\eta_2,t)}{C(\hat{n}_2,t)}\right]_{\hat{n}_2=\xi_2(n)}\right) \tag{3.41}$$

for some differentiable function $\xi_2(n) \in (n,n+1)$.

3. Now from Eq. (3.40) we can re-write equation Eq. (3.37) for the continuous extension $\widetilde{Z}$ in the form:

$$\frac{d\tilde{Z}(n,t)}{dt} = -\frac{\partial}{\partial n}\left[ f(n,t)C(n,t)\left[\frac{\tilde{Z}(n,t)}{C(n,t)} - \frac{\tilde{Z}(n+1,t)}{C(n+1,t)}\right]\right] + \frac{1}{2}\frac{\partial^2}{\partial \hat{n}_1^{\,2}}\left[ f(\hat{n}_1,t)C(\hat{n}_1,t)\left[\frac{\tilde{Z}(\hat{n}_1,t)}{C(\hat{n}_1,t)} - \frac{\tilde{Z}(\hat{n}_1+1,t)}{C(\hat{n}_1+1,t)}\right]\right]_{\hat{n}_1=\xi_1(n)} \quad \textbf{(3.42)}$$

4. Then from Eq. (3.41), equation (3.42) can be written in the continuous form:

$$\frac{d\tilde{Z}(n,t)}{dt} = \frac{\partial}{\partial n}\left[ f(n,t)C(n,t)\left[\left(\frac{\partial}{\partial n}\left[\frac{\tilde{Z}(n,t)}{C(n,t)}\right]\right) + \frac{1}{2}\left(\frac{\partial^2}{\partial \hat{n}_2^{\,2}}\left[\frac{\tilde{Z}(\hat{n}_2,t)}{C(\hat{n}_2,t)}\right]_{\hat{n}_2=\xi_2(n)}\right)\right]\right] - \frac{1}{2}\frac{\partial^2}{\partial \hat{n}_1^{\,2}}\left[ f(\hat{n}_1,t)C(\hat{n}_1,t)\left[\left(\frac{\partial}{\partial \hat{n}_1}\left[\frac{\tilde{Z}(\hat{n}_1,t)}{C(\hat{n}_1,t)}\right]\right) + \frac{1}{2}\left(\frac{\partial^2}{\partial \hat{n}_2^{\,2}}\left[\frac{\tilde{Z}(\hat{n}_2,t)}{C(\hat{n}_2,t)}\right]_{\hat{n}_2=\xi_2(\eta_1)}\right)\right]\right]_{\hat{n}_1=\xi_1(n)} \quad \textbf{(3.43)}$$

5. After separating all terms containing the unknown functions $\xi_1$ and $\xi_2$, the resulting continuous equation that is equivalent to the discrete Master rate equation (3.37) can be written as:

$$\frac{d\tilde{Z}(n,t)}{dt} = \frac{\partial}{\partial n}\left[ f(n,t)C(n,t)\left(\frac{\partial}{\partial n}\left[\frac{\tilde{Z}(n,t)}{C(n,t)}\right]\right)\right] + Err(n,t) \quad \textbf{(3.44)}$$

where:

$$Err(n,t) := \frac{1}{2}\frac{\partial}{\partial n}\left[ f(n,t)C(n,t)\left(\frac{\partial^2}{\partial \eta_2^{\,2}}\left[\frac{\tilde{Z}(\hat{n}_2,t)}{C(\hat{n}_2,t)}\right]_{\hat{n}_2=\xi_2(n)}\right)\right] - \frac{1}{2}\frac{\partial^2}{\partial \hat{n}_1^{\,2}}\left[ f(\hat{n}_1,t)C(\hat{n}_1,t)\left(\frac{\partial}{\partial \eta}\left[\frac{\tilde{Z}(\hat{n}_1,t)}{C(\hat{n}_1,t)}\right]\right)\right]_{\hat{n}_1=\xi_1(n)} - \frac{1}{4}\frac{\partial^2}{\partial \hat{n}_1^{\,2}}\left[ f(\hat{n}_1,t)C(\hat{n}_1,t)\left(\frac{\partial^2}{\partial \hat{n}_2^{\,2}}\left[\frac{\tilde{Z}(\hat{n}_2,t)}{C(\hat{n}_2,t)}\right]_{\hat{n}_2=\xi_2(\eta_1)}\right)\right]_{\hat{n}_1=\xi_1(n)} \quad \textbf{(3.45)}$$

A further calculation of the derivatives in Eq. (3.45) would result in more complicated formulas, involving the given functions $f(n,t)$ and $C(n,t)$, as well as the unknown functions $\tilde{\tilde{Z}}$, $\xi_1$ and $\xi_2$ in the continuous variable $n$. Moreover, any attempt to define a bound of this error would require further assumptions regarding the smoothness and boundedness of the functions $\tilde{\tilde{Z}}$, $\xi_1$and $\xi_2$, which might lack to the acceptable justification from the theoretical and numerical prospective. Therefore, this derivation will not go beyond Eq. (3.45) and will leave the analysis and measure of the error to future studies. Nevertheless, if the error term is assumed to be negligible compared to the first term in the right-hand side of Eq. (3.44), then the solution $\tilde{\tilde{Z}}$ of the continuous Master rate equation:

$$\frac{d\tilde{\tilde{Z}}(n,t)}{dt} = \frac{\partial}{\partial n}\left[ f(n,t)C(n,t)\left( \frac{\partial}{\partial n}\left[ \frac{\tilde{\tilde{Z}}(n,t)}{C(n,t)} \right] \right) \right] \tag{3.46}$$

can be considered as an approximation to the solution $\tilde{Z}$ of the continuous equation (3.44) for $n \in R^+$, and hence an approximation to the solution $Z$ of the discrete Master rate equation (3.37). However, comparing the error terms of Eq. (3.45) to the right hand side of the truncated equation (3.46), it can be noticed that the main functions $f(n,t)$ and $C(n,t)$, and their derivatives are included in all error terms. This might give a reasonable expectation that truncating error terms of Eq. (3.45) to obtain the truncated equation (3.46) would result in inaccurate approximations of the solution of the Eq. (3.44). This particularly true, when the rate change (with respect to the continuous variable $n$) of the right-hand side of Eq. (3.46) is relatively large.

The solution of the Master rate equation represents the cluster size distribution function $Z$ which is the basis of quantifying the crystallization fraction. Hence, any inaccuracy in $Z$

might have a significant effect on the crystallization dynamics. In the next section, a comparison between both discrete and continuous forms of Master rate equation is carried out using same set of parameters with different upper limit of cluster size. This simulation is also used to test the reliability of these approaches in modelling phase-change materials.

#### 3.5.2.2 The effect of maximum cluster sizes on the crystallization dynamics

The crystallization dynamics in phase-change materials using the Master rate equation model is described through the interaction of clusters of different sizes governed by the thermodynamic and kinetic parameters supplied to the model and their temperature dependence. Thus, it is expected that the maximum cluster size, $L$ (upper limit of cluster size), in this model might have an effect on the calculated crystallization dynamics in general in the discrete Master rate equation, and particularly in the approximate continuous form of this equation. Therefore, the effects of maximum cluster size on the calculated crystallization dynamics in both discrete and continuous forms of the rate equation will be compared. Ramped annealing using constant heating rate is applied in the following simulated crystallization curves using the thermodynamic and materials parameters listed in Table 3.2, and represent typical parameters of the GST phase-change material (to be discussed in more detail in chapter 4 of this thesis). The MYEGA model was used to describe the viscosity for the comparison in this section [39].

Starting with the continuous Master rate equation, simulations of crystallization curves over the finite interval [2,$L$] are carried out using different values (for comparison purpose) for the subintervals, $\Delta L$, ranging from 100 to 300. $\Delta L$=100 was initially chosen because it provided convergence of the solution within reasonable simulation time. Moreover, the maximum cluster size $L$ was varied within the range of $L$ = 40 - 80 monomers in the continuous rate

equation simulations, which is practical for the temperatures and cluster sizes considered in this work while providing practical computational times using the NAG solver. The calculated crystalline volume fractions when $\Delta L$ = 100 are shown in Figure 3.6 (a) and Figure 3.6 (b) for the heating rates of 50 K/s and 40,000 K/s respectively. Figure 3.6 illustrates the numerical effect of increasing the maximum cluster size, $L$, on reducing the calculated crystallization temperature (defined as the temperature where the crystallization rate is maximum, and important later for characterisation of crystallization dynamics) and increasing the crystallization speeds for low and high heating rates.

**Table 3.2 Thermodynamic and material parameters used for the numerical simulations**

| Parameter | Value | unit |
|---|---|---|
| Volume of a monomer $\sigma_0$ | $2.9 \times 10^{-28}$ [a] | $m^3$ |
| Enthalpy of fusion $\Delta H_f$ | $6.18 \times 10^{8}$ [a] | $J/m^3$ |
| Melting temperature $T_m$ | 889 [b] | K |
| Specific surface energy $\sigma$ | 0.066[c] | $J/m^2$ |
| Wetting angle $\theta_w$ | 100[d] | deg |
| Glass transition temperature $T_g$ | 383[e] | K |
| Infinite temperature viscosity $\eta_\infty$ | $1 \times 10^{-5}$ [f] | (Pa s) |
| Fragility index $m$ | 47[g] | |

[a] Ref. [32][69].

[b] Ref.[76].

[c] Ref [77].

[d] Ref. [32].

[e] Refs.[28][73][74][75].

[f] Extrapolated from Ref. [28]at $T>T_m$.

[g] Ref. [78].

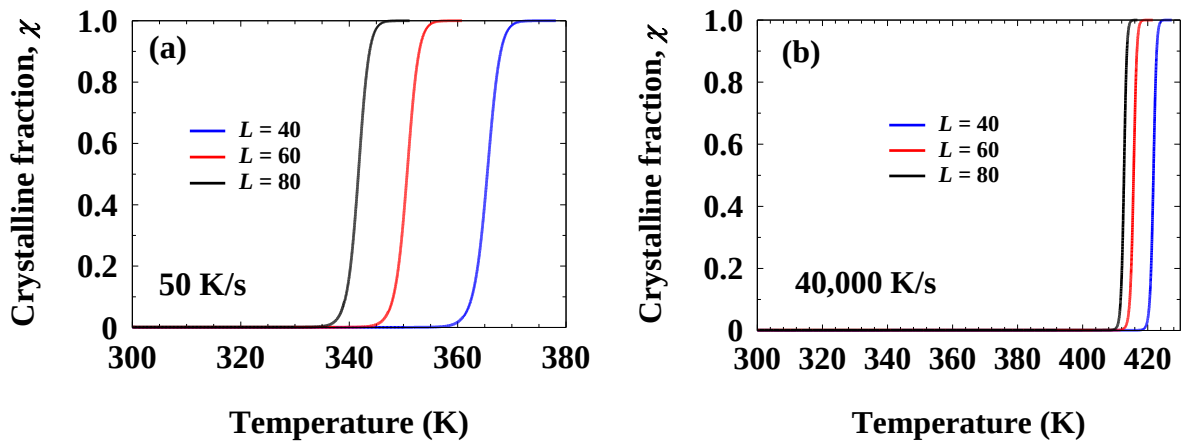


**Figure 3.6 Numerical solution of the continuous Master rate equation for different number *L* of maximum cluster sizes with $\Delta L$=100. (a) Ramped annealing results at heating rate 50 K/s, and (b) at heating rate 40,000K/s. Model parameters are listed in Table 3.2.**

It is also of interest to investigate whether the number of subintervals can lead to significant changes in the computed crystallization curves. Next the interval [2,*L*] is divided into 300 subintervals ($\Delta L$ = 300) in the solver and crystallization curves were recalculated using the same heat source and material parameters and shown in Figure 3.7. It is observed from Figure 3.7 (a) and Figure 3.7 (b) for a low and high heating rate respectively, that increasing $\Delta L$ causes shift in the crystallization temperature to higher temperature (in comparison to Figure 3.6).

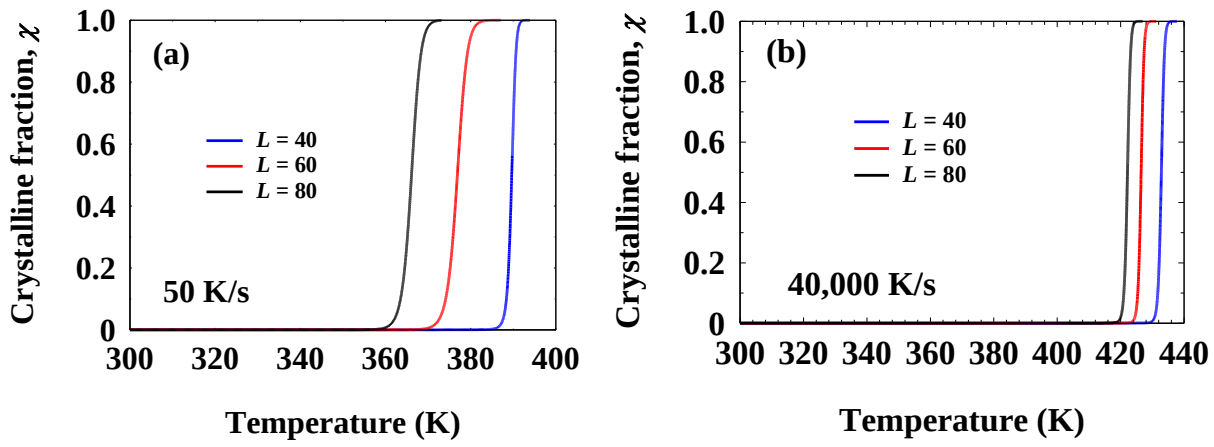


**Figure 3.7 Numerical solution of the continuous Master rate equation for different number *L* of maximum cluster sizes with Δ*L*=300. (a) Ramped annealing results at heating rate 50 K/s, and (b) at heating rate 40,000K/s. Model parameters are listed in Table 3.2.**

Now, the discrete Master rate equation (original) is used to investigate the effect of maximum cluster size on computed crystallization dynamics. Simulations were carried out using the discrete Master rate equation solver with up to 1000 monomers and found a negligible effect of maximum cluster size on the transient behaviour for different heating rates. The simulation results are shown in Figure 3.8 for the low and high heating rates of 50 K/s and 40,000 K/s respectively.

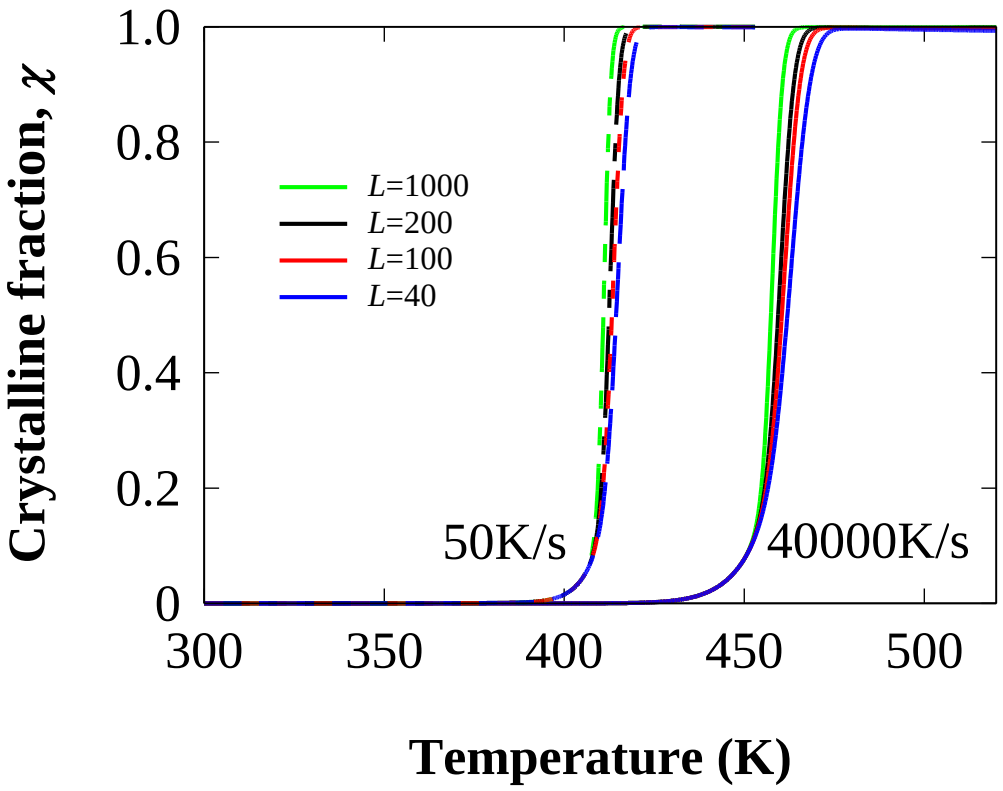


**Figure 3.8 Calculated crystalline volume as a function of temperature during ramped anneals at different heating rates with up to 1000 monomers. Model parameters are listed in Table 3.2.**

The results in Figure 3.6 and Figure 3.7 demonstrate that while the continuous Master rate equation can be used for phase-change modelling with limited maximum number of monomers and subinterval values, they relatively affect the computed crystallization dynamics. However, calculations using the discrete Master rate equation in Figure 3.8 showed that the simulated crystallization curves (for the temperature range used in these calculations) are less sensitive to the maximum number of monomers for the different heating rates.

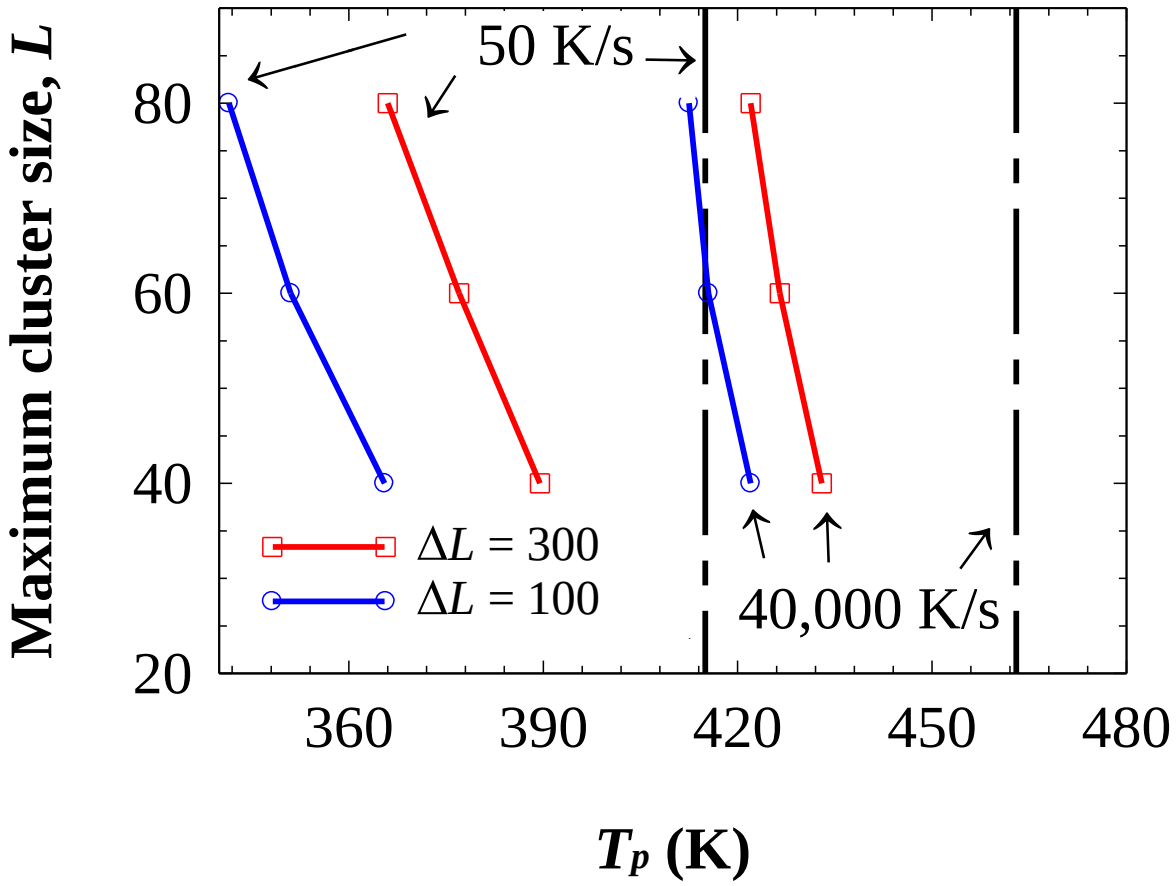


**Figure 3.9 Maximum cluster size as a function of extracted values of *Tp* of the continuous Master rate equation from Figure 3.6 and Figure 3.7 (solid blue and solid red lines) with different sub-intervals showing the effect of these numerical parameters on crystallization dynamics compared to extracted values of *Tp* of the discrete Master rate equation simulations, for different heating rates, from Figure 3.8 (dashed black lines).**

The maximum cluster size, $L$, is plotted in Figure 3.9 as a function of crystallization temperature, $T_p$, to show more clearly how the peak temperature values are affected by varying the maximum cluster size and the subinterval lengths in the continuous Master rate equation solutions compared to those of discrete Master rate equation (original). The discrepancies between the crystallization temperatures illustrate that the continuous model solution is sensitive to the maximum cluster size and the number of subintervals. This inaccuracy may be attributed to the truncated error terms in (3.46).

## 3.6 Chapter summary

In this chapter, a mathematical review of the Master rate equation and its implementation for modelling crystallization dynamics in phase-change materials was presented. It was shown that the continuous Master rate equation is an approximation of the discrete due to truncated terms. This approximation may lead to quantitative errors when modelling the crystallization dynamics. A comparison between continuous and discrete forms was carried out investigating the effect numerical solver parameters such as the upper limit of cluster size and cluster size sub-interval on the crystallization dynamics at low and high heating rates. It was found that the upper limit of cluster sizes along with the number of subintervals has a significant effect on the crystallization dynamics for different heating rates with the use of the continuous Master rate equation. On the other hand, it was found that crystallization curves calculated using the discrete form of the Master rate equation were less sensitive to increases in the maximum cluster size for clusters greater than 40 monomers. The discrete Master rate equation could successfully model the transient behaviour of phase-change material. The simulations and analyses carried out in this chapter provide some confidence in the discrete model and parameters used in the simulations, and will thus be used in all the simulations and analysis in the following chapters of this thesis.

# CHAPTER 4: Viscosity models and crystallization dynamics

In the preceding chapter, the characteristics and implementation of the Master rate equation approach to modelling crystallisation dynamics were presented. Through the attachment and detachment of monomers, the Master rate equation naturally traces nucleation and growth of crystallites with temperature history to calculate the transient distribution of clusters sizes in the material. Both the attachment and detachment rates in this theory are strong functions of viscosity and thus the value of viscosity and its dependence on temperature significantly affects the crystallization process. In this chapter, the Master equation approach is augmented with a physically founded model for the viscosity dependence on temperature. The Master rate equation is now used to understand the role of viscosity model parameters on the crystallization process through modelling.

## 4.1 Introduction

Modelling crystallization dynamics of phase-change material under fast annealing conditions is of importance to understand the requirements for achieving high data rates during the write and erase processes in optical and electronic memories [21]. While quenching from the melt and re-amorphisation is a relatively fast process, crystallization from the amorphous phase remains to be the time limiting process in phase-change based memories [34]. The viscosity dependence on temperature directly affects the speed of crystallization of the phase-change material. Therefore, understanding the role of viscosity parameters on the crystallization process through modelling is crucial for the development of modern, high-speed phase-change memory devices and technologies.

The crystallization process in phase-change materials has been modelled using different approaches (see Chapter 2), One of the approaches for bridging the gap between the large-scale, simplified analytical models (such as the JMAK description) and the first-principle and numerically intensive atomistic modelling is the robust and more physically realistic Master rate equation method (see Chapter 2 and 3). Nucleation and growth in this model are described by the attachment and detachment of monomers [43]. The rates of attachment and detachment in the Master equation model, which control the speed of crystallization, are functions of temperature dependent viscosity and hence the simulations are sensitively characterized by the mathematical expression used for viscosity.

A number of models have been developed to describe the viscosities of glasses in a broad range of chemical compositions and temperatures [79]. The Arrhenius viscosity model [80], is commonly used in investigations of crystallization dynamics in GST [32] [81]. However, extracted viscosities for GST from ultrafast DSC measurements and growth rate measurements showed deviation from the Arrhenuis temperature dependence, particularly demonstrating a fragile behaviour in the supercooled region [28][78]. Other non-Arrhenius models for viscosity in phase-change materials were therefore adopted including the Cohen and Grest viscosity model, and the three-parameter models. The Cohen and Grest viscosity model has four adjustable parameters to fit measured viscosity data experimentally [82]. This model was used in [28] to extract the dependence of viscosity and crystal growth rates on temperature from DSC measurements for GST. The fitting constants in this viscosity model are not related to physical parameters of viscosity. It was also noted that the Cohen and Grest viscosity model over-estimated crystal growth rates in Ge-Sb alloys by 2-3 orders of magnitude compared to the three-parameter models [29], and was not able to provide accurate fitting to Kissinger plots at high heating rates for AgInSbTe phase-change material [30].

The three-parameter viscosity models include the well-known Vogel–Fulcher−Tammann (VFT) model [83], the Avramov–Milchev (AM) model [84] and the more widely accepted Mauro−Yue−Ellison−Gupta−Allan (MYEGA) model [38]. The VFT model has three fitting parameters and was used to describe the temperature dependence of viscosity of GST (for example [85] [78]). The more robust MYEGA viscosity model has physical foundation with the three physical parameters including the glass transition temperature $T_g$, the fragility $m$, and extrapolated infinite temperature viscosity parameter, $\eta_\infty$ [38]. This model was successfully used to describe the temperature dependence of viscosity and crystal growth rates for AIST [86][87], GeSb [29] and GST [73]. The extended, five parameter generalised MYEGA model [88] was also used to describe the fragile-to-strong cross-over of viscosity in AgInSbTe phase-change material (which is not apparent in GST) [30]. This Chapter is therefore concerned with implementing the MYEGA model for the viscosity dependence on temperature in the Master equation system to simulate crystallization in GST at high heating rates.

The fragility index $m$ in the MYEGA viscosity model represents the slope of the viscosity in the Angell plot at the glass transition temperature, and indicates the degree of deviation from the strong, Arrhenius temperature dependence of viscosity. For the GST phase-change material, the fragility index has been extracted from fitting simplified (growth dominated) JMAK formulation with the Cohen and Grest viscosity model to Kissinger plots measured using ultrafast differential scanning calorimetry (DSC), with a reported value of ~90 [28]. Mechanical stress measurements on GST films at relatively low heating rates (assuming Arrhenius temperature dependence of viscosity and heating rate dependent $T_g$) indicated fragilities of 47 and 20 for pure and doped GST, respectively [78] . Higher values of fragility

of 140 were also estimated from fitting to device level measurements of crystal growth rates as function of temperature [73]. There is thus dispersion and uncertainty in the extracted values of fragility, but they all indicate the fragile nature of GST, which contributes to the high atomic mobility and fast crystallization of this phase-change material heated at the relevant temperatures.

Published values of the glass transition temperature $T_g$ for GST also vary, with 373 K reported for thin (as-deposited) amorphous films using impedance, transmission and heat capacity measurements [74]. This value is in agreement with a glass transition temperature of 384 K determined from theory based on the enthalpy of atomization for GST [89], and therefore adopted in the theoretical analysis and fitting to measured Kissinger plots in ultrafast DSC simulations in [28]. However, DSC measurements of pre-annealed thin amorphous films of phase-change material at relatively low heating rates (40 K/min) revealed glass transition temperatures within 10 K of the peak crystallization temperature (456 K for GST), and hence difficult to resolve from the main crystallization peak in the measurement [75]. The highest value reported of $T_g$ for GST was estimated from fitting the MYEGA model for the viscosity to crystal growth velocity measurements at device level, and was 472K [73]. The infinite temperature viscosity parameter, $\eta_\infty$, can be extracted from Angell plots extrapolated to high temperatures, and is typically in the range $10^{-5}$ - $10^{-3}$ (P as) [28].

It is clear from the brief overview of reported viscosity parameters above that there are uncertainties in the values of fragility and glass transition temperature for GST in the MYEGA model. The effect of these uncertainties on the crystallization dynamics of phase-change materials is not well understood. In this Chapter, a more detailed Master equation approach was used, which includes both transient nucleation and growth processes with viscosity described by the MYEGA model, to study the crystallization dynamics of GST over

a wide range of heating rates. In particular, the role of the viscosity model and its parameters on the crystallization dynamics using Master equation simulations is investigated.

## 4.2 Methodology

This section concerned with implementing the MYEGA model for the viscosity dependence on temperature in the Master equation system to simulate crystallization in GST at high heating rates.

### 4.2.1 Mathematical formulation of the viscosity models

In this section both the Arrhenius and non-Arrhenius (MYEGA) models of viscosity dependence on temperature are presented. In the Arrhenius model, the viscosity is described by:

$$\eta(T) = K_\eta \exp\left[\frac{E_a}{\kappa_\beta T}\right] \qquad \textbf{(4.1)}$$

where $K_\eta$ is a pre-factor and $E_a$ is the activation energy for viscous flow. This model has been previously employed in reaction rate modelling of crystallization in phase-change materials and yielded good agreement between simulations and measurements, for isothermal annealing and at low heating rates [69][32]. Recent ultra-high heating rate DSC measurements, however, indicated deviation of the viscosity from the Arrhenius behaviour for GST[28] and other phase-change material including AIST[86][87], and GeSb [29].

This thesis focuses on the more robust and widely accepted viscosity model of Mauro-Yue-Ellison-Gupta-Allan (MYEGA) [38]. This model has physical grounding and is able to describe different viscosity behaviours over a wide temperature range from $T_g$ (glass transition temperature) to $T_m$ (melting temperature), and is given by:

$$\log_{10}\eta(T) = \log_{10}\eta_\infty + (12-\log_{10}\eta_\infty)\frac{T_g}{T}\exp\left[\left(\frac{m}{(12-\log_{10}\eta_\infty)}-1\right)\left(\frac{T_g}{T}-1\right)\right] \quad \textbf{(4.2)}$$

for $T \geq T_g$. The three parameters in the MYEGA model are: $\eta_\infty$ which is the extrapolated infinite temperature viscosity, $T_g$ is the glass transition temperature at which the shear viscosity is equal to $10^{12}$ (Pa s) [90], and $m$ is the fragility index of the material, defined as:

$$m = \left.\frac{\partial \log_{10}(\eta(T))}{\partial(T_g/T)}\right|_{T=T_g} \quad \textbf{(4.3)}$$

The fragility index is the slope of the viscosity curve at the glass transition temperature in the Angell plot as shown in the example plot of Figure 4.1, and indicates the degree of deviation from the Arrhenius behaviour in the supercooled region.

The MYEGA model is also able to describe the viscosity of a wide class of phase-change materials and behaviours including the Arrhenius behaviour. This can be illustrated by taking the logarithm on both sides of Eq. (4.1) to yield:

$$\log_{10}\eta(T) = \log_{10}K_\eta + \left[\frac{E_a\log_{10}(e)}{k_B T_g}\right]\times\frac{T_g}{T} \quad \textbf{(4.4)}$$

By comparing Eq. (4.2) to Eq. (4.4) it can be readily shown that the MYEGA model can describe the Arrhenius temperature dependence provided that:

$$\log_{10} K_\eta = \log_{10} \eta_\infty$$

and:

$$12 - \log_{10} \eta_\infty = \left[ \frac{E_a \log_{10}(e)}{k_B T_g} \right]$$

while the exponential term in Eq. (4.2) equates to:

$$\exp\left[ \left( \frac{m}{(12 - \log_{10} \eta_\infty)} - 1 \right) \left( \frac{T_g}{T} - 1 \right) \right] = 1 \qquad \textbf{(4.5)}$$

The above equalities show that through appropriate choice of the three parameters, the MYEGA model can describe the strong, Arrhenius temperature dependence of viscosity near the glass transition temperature for small fragilities where $m \to (12 - \log_{10} \eta_\infty)$.

For temperatures $T < T_g$, the viscosity dependence on temperature is taken to be Arrhenius as defined in Eq. (4.1), with activation energy $E_a$ = 1.76±0.05 eV [91]. The pre-factor $K_\eta$ in Eq. (4.1) in this case was determined from the requirement that $\log_{10} \eta(T) = 12$ at $T = T_g$ to match the viscosity of the MYEGA model. Hence the complete viscosity model used in this thesis is given by:

$$\log_{10}\eta(T)=\begin{cases}12-\log_{10}\left(\exp\left[\dfrac{E_a}{\kappa_\beta}\left(\dfrac{1}{T}-\dfrac{1}{T_g}\right)\right]\right) & T<T_g \\ MYEGA & T\geq T_g\end{cases} \qquad \textbf{(4.6)}$$

Figure 4.1 illustrates the temperature dependence of viscosity calculated using the MYEGA model for different values of fragility. The viscosity model in Eq. (4.6) is used in the subsequent simulations in this thesis.

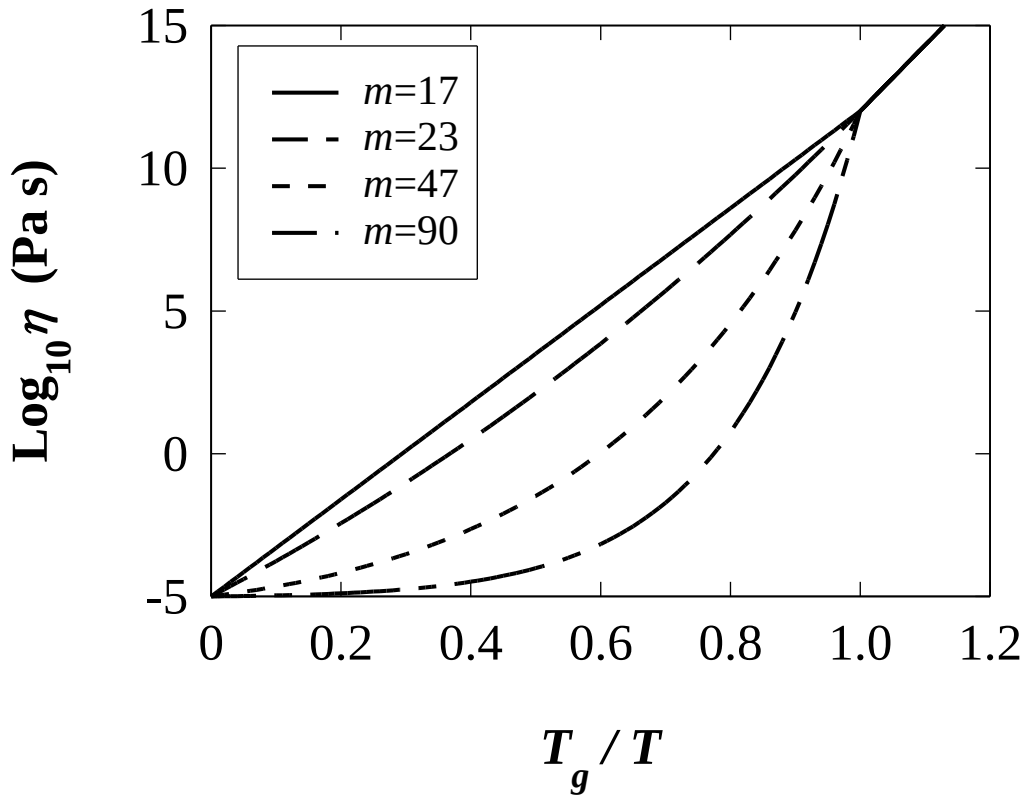


**Figure 4.1 Angell plot for the temperature dependence of calculated viscosity using the complete viscosity model described in Eq. (4.6) with parameter values: $\eta_\infty = 10^{-5}$ (P as), $T_g = 383K$, and $E_a = 1.76$ eV in the Arrhenius model for $T < T_g$.**

The viscosity model in Eq. (4.6) (plotted in Figure 4.1) is based on the physically realistic MYEGA model for temperatures > $T_g$, and the experimentally observed Arrhenius dependence for temperatures < $T_g$. The two viscosity functions are matched at $T_g$, however they are discontinuous in their first derivatives at this temperature as indicated in Figure 4.1. To study the effect of this discontinuity on the simulation work in this thesis, crystallization simulations were carried out with varied activation energies up to 3.0 eV for the Arrhenius temperature dependence of viscosity with negligible effect on the crystallisation dynamics or fittings to experimental Kissinger plots. Further simulations were also carried out without dividing the viscosity into two regions by using the MYEGA viscosity model for all temperatures and thus without discontinuity at $T_g$, again showing negligible effects on the crystallisation dynamics and fittings to experimental measurements. However the effect of this discontinuity require more investigation for different values of the glass transition temperature and when using different viscosity models for temperatures > $T_g$ in the simulations. The alternative is to seek another viscosity model that is physically realistic while continuous over a wide temperature range starting from room temperature to the material's melting point.

The simulations carried out in this thesis assumed the applicability of the Stokes-Einstein equation of Eq. (3.31) to describe the relationship between the diffusion coefficient and viscosity. Deviation from the form $D \propto 1/\eta^{\zeta}$ where $\zeta < 1$ for temperatures down to $T_g$ was indicated using molecular dynamic simulations for the GeTe compound (not GST) in [31]. The decoupling between diffusion and viscosity was also suggested and introduced in [28] for GST, however mainly to overcome the inability of the Cohen and Grest viscosity model used in the analysis of Kissinger data to correctly describe the viscosity behaviour at $T_g$ (with

value $10^{12}$ Pa.s). This limitation that was highlighted in [86] and [30] for AIST (and indicated that the more physically realistic MYEGA models for viscosity can alternatively provide accurate analysis of DSC measurements without the need for decoupling), and [29] for GeSb. Moreover, fittings to device level measurements in [73] found no sufficient evidence for the need for this decoupling for GST. There is thus currently little concrete evidence that confirms the breakdown of the Stokes-Einstein equation for GST nor confirmed values for the decoupling factor in the literature, which is also made difficult by the disparity of reported values of $T_g$ and fragility index.

## 4.3 Results and Discussion

In this section, transient simulations of crystallization over a wide range of heating rates are carried out by solving the Master equation, to determine the key parameters within the MYEGA viscosity model that affect the crystallization dynamics.

The maximum number of equations solved in the Master rate equation system (upper limit of cluster sizes) was 40 (see Section 3.5.2.2). The thermodynamic and material parameters used in the simulations are listed in Table 3.2. The viscosity model parameters were varied in the simulations within the range of reported values in the literature to investigate their effect on the transient crystallization behaviour.

### 4.3.1 The effects of viscosity parameters on crystallization dynamics

The fragility index, the glass transition temperature, and the infinite temperature viscosity parameter are the main parameters which describe the temperature dependence of viscosity in the MYEGA model, and influence the rates of attachment and detachment of monomers (and

therefore crystal nucleation and growth rates) in the Master rate equation. The effects of these parameters on the crystallization dynamics is studied using the Master rate equation simulations; in particular on the transient rate of crystallization, and on the peak crystallization temperature $T_p$ - defined here as temperature at which the crystallization rate is maximum - at different heating rates.

Figure 4.2 (a) starts by illustrating the effects of the fragility index on the crystalline volume fraction transformed, where low fragility values ($m$ = 23) decrease the rate of crystallization and increases the peak crystallization temperature, leading to incomplete crystallization at high heating rates. This is attributed to the reduction in the diffusion coefficient (atomic mobility) in the rate equation with increasing viscosity, which increases the transient nucleation time for the clusters (time for the onset of steady-state nucleation in $Z$) as shown in Figure 4.2 (b) for relatively low heating rates (50 K/s) and in Figure 4.2 (c) for the highest heating rate (40000 K/s). On the other hand, high fragility values ($m$ = 90) increase the atomic mobility in the supercooled region, therefore reducing the transient nucleation time and increasing the crystallization rates. This is illustrated by the sharp increase in the cluster size distributions for $n$ = 3 in Figure 4.2 (b) and Figure 4.2 (c) around 1.7 s and 2 ms respectively, marking the sharp drop in viscosity as the temperature reaching the glass transition temperature in the simulations. In this case (higher $m$) full crystallization is achieved even at relatively high heating rates with modest increase in $T_p$ as indicated in Figure 4.2 (a). It can also be observed from Figure 4.2 (b) and (c) that the transient nucleation rate of clusters of different sizes is not uniform and changes with heating rate. In particular showing the influence of increasing the fragility on reducing the cluster nucleation time and increasing the crystallization speed.

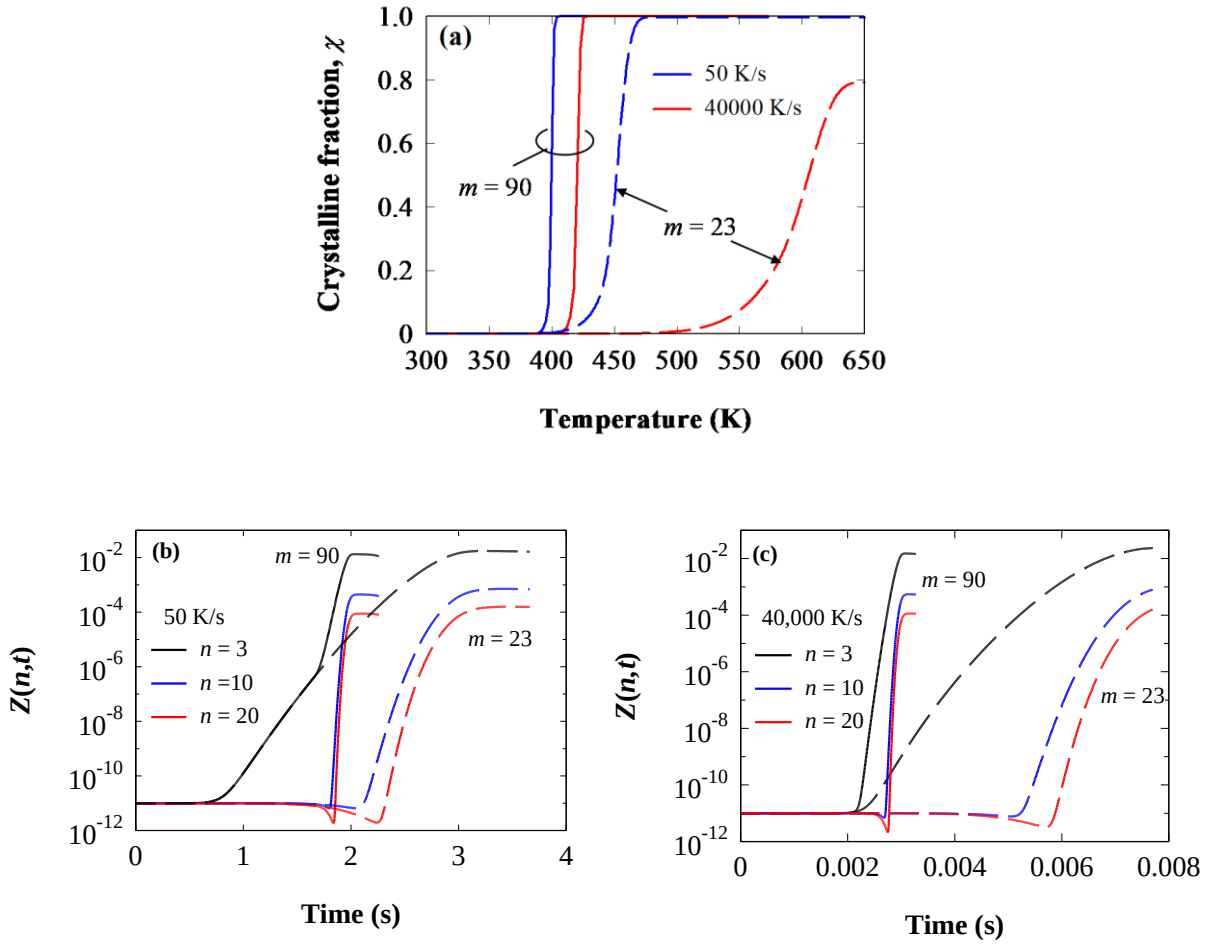


**Figure 4.2 (a) Calculated crystalline volume as a function of temperature during ramped anneals at different heating rates for two different fragility values: *m* = 90 (solid lines) and *m* = 23 (dashed lines). The calculated transient cluster densities for different cluster sizes at heating rates of (b) 50 K/s and (c) 40000 K/s, showing non-uniform transient nucleation and the influence of increasing the fragility parameters on reducing the cluster nucleation time and incrasing the crystallization speed. In these plots the fragilities values used in the calculations are *m* = 90 (solid line) and *m* = 23 (dashed line).**

The glass transition temperature $T_g$ was next varied within the range of published values in the Master equation simulations. The calculated crystalline volume fractions are shown in Figure 4.3 (a) for a strong glass with $m$ = 23 in the MYEGA model, illustrating an increase of $T_p$ following the increase in $T_g$ (compare dashed lines versus solid lines), leading to incomplete crystallization and increased temperature difference $T_p - T_g$ at high heating rates. The crystallization simulations in Figure 4.3 (b) also illustrate an increase of $T_p$ with

increasing $T_g$ for a fragile material with $m$ = 90, with modest changes of in the temperature $T_p$ – $T_g$ with increasing heating rate due to the high atomic mobility of the glass in this case.

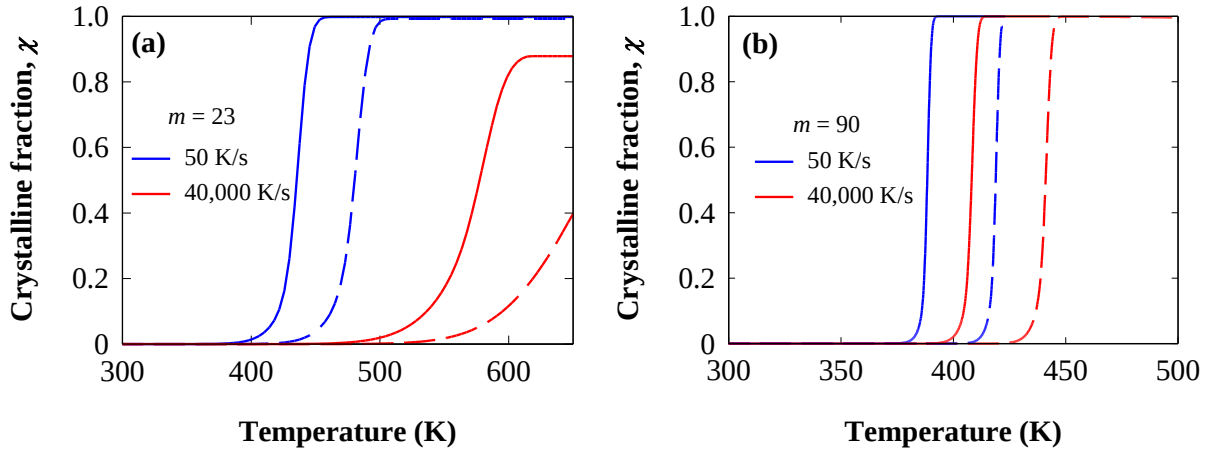


**Figure 4.3 Calculated crystalline volume fraction as a function of temperature during ramped anneals at different heating rates. Two different values of $T_g$ are used in the calculations: $T_g$ = 373K (solid line), and $T_g$ = 400K (dashed line) at different heating rates for (a) $m$ = 23, and (b) $m$ = 90.**

The infinite temperature viscosity parameter, $\eta_\infty$ was varied within the range 0.012 – $10^{-5}$ (P as) [28] [73] in the Master equation simulations for the fragilities $m$ = 23 and $m$ = 90 and at different heating rates. It is expected that the influnce of this parameter becomes important only at high temperatures near the melting point. As shown in Figure 4.4 (b), varying $\eta_\infty$ over this large range of values has a relatively small effect on the crystallization dynamics for high fragility values in the viscosity model, where the high diffusivities increase the crystallization rate and lower $T_p$ well below the melting point $T_m$. For low fragility values the influence of $\eta_\infty$ on the crystallization dynamics depends on the heating rate (which controls $T_p$). At low heating rates, $T_p$ is again well below $T_m$ and the value of $\eta_\infty$ has negligible effect on the crystallization dyanmics as shown in Figure 4.4 (a) at 50 K/s. Increasing the heating rates increases $T_p$ to higher temperatures towards the melting point, where smaller values of

$\eta_\infty$ increase the crystallization rate and final crystalline volume fraction as shown in Figure 4.4 (a). Since the simulations in this work occur within temperatures lower than the melting point for GST, a constant value of $\eta_\infty = 10^{-5}$ (Pa s) was employed in this work, allowing focus on the fragility index and glass transition temperature as variable parameters in the DSC simulations.

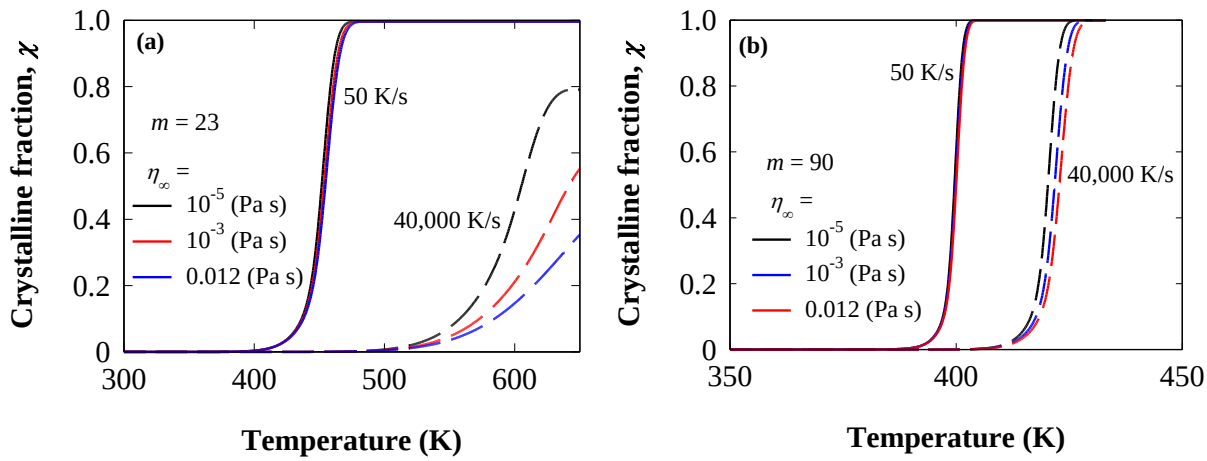


**Figure 4.4 : Calculated crystalline volume fraction as a function of temperature during ramped anneals at different heating rates. Three different values of $\eta_\infty$ were used at the heating rates 50 K/s (dashed lines) and 40000 K/s (solid lines). *Tg* = 383 K was used in the simulations for the fragilities (a) *m* = 23, and (b) *m* = 90.**

### 4.3.2 Chapter summary

In this chapter, it was shown that it is essential to use the physically realistic MYEGA viscosity model in the Master equation approach, and to investigate the impact of viscosity parameters on the crystallization dynamics. It was found that, with increasing heating rate, high fragility values ($m$ = 90) lead to modest increases in crystallization temperature. Lower values of fragility ($m$ = 23) reduced the crystallization rate due to reduced atomic mobility, leading to increased crystallization temperature and to incomplete crystallization at high heating rates. Moreover, increasing the glass transition temperature can produce a corresponding shift in crystallization temperature towards higher values. Furthermore, at low heating rates, infinite temperature viscosity parameter has negligible effect on the crystallization dynamics while, at higher heating rates, smaller values of infinite temperature viscosity parameter increase the crystallization rate and final crystalline volume. Those results lead to further understanding of fundamental physical processes that affect crystallization dynamics physics of the phase change processes. The results are also very promising for the future development of phase change modelling.

# CHAPTER 5: Modelling calorimety measurements using the Master rate equation at high heating rates

In the preceding chapter, the effects of the viscosity parameters on the crystallization dynamics have been investigated. This was carried out by implementing the MYEGA model for the viscosity dependence on temperature in the Master rate equation system. It is worth recalling some key characteristics of the Master rate equation model before using it for extracting viscosity model parameters and DSC measurement analysis. It is considered a comprehensive model that describes transient nucleation and growth based on the mechanism by which monomers are attached and detached to and from clusters with temperature history. Therefore, it is a dynamic model that more physically realistic than the simplified JMAK model (which assumes nucleation is random, uniform and stationary). It is also much less computationally intensive compared to atomistic simulations. In this chapter, the analysis and extraction of viscosity model parameters will be carried out using a developed algorithm based on a given DSC measurement.

## 5.1 Introduction

The disparity in the estimated viscosity parameters (see chapter 4) may arise due to the differing types of samples (powder, flake, thin-film), preparation conditions, pre-annealing, heating and rates, and more fundamentally the nature of the crystallization and viscosity models imposed for fitting to experimental data. An example is the large difference in the value of fragility $m > 100$ derived for AIST from fitting the MYEGA model to growth velocity measurements [86], compared to the value of $m \sim 37$ derived for the same material using the generalised MYEGA model accounting for the fragile-to-strong transition

behaviour of the viscosity [30]. Furthermore, current methods of extraction of the viscosity parameters rely on simple models of crystallization, such as the JMAK model with constant nucleation rate and growth dominated crystallization which may not be appropriate for nucleation dominated materials such as GST. In this Chapter, the Master rate equation approach, which includes both transient nucleation and growth processes with viscosity described by the MYEGA model is used in order to study the crystallization dynamics of GST over a wide range of heating rates in particular to simulate full Kissinger plots. An iterative numerical algorithm is also developed based on the more physically realistic Master rate equation to estimate the values of the viscosity parameters for GST by comparison to published Kissinger plots from ultrafast DSC measurements. In these analyses, the effects of the dependence of glass transition temperature on heating rate on the extracted fragility values and the strong correlation between the glass transition temperature and fragility values were particularly highlighted and explored.

## 5.2 Methodology

Differential scanning calorimetry (DSC) is a valuable tool to investigate crystallization dynamics and extract important kinetic and thermodynamic parameters of phase-change materials[92]. The peak crystallization temperature $T_p$ is determined from the peaks in the measured DSC traces at different heating rates $\phi$, and used to produce Kissenger plots [92] in which $\ln(\phi/T_p^2)$ is plotted verses $1/T_p$ with the plot being typically a straight line (to describe an Arrhenuis behaviour) enabling the estimation of the activation energy for the reaction [26]. The crystallization dynamics over a broad range of heating rates (50 K/s up to 40,000 K/s) have been measured using ultrafast DSC measurements for GST (see Figure 5.2) [28][29], and for other phase-change materials (GeSb[29] and AIST[30]). A non-Arrhenius behaviour

was observed in the Kissinger plots for GST in these measurements which cannot be described with a single activation energy. Analysis of Kissinger plots is normally carried out using the JMAK theory assuming mainly growth dominated crystallization[93] [28].

Here, however, the Master equation approach that includes both nucleation and growth processes was used instead, and is capable of simulating complete Kissinger plots from consecutive crystallization simulations at increasing heating rates. Typical crystallization simulations using the Master rate equation are presented in Figure 5.1 (a) at increasing heating rates, while Figure 5.1 (b) illustrates the time derivatives of the crystallization curves ($d\chi/dt$) to simulate DSC traces [93], which enable the identification of the peak crystallization temperatures. Figure 5.1 shows progressive increase in the peak crystallization temperature $T_p$ and decrease of the slope of the crystallization curves at the transition temperatures with increasing heating rate, which is normally observed experimentally as shift in the peaks of the DSC traces and broadening of their distribution in differential calorimetry measurements. The calculated crystallization temperatures $T_p$ from the Master equation simulations at different heating rates in Figure 5.1 can thus be used to produce complete theoretical Kissinger plots and compare to experimental measurements.

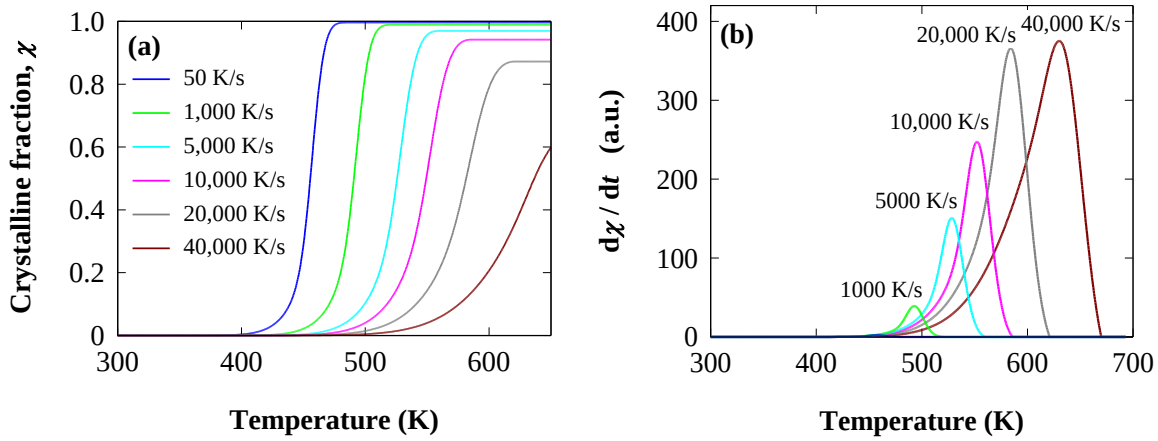


**Figure 5.1 : (a) Calculated crystalline volume fraction as a function of temperature during ramped annealing at different high heating rates. (b) Differentiated crystalline fraction curve (colour designation follows the legend of (a)). The simulations parameters include: $T_g$ = 383 K and $m$ = 23.**

Due to the relatively low computational cost of solving the Master rate equation system and the ability to simulate both nucleation and growth, an iterative numerical approach has been developed to compare simulated and experimental Kissinger plots from ultrafast DSC measurements.

## 5.3 Results

An iterative numerical algorithm based on the Master equation method is developed to compare simulated and measured Kissinger plots from experimental calorimetry studies published in the literature, so as to extract the viscosity model parameters and examine the role of the viscosity and crystallization models on the extracted values.

The iterative algorithm is developed to understand the crystallization process at high heating rates and enable the extraction of the important viscosity model parameters from a more detailed theoretical approach. Preliminary focus will be on implementing the iterative

algorithm to extract the fragility index parameter $m$ for the MYEGA viscosity model from ultrafast DSC experimental measurements reported for GST in [28]. In this case it is assumed that the glass transition temperature is constant (within the range of published values see Chapter 4) for all the simulated heating rates, in accordance with the procedure used in the literature to analyse Kissinger plots[28][29]. The iterative algorithm proceeds by carrying out a complete crystallization simulation using ramped annealing at one heating rate from the solution of the Master equation system, using a starting value of $m$ = 17 for the fragility. The simulated crystallization curve is then differentiated with time and the peak temperature $T_p$ (corresponding to maximum crystallization rate) is compared with the experimental value at the same heating rate (see Figure 5.2) [28][29] and the absolute percentage error between the two temperatures is calculated. Repeated simulations at this heating rate are then carried out to increment $m$ in each iteration until the absolute percentage error of the difference between the experimental and theoretical $T_p$ is less than 0.5%. This whole process is repeated at each heating rate to produce the theoretical Kissinger plot that closely fits the experimental curve as shown in Figure 5.2, and the extracted values of fragility that provide best agreement at each heating rate are recorded as shown in Table 5.1 as an example. Also shown in Figure 5.2 for comparison are simulated Kissinger plots using four constant values of fragility (where $m$ = 17 corresponds to the Arrhenius temperature dependence of viscosity).

**Table 5.1 Simulated Kissinger data and fitted fragility indices for $\sigma$ = 0.066 J/m$^2$ and $T_g$ = 383 K.**

| Heating rate (K/s) | Measured $T_p$ (K) (Ref. [28]) | Fitted $T_p$ (K) | Extracted fragility index $m$ |
|---|---|---|---|
| 50 | 456.3 | 456.8 | 21.99 |
| 100 | 462.3 | 463.0 | 23.18 |
| 500 | 481 | 481.7 | 24.78 |
| 1,000 | 491.5 | 492.5 | 25.04 |
| 5,000 | 527.1 | 528.1 | 24.63 |
| 10,000 | 550.5 | 551.8 | 23.92 |
| 20,000 | 582.7 | 584.0 | 22.95 |
| 40,000 | 629.5 | 631.1 | 21.42 |

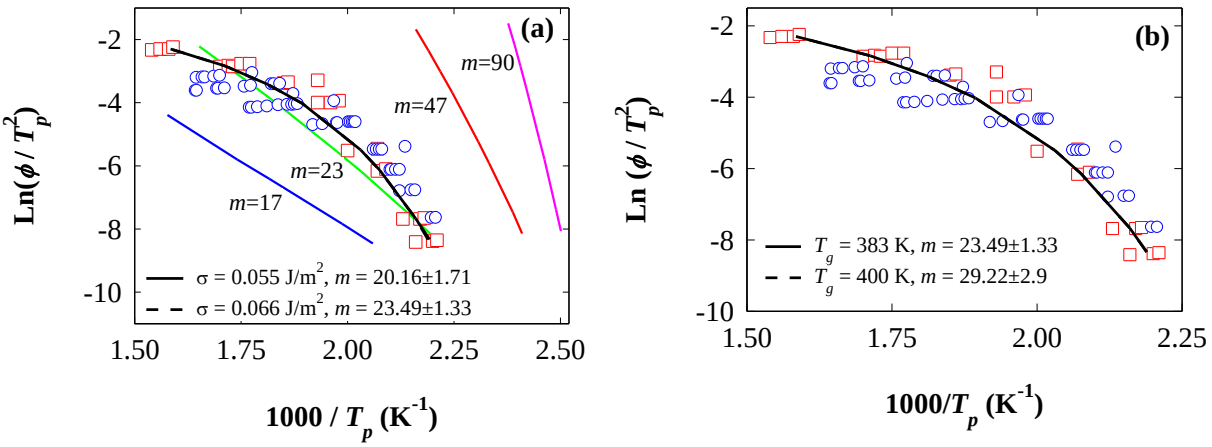


**Figure 5.2 Experimental Kissinger plots for GST using ultrafast DSC measurements from Orava *et al*. (red squares)** [28]**, and simulated plots using the iterative numerical algorithm based on the Master rate equation with the fragility index being the fitting parameter. All the fitting was carried out on the experimental data of Orava *et al*** [28]**. (Chen *et a l*** [29]**. data - blue circles - shown for consistency). (a) Fitting taking into account uncertainty in surface energy with $T_g$ = 383 K and showing simulated Kissinger plots using four constant fragility values for comparison, and (b) fitting for two glass transition temperature values with $\sigma$ = 0.066 J/m$^2$. Simulation parameters are listed in Table 3.2.**

To investigate the effects of the uncertainty in some of the modelling parameters, including the interfacial surface energy $\sigma$ and glass transition temperature $T_g$, on the extracted fragility values these parameters were varied within the range of published values ($\sigma$ = 0.033 - 0.066 J/m$^2$ [94], $T_g$ = (373 – 472K) [28] [73][74][75]) in the iterative algorithm to produce the theoretical Kissinger plots shown in Figure 5.2. It can be observed in Figure 5.2 (a) that increasing the interfacial energy $\sigma$ from 0.055 to 0.066 J/m$^2$ increases slightly the average extracted fragility values from $m \approx 20.16 \pm 1.7$ to $m \approx 23.49 \pm 1.3$ respectively. It can also be observed that increasing the glass transition temperature $T_g$ from 383K to 400K (within accepted values in the literature) also increases slightly the extracted fragility values from $m \approx 23.49 \pm 1.3$ to $m \approx 29.22 \pm 2.9$ respectively, as indicated in Figure 5.2 (b). In general, the effect of uncertainty in $\sigma$ and $T_g$ on the extracted fragility values is modest, and the average value of fragility extracted from the experimental measurements using the iterative algorithm is $m \sim 23$ (assuming constant $T_g$). Moreover, no clear trend was found in the variations of $m$ with increasing heating rate in the iterative algorithm as indicated in Table 5.1. This extracted value of fragility is lower than the value obtained from fitting using the JMAK model of $m \sim 90$ in [28].

## 5.4 Discussion

The ability of the Master equation method to model transient crystallization including nucleation and growth, and its low computational cost permitted the simulation of complete Kissinger plots in this chapter over a wide range of heating rates, and the development of an iterative algorithm for the extraction of the important viscosity parameters from published experimental measurements. The discussion will now focus on the extracted fragility index in this chapter using the Master rate equation in relation to previously published values, and the

important role of the glass transition temperature and its dependence on heating rate on the extracted fragility values.

Extracted values of the fragility index for GST in the literature varied considerably from 20 to 140 [78] [28] [73]. This variation in reported values may be attributed to several factors such as different sample and substrate structures (powder, thin-film, flakes), sample preparation conditions, measurement technique (DSC, mechanical stress, crystal growth velocity), pre-annealing conditions, doping, and heating and cooling rates. An equally important factor that affects the extracted values from measurements is the crystallization and viscosity models employed in the fitting and their parameters. The average fragility value of $m \sim 23$ derived in this work from fitting to the ultrafast DSC measurements is lower than other reported values for GST for example ($m \sim 90$ in [28]). This value was computed using a more physically realistic crystallization model which incorporates both transient nucleation and growth processes. The JMAK model, which assumes stationary nucleation and growth dominated crystallization, was used to extract the fragility values for GST in [28] which is commonly classified as nucleation dominated material [92]. Moreover, in using the JMAK model for fitting to the experimental Kissinger curves in the literature, both the number of pre-existing nuclei and temperature dependant growth rate were combined into a single fitting kinetic coefficient, and the influence of each of these factors acting independently on the fitting process or on the computed fitted parameters was not clarified. Furthermore, the more physically realistic MYEGA model for the viscosity dependence on temperature was implemented here in the Master equation simulations, which has been shown to produce different results from the Cohen and Gerst model [82] employed in [28] to fit to experimental Kissinger curves and extract the fragility.

In further exploring the potential causes for the difference between the extracted fragility values in this work and from literature, it is fundamentally important to emphasise that the

iterative algorithm used here produced complete transient crystallization simulations and extracted a separate fragility value at each heating rate. This is unlike DSC simulations employing the JMAK equation where a single fragility index was extracted over the whole range of heating rates (using a fixed value for $T_g$). This raises the important question of the validity of assuming a fixed viscosity and kinetic behaviour to describe crystallization in phase-change material at different heating rates. In particular it has been shown that the glass transition temperature, due to its kinetic nature, is sensitive to the heating rate and increases with increasing heating rate in amorphous GeTe alloys [95], chalcogenide glasses [96], and in the GST phase-change material [78] [91]. At relatively low heating rates the dependence of the glass transition temperature on heating rate in GST was described by the Moynihan relation $dln(\phi)/d(1/T_g) \approx -E/k_B$ [97], with a relaxation activation energy $E$ corresponding to the activation energy for shear viscous flow [78].

To elucidate the effect of the dependence of the glass transition temperature on heating rate in the Master equation simulations, $T_g$ was allowed to vary in the iterative fitting algorithm to the experimental Kissinger plots in Figure 5.2 while assuming a constant value for the fragility ($m$ = 47 for pure GST from mechanical stress measurements [78]). Figure 5.3 (a) illustrates the extracted values of $T_g$ from the iterative algorithm required to achieve the closest fit to the experimental data (within 0.5% difference error). This figure shows the clear trend of increasing $T_g$ from 416 K to 488 K with the increase in heating rate in the experiment (50 K/s to 40000 K/s), which is within the range of reported values for $T_g$ in the literature for GST. Moreover, the difference between the experimental peak crystallization temperature and fitted glass transition temperature, $T_p$–$T_g$ (reflecting the degree of mobility in the supercooled region) in Figure 5.3 (b) is approximately 40 K at low heating rates, in agreement with the DSC measurements for GST at low heating rates in [75]. Increasing the fragility in the iterative algorithm to $m$ = 90 increases the diffusivity and crystallization rate

therefore reducing the peak crystallization temperature in the simulations. This requires further increases in $T_g$ with increasing heating rate in the fitting algorithm to achieve the closest fit to the experimental Kissinger data in Figure 5.2, as indicated in Figure 5.3 (a). Furthermore, the sharp drop of the viscosity with temperature near $T_g$ for $m$ = 90 reduces the temperature difference $T_p$–$T_g$ as indicated in Figure 5.3 (b), which at low heating rates is ~ 22 K (again in agreement with [75]). The increase in fitted values for $T_g$ for $m$ = 90 at high heating rates go beyond any reported values for GST in the literature.

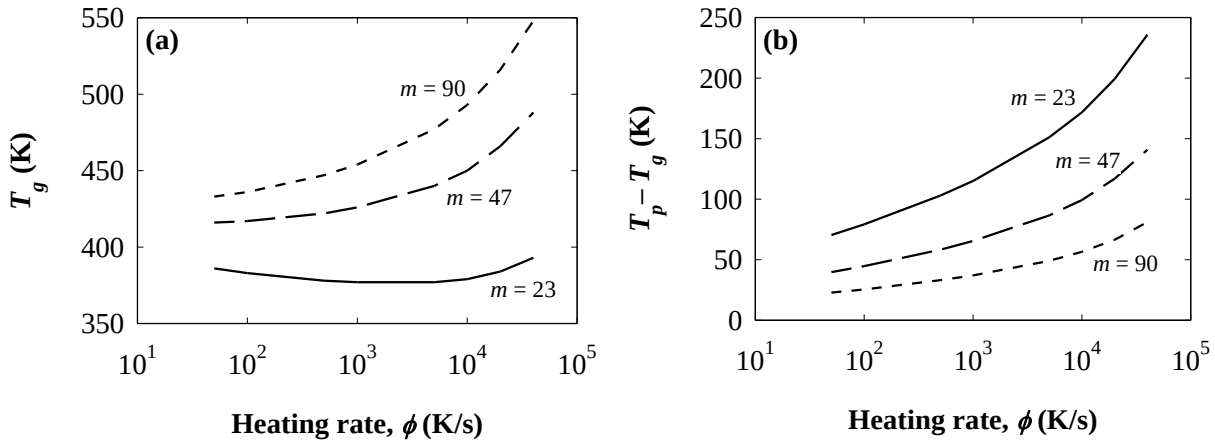


**Figure 5.3 (a) The glass transition temperature as a function of heating rate determined from fitting the Master rate equation to experimental Kissinger plots, assuming constant values for the fragility. (b) The computed difference between the experimental peak crystallization temperature and derived glass transition temperature from (a). The glass transition temperatures and temperature differences for low fragility at $m$ = 23 is shown for comparison. (Note measured values of the glass transition temperature, $T_g$ , are within the range of 373K - 472K** [28] [73][74][75]**).**

In the above simulations and fittings, the representative value of $m$ = 47 for the fragility index (from[78]) produced values of $T_g$ that are in general agreement with reported values in the literature for GST. This agreement may suggest that this lower value of fragility is more reasonable than larger values found in the literature based on a constant $T_g$. However, this

fragility value ($m$ = 47) remains to be an assumption which can still be further refined to produce a modified range of values of $T_g$ with increasing heating rate, particularly in the absence of experimental measurements or theory that confirm the dependence of $T_g$ on heating rate for GST. Thus the Master rate equation simulations and fittings highlight the important observations that:

a) the fragility index and glass transition parameters in the viscosity and crystallization simulations are coupled, and evaluation or extraction of one from experimental measurements requires that the other is available from experiment or theory, and thus

b) the accurate estimation of the fragility index from DSC measurements and Kissinger plots require information on the dependence of the glass transition temperature on heating rate.

The Master rate equation simulations and analysis of previously published ultrafast DSC measurements carried out in this work highlighted the fundamental need to measure and understand the heating rate dependence of the glass transition temperature for the correct analysis of DSC measurements and estimation of the viscosity parameters necessary for modelling and characterising the crystallization dynamics in phase-change materials. This dependence will also have impact on the estimation of crystal growth rates from DSC measurements for phase-change materials (since the growth velocity for interface controlled growth depends on viscosity) [98]. Alternatively, and if the fragility index is known for the phase-change material, then the iterative algorithm developed in this work can potentially be used to estimate the glass transition temperature and its dependence on heating rate from DSC measurements.

## 5.5 Chapter summary

The crystallization dynamics in $Ge_2Sb_2Te_5$ were modelled using the Master equation approach which includes both nucleation and growth processes, under ramped annealing over wide range of heating rates, spanned between 50 K/s to 40,000 K/s. The temperature dependence of viscosity was implemented in this numerical approach using the physically founded MYEGA model. The relatively low computational cost of solving the Master rate equation for a practical system enabled the use of more rigorous crystallization model for the analysis of experimental measurements of crystallization kinetics in phase-change materials. An iterative numerical method based on the Master rate equation was therefore developed and used to fit to experimental Kissinger plots taken from ultrafast calorimetry measurements for GST, and extract the MYEGA viscosity model parameters. The outcomes of the simulations and fittings highlighted the coupling between the fragility index and glass transition temperature parameters in the viscosity and crystallization models. Moreover, the results showed the need for the experimental or theoretical determination of the dependence of glass transition temperature on heating rate for accurate estimation of the viscosity parameters from experimental measurements. This enables the accurate modelling and characterisation of phase-change materials, and provides deeper understanding of the crystallization dynamics necessary for development of high data rate phase-change memories and devices.

# CHAPTER 6: Initial cluster size distribution and crystallization dynamics in phase-change materials

In the preceding chapter, it was demonstrated that the Master rate equation can be used to describe the crystallization behaviour at high heating rates in phase-change materials, showing non-uniform nucleation and growth of clusters of different sizes. This indicates that the distribution of cluster sizes in the amorphous starting phase prior to annealing at temperature higher than glass transition temperature, $T_g$, may influence the dynamics of crystallization during annealing particularly for nucleation dominated materials such as GST. In this chapter, the influence of the preparation condition of amorphous GST material on the crystallization dynamics is theoretically investigated by implementing initial distributions of cluster sizes resulting from different thermal treatments such as melt-quenching and pre-annealing, and theoretical Gaussian initial cluster size distributions.

## 6.1 Introduction

The phase transformation in phase-change materials from the initial amorphous phase often starts with the formation of nuclei, which then grow and consequently crystallizes the material. Controlling and reducing the crystallization time during the writing and erasing stages is critically important for the development of high-speed, low-power phase-change memories. Moreover, repeated writing, erasing and per-annealing (priming) causes microstructural changes to the starting amorphous phase leading to deviations in the optical and electrical properties of the material compared to the as-deposited case, which has an impact on the intended device operation and specified operating parameters.

Experimental studies using static laser testers on thin GST films (25 - 70nm thick) indicated reduction of the crystallization times from hundreds of nanoseconds in the as-deposited state, to tens of nanoseconds in the melt-quenched or pre-annealed state (at temperature below the crystallization temperature) [34] [99]. These effects were attributed to formation of nano-crystal nuclei which greatly reduce the time of formation of the critical crystal nuclei and therefore increase the nucleation rate and reduce crystallization time. Thus pre-pulse annealing (using electrical pulses) was exploited to reduce the switching times between the amorphous and crystalline phases in GST films in phase-change random access memories (PCRAM) [10]. More recently and to elucidate the nature and sizes of these nano-clusters, statistics-based detection using fluctuation transmission electron microscopy (FTEM) and high-resolution TEM (HRTEM) experimental studies have revealed that thermal treatment of GST films using temperatures lower than the crystallization temperature can increase the number and size of clusters in the amorphous phase [25][100][35]. The size of these clusters were in the range 2 - 8 nm. Theoretical work using the Master rate equation also highlighted the importance of understanding the effect of initial cluster size distribution on the crystallization behaviour in phase change material [58].

There is still however a lack of a thorough understanding of the cluster size distributions resulting from the various thermal treatments that phase-change material undergo during operation, and the influences of these resulting initial cluster size distributions on the crystallization dynamics during annealing at low and high heating rates. Hence in this chapter, the effects of a variety of initial cluster size distributions on the crystallization dynamics of an initially amorphous GST phase-change material is studied theoretically at different heating rates using the Master rate equation. The simulated initial states include the as-deposited, melt-quenched, and pre-annealed states. Moreover, theoretical and non-

uniform initial cluster size distribution accommodating different initial cluster sizes will be used to complete the investigation, and in particular to study the impact of an initial amorphous phase with concentration of large clusters on subsequent crystallization.

The Master rate equation method described in Chapters 2 and 3 of this thesis models both nucleation and growth by the attachment and detachment of monomers [43], yielding transient cluster size distributions in subcritical and supercritical regimes under isothermal and non-isothermal annealing conditions [56][32]. Moreover, various initial cluster size distributions can be specified to describe the initial state of material, hence the Master rate equation model is ideally suited for investigating the effect of initial cluster size distribution on crystallization dynamics.

## 6.2 Master rate equation simulations

The system of coupled equations in Eq. (3.9) was solved numerically as described in Chapter 3 with different initial conditions. In order to simulate the crystallization volume fraction in a physically realistic way, the MYEGA viscosity model was implemented which is explained in Chapter 4. The initial starting state of the material in each simulation will be either in the as-deposited, melt-quenched, or pre-annealed state. The as-deposited state refers to the initially amorphous phase with no pre-existing nuclei. This is easily modelled in the Master rate equation as an initial and uniform cluster size density of $Z(n,0) = 10^{-11}$ clusters/m$^3$, and will be used throughout this Chapter to describe the as-deposited state. The implementation of the melt-quenched and the pre-annealed initial states will be described in detail in the simulations section.

Following the implementation of the initial cluster size distribution in the Master rate equation, numerical simulations of crystallization were performed by application of ramped and uniform temperatures at two different heating rates of 50 K/s and 40,000 K/s according to Eq. (3.32). These heating rates are commensurate with published ultrafast calorimetry experiments in [28][29] and enable the investigation of crystallization dynamics at different annealing conditions. The maximum number of equations (upper limit of cluster sizes) was considered assuming a circular geometry for clusters in the size range 2 - 8 nm [25][100][35] corresponding to approximately 10 - 40 monomers. However to account for volumetric distributions and larger clusters, a maximum size of 200 monomers is used in the simulations that follow. The material parameters used in this chapter are listed in Table 3.2.

In sub-section 6.2.1 below, the melt-quenched state is simulated, and the computed initial cluster size is then used in crystallization simulations. In sub-section 6.2.2, practical initial cluster size distributions are simulated by pre-annealing the amorphous state to temperatures below the crystallization temperature, and the resulting initial cluster size distributions are then used to study crystallization dynamics under ramped annealing conditions. Moreover, and to complete this systematic investigation, hypothetical Gaussian initial cluster size distributions with different cluster size means, widths and densities are implemented in the simulations. This is then followed by simulations of crystallization from these initial states to study their effects on the crystallization dynamics by comparison to simulations from the as-deposited initial state.

### 6.2.1 Melt-quenched simulations

Melt-quenching occurs repeatedly during the writing and erasure processes in phase-change memories to arrive at the amorphous starting phase for subsequent annealing operations. Thus it is of interest to study the resulting cluster size distributions following this operation and how they affect the crystallization speed when the material is subsequently annealed. Obtaining a melt-quenched amorphous state requires that the applied temperature in the GST material exceeds the melting point of 889 K. This is then followed by cooling at high rates, to quench the melted region into the amorphous state. Typical cooling rates required for re-amorphisation of GST are of the order of tens of degrees per nanosecond [17].

Melt-quenching is modelled and simulated here at three different cooling rates, to determine the appropriate cooling rate at which the crystalline volume fraction is minimum. Starting with the fully crystalline material, a constant temperature of 976 K that exceeds the melting point for GST was initially applied in the simulations for a very short period of time (1 ns chosen here), followed by linear cooling down to room temperature over the three time durations of 1 ns, 10 ns, and 100 ns (corresponding to the cooling rates 676 K/ns, 67.6 K/ns, and 6.76 K/ns respectively) as shown in Figure 6.1(a). Figure 6.1(b) shows the corresponding calculated crystalline fractions, with the minimum fraction obtained at steady state when the cooling time is 1 ns.

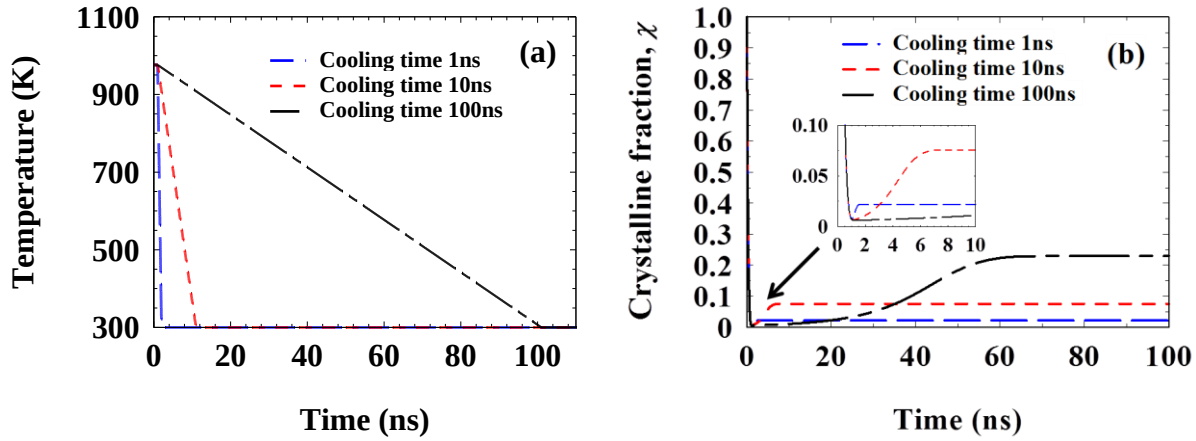


**Figure 6.1(a) Temperature profile in the melt-quench simulations with three different cooling times to room temperature. (b) Transient crystallization curves following the application of the temperature profiles in (a). The steady-state crystalline fraction (blue line) at the cooling time of 1 ns is 0.0219.**

Figure 6.2 (a) shows the unique steady-state cluster size distributions produced from the simulations for the three cooling times, illustrating the very narrow distribution of smaller clusters at the lowest cooling time of 1 ns, consistent with the lowest crystalline volume fraction. For the longest cooling time of 100 ns, there is a wider distribution of cluster sizes including small and larger cluster. Figure 6.2 (b-d) are graphic illustrations of a random distribution of the steady-state cluster sizes in the simulation space corresponding to the curves in (a) for the three different cooling times. Figure 6.2 (b) shows the formation of only small clusters of few monomers due to the short cooling time, while longer cooling times permit the growth of larger clusters in Figure 6.2 (c) and (d) leading to the increased crystalline volume fraction shown in Figure 6.1 (b) [35].

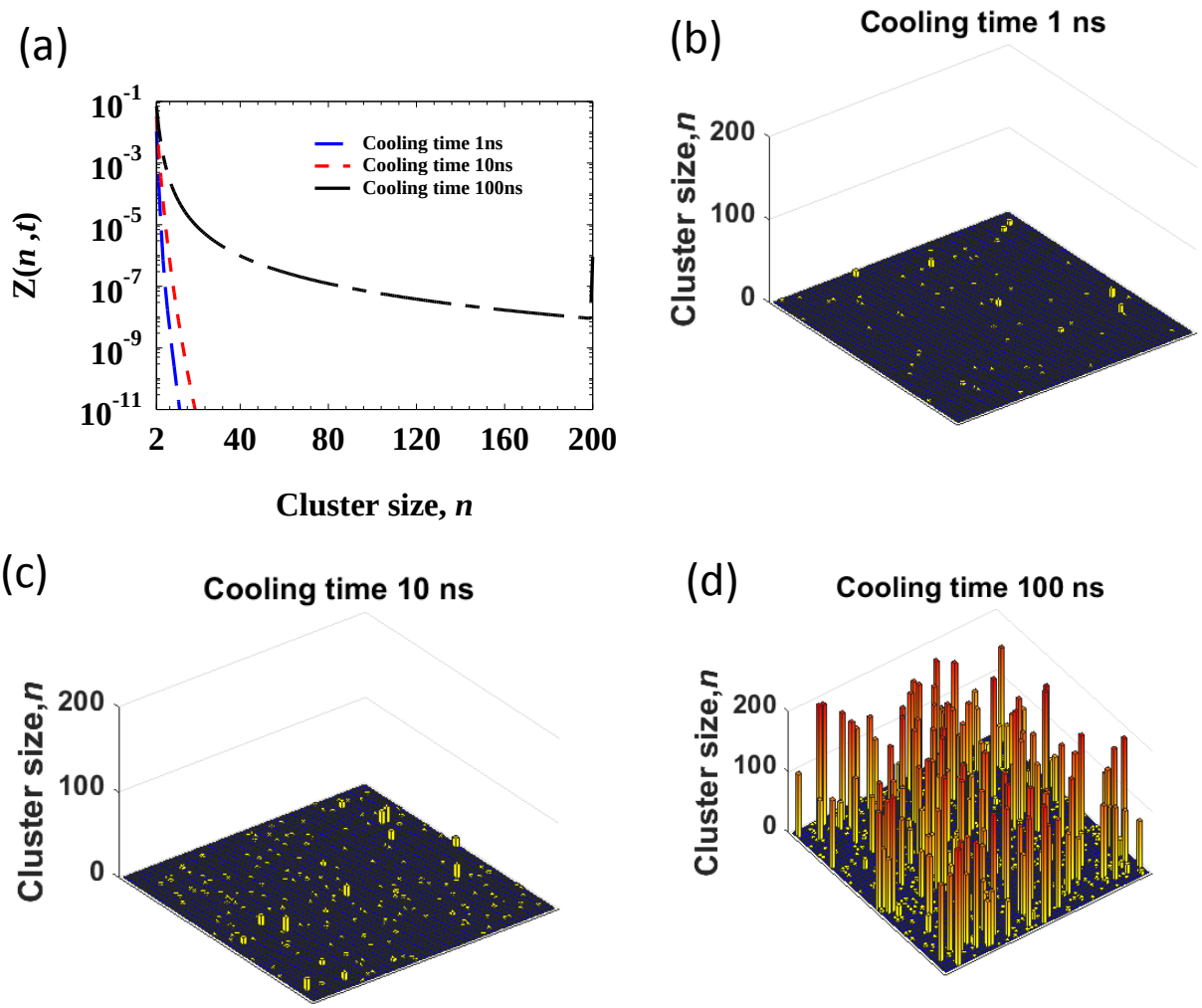


**Figure 6.2 (a) Steady-state cluster size distribution following the melt-quench simulations for three different cooling times. (b) - (d) Three-dimensional plots depicting the steady-state cluster sizes in the simulation spaces for the three cooling times of 1 ns, 10 ns, and 100 ns respectively. Note: The three-dimensional plots have been converted from the vector one-dimensional plots in (a) to a two-dimensional, arbitrary space of cluster size height matrix for better visualisation.**

The three quantifiable cluster size distributions resulting from the melt-quenching simulations are now used as initial states in crystallization dynamics simulations at different heating rates.

Figure 6.3 illustrates the effect of the initial amorphous states on the crystalline volume fraction, compared to the as-deposited state. At longer cooling times following melting, the existence of large clusters increases the initial crystalline volume fraction and reduces the

crystallization temperature (defined as the temperature where the crystallization rate is maximum). With reduced cooling time from the melt, the crystallization temperature increases towards the as-deposited value due to the narrow distribution of smaller clusters in the initial amorphous state. These observations were found to be applicable at the 50 K/s heating rate (Figure 6.3(a) and (b)) and at the 40,000 K/s heating rate (Figure 6.3(c) and (d)) as well.

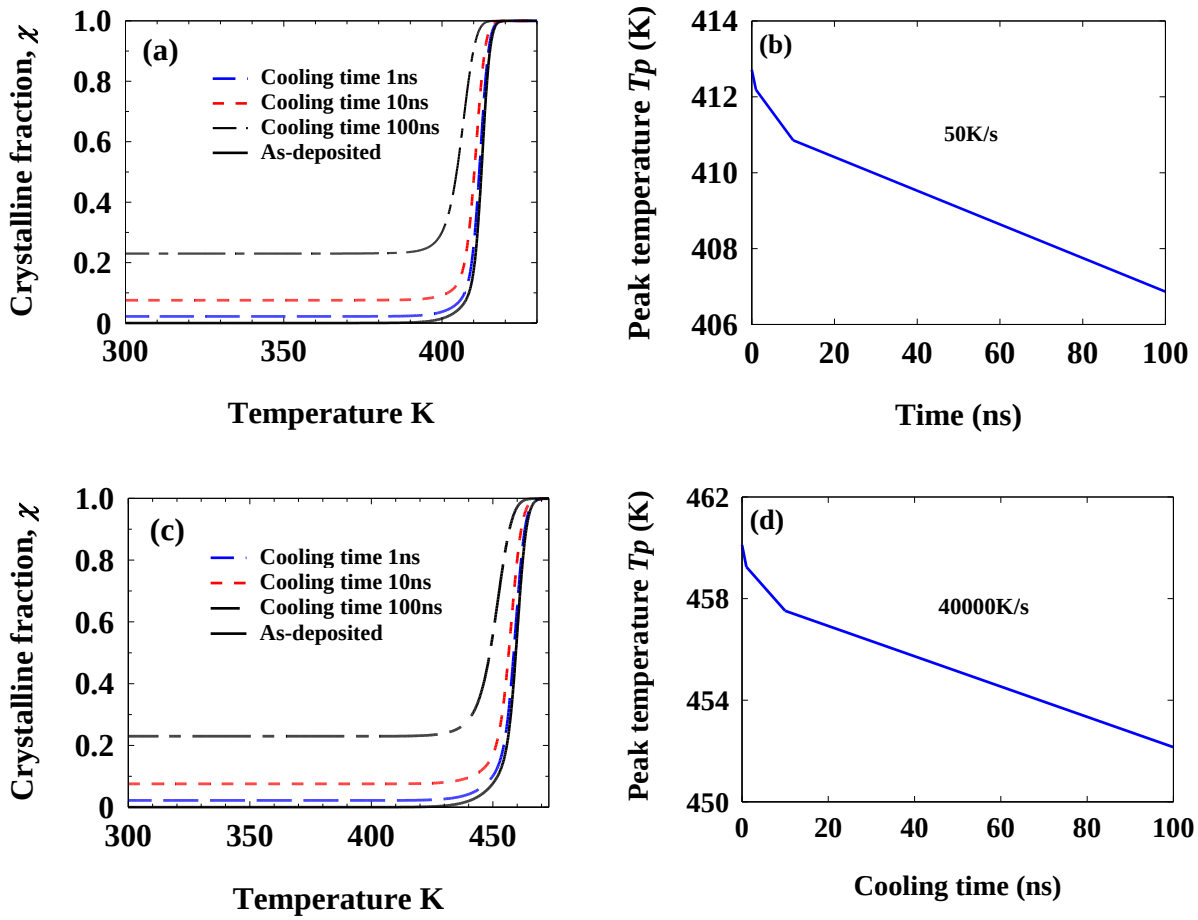


**Figure 6.3 Calculated crystalline volume fraction as a function of temperature during ramped anneals at two different heating rates with three different melt-quenched initial state (a) 50K/s. (c) 40000K/s. (b) and (d) Peak temperature, $T_p$ as a function of cooling time, determined from the 1st derivatives of the crystalline fraction curves in (a) and (c), indicating that reducing cooling time can lead to decrease peak temperature (crystallization temperature).**

### 6.2.2 Pre-annealing treatment

In this section, practical pre-annealing treatments at temperatures well below the crystallization temperature for GST are considered to investigate the effects of the different resulting initial amorphous states on crystallization dynamics. Moreover, hypothetical initial distributions are also investigated that are not necessarily produced by the thermal treatments above, with different size means spanning the entire range of cluster sizes and used in crystallization simulations at different heating rates.

#### 6.2.2.1 Practical pre-annealing treatment

In this section, the as-deposited amorphous material is heated using ramped annealing to temperatures well below the crystallization temperature, to investigate the resulting steady-state cluster size distributions, and to use this practical distribution as an initial state for the simulation of crystallization dynamics under ramped annealing conditions. The pre-annealing simulation is carried out by applying ramped annealing over the temperatures range 300K to 353K which is lower than the crystallization temperature reported (~ 403 - 423 K) for $Ge_2Sb_2Te_5$ thin films [25][101], with a relatively low heating rate of 0.033 K/s (to ensure that nucleation will take place in the simulation). Figure 6.4 plots the calculated steady-state pre-annealed cluster size distribution (blue line), and compares it to the as-deposited distribution (red line). This figure shows that pre-annealing at this heating rate produces a large density of smaller cluster sizes up to 20 monomers, a low concentration of larger clusters with almost uniform distribution, and a very narrow distribution of clusters of 200 monomers in size, embedded in the parent amorphous phase. The size of smaller clusters up to 20 monomers is consistent with the nano-cluster sizes of 5 - 8 nm observed experimentally for GST using high-resolution TEM under the same pre-annealing condition [25][100][35].

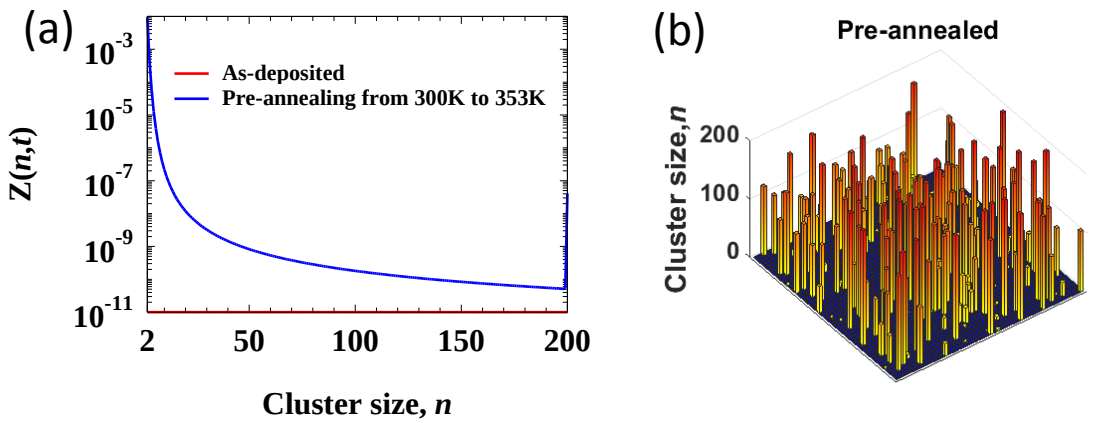


**Figure 6.4 (a) As-deposited and pre-annealed cluster size distribution following ramped annealing to temperature 353 K (well below the crystallization temperature for GST).**

The pre-annealed cluster size distribution in Figure 6.4 was used as the initial state for transient crystallization simulations using the Master rate equation with ramped annealing at the heating rates 50 K/s and 40,000 K/s. Figure 6.4 (b) is graphic illustrations of a random distribution of the cluster sizes in the simulation space corresponding to the curves in Figure 6.4 (a) (blue line). The simulations yielded the crystalline volume fractions shown in Figure 6.5. As indicated in this figure, the effect of the pre-annealed initial cluster size distribution is to increase slightly the initial crystalline volume fraction, and slightly reduce the crystallization temperature and crystallization time compared to the as-deposited state. This is due to the existence of nucleation centres from pre-annealing that enhances nucleation. The change in crystallization temperature is better illustrated using the time derivative of the crystalline volume fractions shown in Figure 6.5(b) and (d).

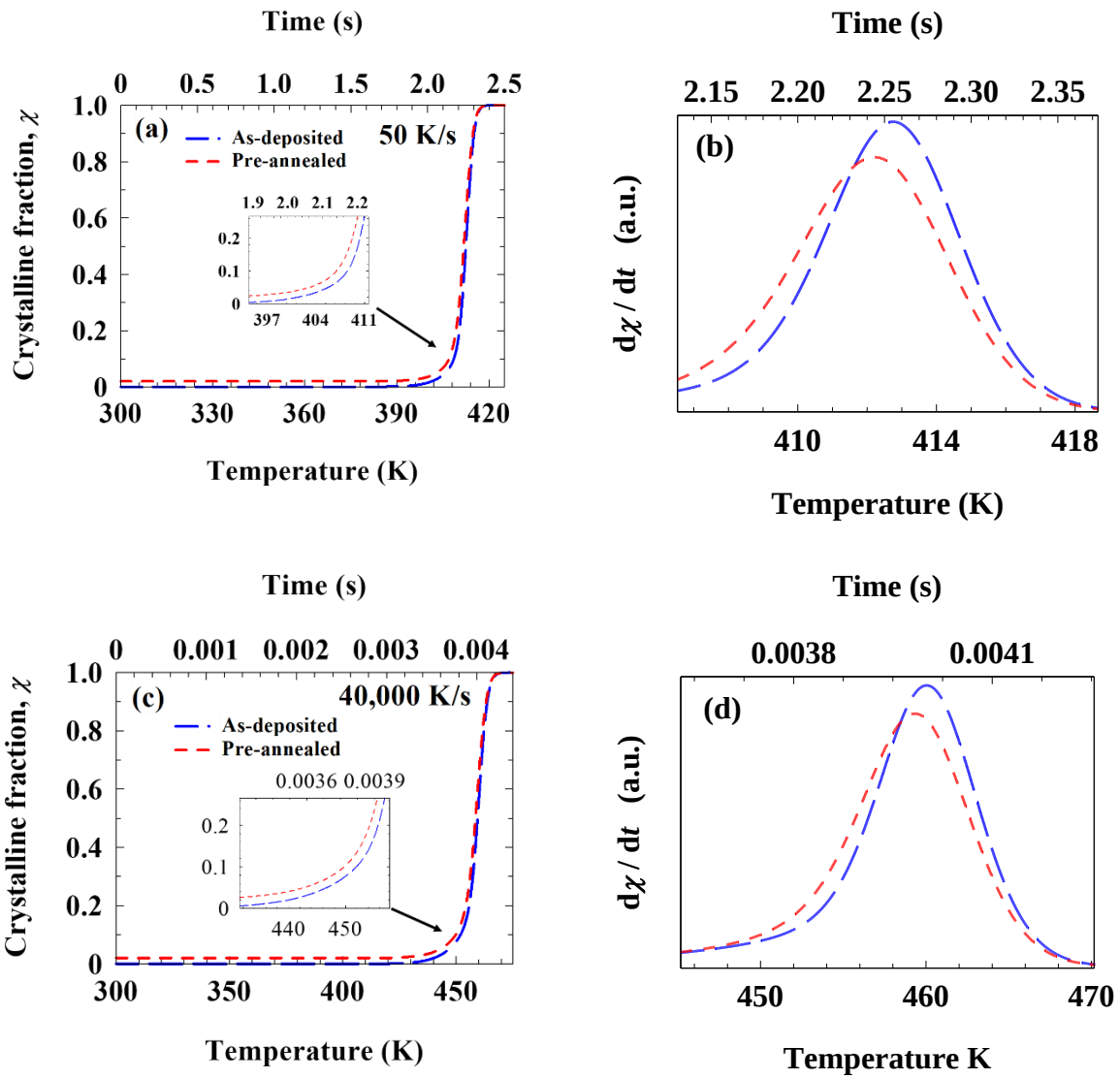


**Figure 6.5 Calculated crystalline volume fraction as a function of temperature during ramped anneals at two different heating rates with pre-annealed initial state (a) 50K/s heating rate. (b) 40000K/s heating rate. (c) and (d) are the 1st derivatives of the crystalline fraction curves in (a) and (b), with their peaks determining the crystallization temperature.**

The transient cluster density changes corresponding to the crystallization curves in Figure 6.5 are illustrated in Figure 6.6 for a selection of cluster sizes. Figure 6.6 shows the non-uniform transient nucleation for the different cluster sizes at the heating rates of 50 K/s and 40,000 K/s. Smaller clusters (e.g $n$ = 3) of the as-deposited state require longer time to be formed, which consequently delays the formation and growth of larger clusters as illustrated by the dashed lines in Figure 6.6. The existence of a distribution of smaller cluster from pre-

annealing (e.g $n$ = 3), on the other hand, speeds up the formation of larger clusters through the attachment of monomers and therefore reduces the crystallization time (compared to the as-deposited state) as shown by the solid lines in Figure 6.6.

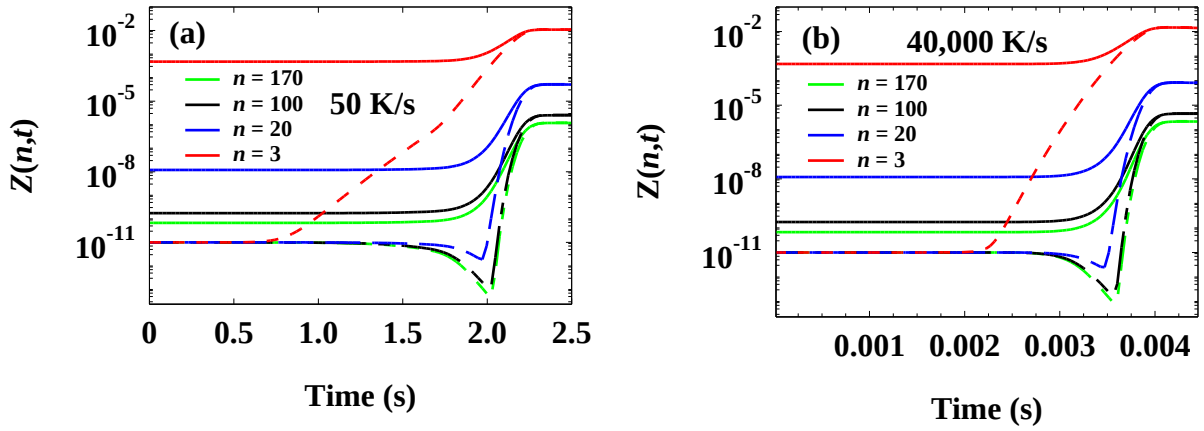


**Figure 6.6 The calculated transient cluster densities for different initial cluster sizes as-deposited (Dashed lines), and pre-annealed (solid lines) at heating rates of (a) 50 K/s and (b) 40 000 K/s.**

To systematically study the effects of non-uniform initial cluster size distribution on the crystallization dynamics in phase-change materials, theoretical Gaussian cluster size distributions with different monomer means, widths and density will be implemented as initial states in the Master rate equation during ramped annealing transient simulations next.

### 6.2.2.2 Theoretical cluster size distributions

The Gaussian distribution function is implemented here to describe the pre-existing cluster size distribution $Z(n,0)$, which is written as:

$$Z(n,0) = A_0 \exp(-(n-\mu)^2 / v^2) \qquad \textbf{(6.1)}$$

where $n \geq 2$, $A_0$ is a factor for setting the required volume fraction of crystallized material, $n$ is cluster size, $\mu$ is the cluster distribution mean with standard deviation $\nu$. The monomer mean and standard deviation were chosen to provide various initial cluster size distributions, and $A_0$ was used to set the required initial crystalline volume fraction $\chi_0$ from substituting Eq. (6.1) into Eq. (3.29) and solving to yield:

$$A_0 = \chi_0 Z_0 \Big/ \sum_{n=2}^{n_{\max}} n \exp\left(-(n-\mu)^2 / \nu^2\right)$$

A very low initial crystalline volume fraction of $\chi_0$ = 0.05 was used consistently throughout the forthcoming simulations, and ramped annealing with constant heating rates of 50 K/s and 40,000 K/s will be applied in the Master rate equation calculations. Figure 6.7 shows the assumed initial Gaussian cluster size distributions in this work, with narrow and wide distributions of small, medium-sized and large clusters (preserving the initial volume fraction at 5%).

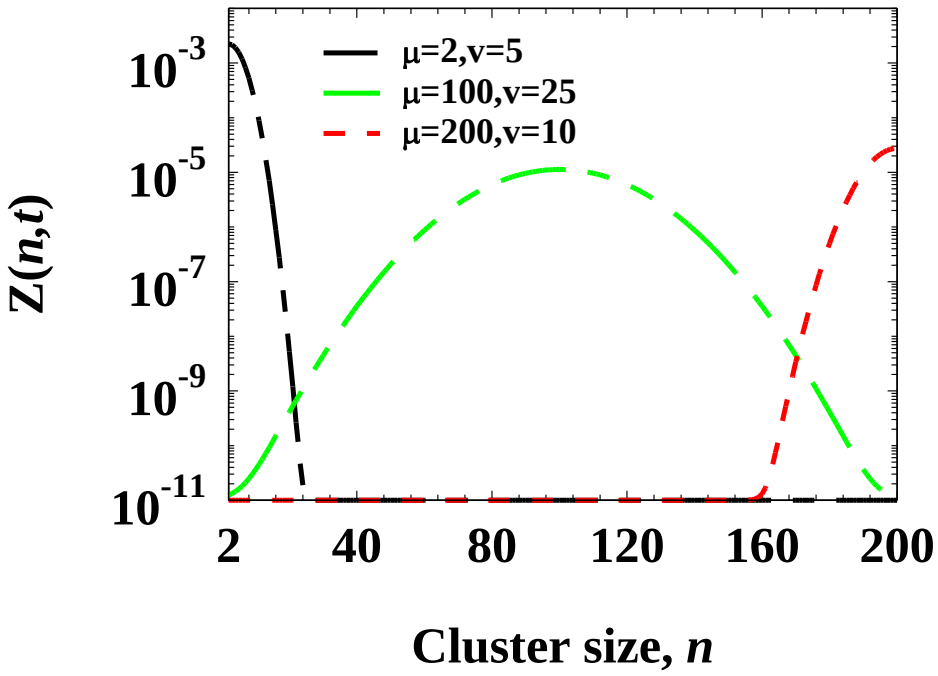


**Figure 6.7 Gaussian distribution with different means and variances as labelled, providing different initial cluster size distributions with partial crystallization of 5%. The states used in the simulations as initial conditions for the numerical solution of the Master rate equation.**

Figure 6.8 shows the simulated crystalline volume fractions for the different initial amorphous states using the parameters listed in Table 3.1 for GST, compared to the as-deposited amorphous state. This figure shows the general effects of initial cluster size distributions on increasing the initial crystalline fraction, reducing the onset time for crystallization and crystallization time, and reducing the peak temperature compared to the as-deposited state. These effects are more notable for the narrow distribution of small cluster sizes (black line when $\mu = 2$ and $\nu = 5$), while the wider distribution of larger cluster sizes (green line with $\mu = 100$) having a modest effect on the crystallization dynamics. When there is a narrow distribution of larger clusters only (red line with $\mu = 200$), the crystallization curve approaches that for the as-deposited initial state. This is true for both low (50 K/s) and high (40,000 K/s) heating rates. Figure 6.8(c) shows the extracted peak temperatures (from

the time derivative of the crystallization curves - not shown here) for each of the simulations in Figure 6.8(a) and Figure 6.8(b), demonstrating the decrease in peak temperature with smaller mean cluster sizes.

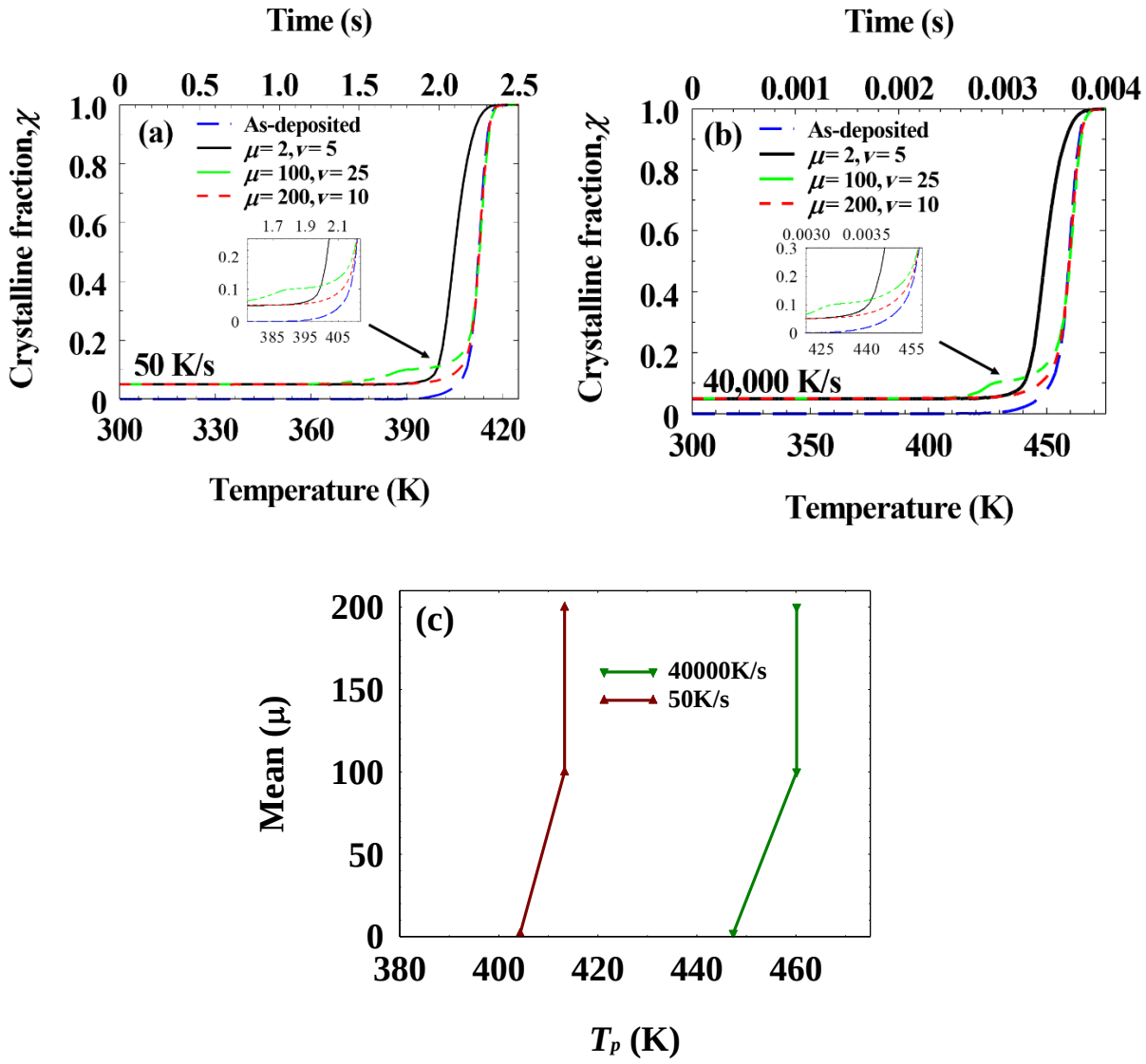


**Figure 6.8 Calculated crystalline volume as a function of temperature during ramped anneals at two different heating rates with different Gaussian distribution as an initial state. (a) 50K/s. (b) 40000K/s. (c) Extracted peak temperatures from (a) and (b).**

The simulated transient cluster size distributions corresponding to the crystallization curves in Figure 6.8 are presented in Figure 6.9 for a selection of cluster sizes. For initial Gaussian distributions where small clusters are either absent (Figure 6.9(a) and (b) where $\mu$ = 200) or relatively low (Figure 6.9(c) and (d) with $\mu$ = 100), the small clusters require longer time to nucleate and grow, and the larger clusters tend to dissociate and contribute to enhancing the growth of the smaller clusters. Both of these effects cause modest decreases in crystallization time and temperature, leading to crystallization curves approaching those produces with the as-deposited initial state. On the other hand, for initial Gaussian distribution where the concentration of small clusters is high (Figure 6.9(e) and (f) where $\mu$ = 2), the abundance of smaller clusters enhances the formation and growth of larger clusters leading to the marked decrease in crystallization time and temperature. The same crystallization trends are observed for the simulations at both heating rates of 50 K/s (Figure 6.9(a), (c), and (e)) and 40,000 K/s (Figure 6.9(b), (d), and (f)).

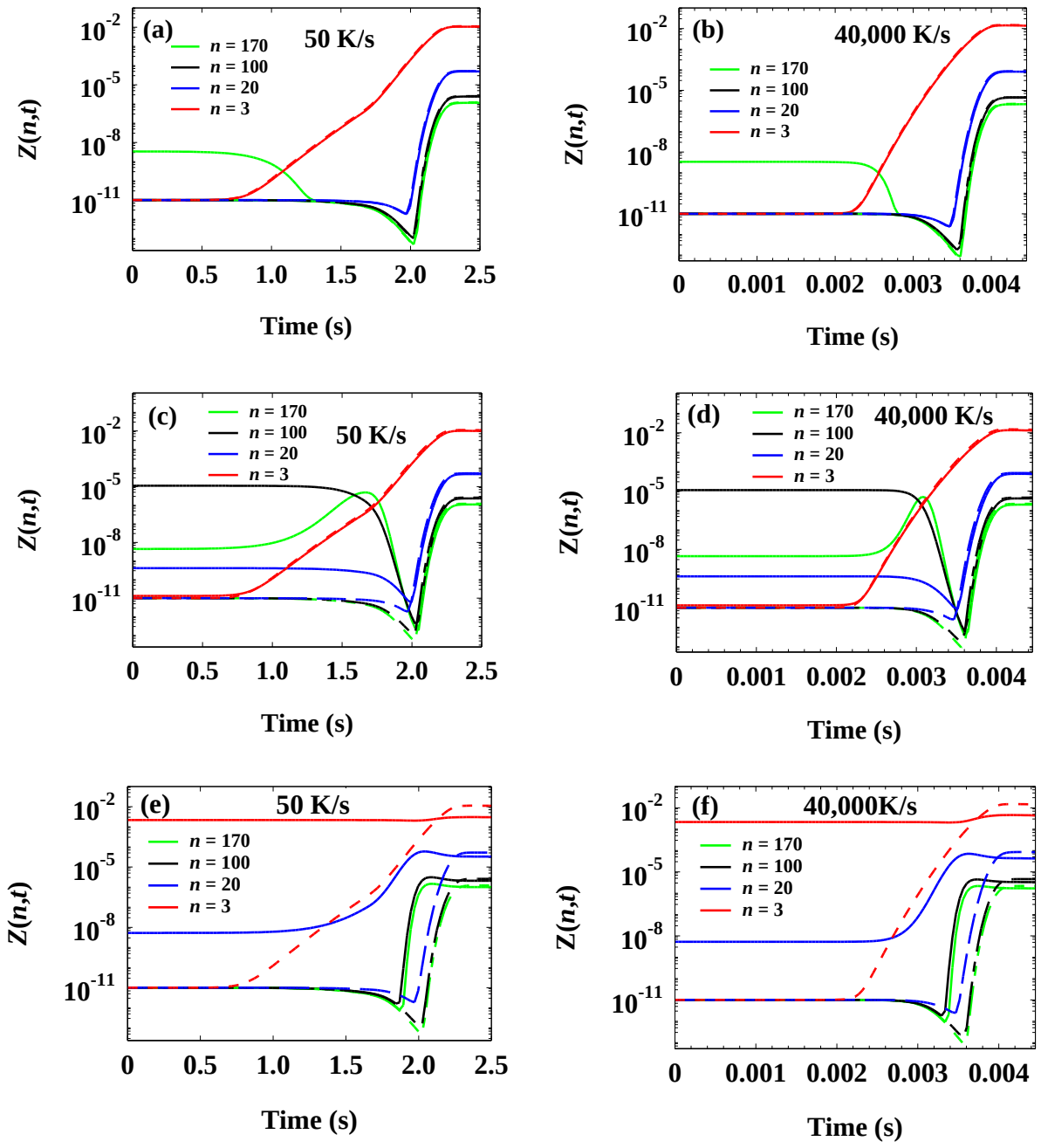


**Figure 6.9** The calculated transient cluster densities for different initial cluster sizes, as-deposited (Dashed lines), Gaussian cluster size distributions (solid lines) for (a) and (b) ($\mu$=200, $\nu$=10), (c) and (d) ($\mu$=100, $\nu$=25), and (e) and (f) ($\mu$=2, $\nu$=5) at heating rates of 50 K/s and 40,000 K/s as labelled.

## 6.3 Chapter summary

This chapter was concerned with understanding the effects of the initial state of the amorphous phase on the crystallization dynamics in the GST phase-change material. The Master rate equation was used to simulate the cluster size distributions from thermal treatments such as melt-quenching and pre-annealing to temperatures below the crystallization temperature for GST. The simulations revealed steady-state cluster size distributions exhibiting a large number of smaller clusters (~ 20 monomers) and low density of larger clusters with almost uniform distribution, in agreement with high-resolution TEM measurements of crystalline nano-clusters in GST. Application of these as initial states for crystallization simulations in the Master rate equation lead to relative reductions in crystallization time and crystallization temperature due to the existence of these nano-clusters promoting and speeding up the formation of larger clusters. This approach was systematically generalised and extended by using a theoretical Gaussian distribution of the initial cluster size in the Master rate equation with different cluster size mean, standard deviation and initial volume fraction. The simulations explicitly shown the marked decrease in crystallization speed and temperature (and therefore increase in crystallization speed) when there is predominately a narrow distribution of smaller crystalline clusters embedded in the initial amorphous phase.

# CHAPTER 7: Summary and Outlook

## 7.1 Research summary and outcomes

Over the last two decades, phase-change materials showed high potential for the development of computer memories, including non-volatile electronic phase-change random access memories and optical memories (the CD, DVD and Blu-Ray disk). Phase-change technologies are based on the fast and reversible switching between the amorphous phase and the crystalline phase upon heating of chalcogenide materials (such as GeSbTe) through the absorption of optical energy or through resistive Joule heating using electrical pulses. These phases can be distinguished by the contrast in their electrical and optical properties, which explains their capability of not only binary data storage, but also multi-level storage with appropriate control of the duration and magnitude of the exciting heat source. Crystallization occurs due to heating from the amorphous phase to the characteristic crystallization temperature, and involves nucleation of small polycrystalline nano-clusters followed by their growth. Amorphisation on the other hand occurs when the initially crystallized material is heated to a temperature that exceeds the melting point for the chalcogenide material, followed by quick cooling and quenching of the melt at cooling rates of tens of Kelvins per nanosecond into the amorphous phase.

The crystallization process is complicated by the nature of the phase-change material (whether nucleation or growth dominated) and its thermodynamic parameters, strongly affected by neighbouring interfaces and presence of defects which act as nucleation centres, sensitive to material thickness and thicknesses and thermal properties of adjacent layers, and a function of the thermal history and gradients during operation. Due to the sensitivity to

these factors, crystallization is often the timing limiting process in phase-change technologies. Hence extensive research efforts, both theoretical and experimental, have been carried out over the last few decades to better understand the crystallization process and reduce crystallization time, to increase the operating speeds and data rates of phase-change devices and memories and to ensure consistent and stable operation of these devices.

Viscosity is one of the important parameters that describes the atomic mobility of phase-change materials over the relevant temperatures during crystallization and therefore controls the crystallization rate. The strong correlation between the viscosity and crystal growth is also established in the classical nucleation and growth theory. Therefore, knowledge of the temperature dependence of viscosity for phase-change materials is important for understanding the crystallization dynamics and prediction of material performance. However, the temperature dependence of viscosity for the technologically important phase-change materials (such as GST) over wide temperatures from room temperature to the melting point is not available from experimental measurements (and limited to few chalcogenide alloys). Attempts have been carried out to extract the viscosity from calorimetry and crystal growth measurements, particularly recently at ultra-fast heating rates approaching the thermal gradients expected during practical device operations. However, these attempts are hampered by the use of over simplified, less physically realistic analytical models of crystallization and viscosity to fit to experimental measurements, and by the disparity in the reported thermodynamic and kinetic parameters of phase-change materials in the literature used in these models. These drawbacks lead to the disparity in the reported viscosity parameters and fully understanding the crystallization dynamics of phase-change materials particularly at the very high heating rates expected in practical devices.

Another important factor affecting the crystallization dynamics in phase-change materials, which is the focus of this research, is the state of the initial amorphous phase following the thermal treatments expected in priming the phase-change active material in devices, and following repeated operations. It has been shown experimentally that melt-quenched amorphous phase-change material exhibits shorter crystallization times compared to the as-deposited state, as a result of the formation of nucleation centres when cooling from the melt even though the crystallized volume fraction is very low consistent with that of the as-deposited state. This was elucidated more recently using high resolution TEM, showing the formation of nano-clusters with sizes 2 - 8 nm in the amorphous phase following ramped annealing at temperatures much lower than the characteristic crystallization temperature, yet with crystalline volume fractions consistent with the as-deposited amorphous material. The size and distribution of the nano-clusters embedded in the amorphous phase are important in determining the crystallization rate in phase-change material and also the stability of the amorphous phase during practical operation of devices. There is currently no detailed or systematic study on the size and distribution of nano-clusters in amorphous phase-change material, and their correlation to the form of the different thermal treatments and ultimately on crystallization dynamics on phase-change technologies.

In the absence of experimental measurements, or for analysis of experimental data and interpretation, mathematical modelling plays a vital role in simulating the overall behaviour of phase-change materials. However, a physically realistic and comprehensive model should be used to capture the complexities of the material and be robust to enable modelling different material properties and heating conditions. In this research programme, the Master rate equation approach, which fits the above criteria, was used to describe phase transformation in the technologically important GST phase-change material. The Master rate

equation can describe the interaction of an ensemble of monomers through thermodynamic attachment and detachment processes in response to transient temperature changes. Thus it is capable of modelling the non-uniform nucleation and growth processes with sufficient detail, yet at practical computational times much shorter than the atomistic level simulations. Therefore, it is robust to allow inclusion of more physically realistic viscosity models, and be used iteratively to fit to experimental measurements to extract pertinent parameters characterising the crystallization dynamics in phase-change materials.

This thesis contributes to a fundamental understanding of the use of a suitable mathematical model and numerical implementation to investigate the crystallization kinetics in the GST phase-change materials. This was possible by answering the following research questions:

- How important is it to use a more realistic model such as the Master rate equation in modelling the crystallization dynamics of phase-change material?
- Do viscosity parameters affect the crystallization dynamics significantly? If so, how this effect can be implemented in modelling phase-change material using Master rate equation?
- Can viscosity parameters be extracted using the Master equation approach?
- Can the material initial state affect the crystallization dynamics? Are the cluster evolutions the key to understand this effect? And how can this be studied using the Master rate equation?

This thesis was structured in chapters through which the preceding questions have been systematically answered. The principle key findings of this study along with highlighted discussions are presented as follows:

In chapter 1, the thesis starts with a brief background of phase-change materials and memories. The characteristics and properties of the phase-change materials along with the crystallization kinetics are also introduced. This was followed by the aims and objectives of this research programme.

In chapter 2, an overview of the different approaches for modelling the phase change process was presented, highlighting their applicability, advantages and shortcomings. Due to the ability of the Master rate equation of bridging the gap between the large-scale, simplified analytical models (such as the JMAK description) and the first-principle and numerically intensive atomistic modelling, this modelling approach was deemed suitable for the realistic simulations of crystallization dynamics in the GST phase-change material needed for this research programme. In this rate equation approach, nucleation and growth are traced by the attachment and detachment of monomers, with temperature history, to calculate the transient distribution of cluster sizes in the material. Both the attachment and detachment rates in this model are strong functions of viscosity, and thus, the value of viscosity and its dependence on temperature significantly affect the crystallization process.

In chapter 3, a mathematical review of the continuous and discrete forms of the Master rate equation is presented. It is well known that the continuous Master rate equation is an

approximation of the discrete model as a consequence of approximating discrete terms using a Taylor expansion. Consequently, there are error terms due to the Taylor truncation used for derivation of the continuous model from the discrete one. To investigate the role of numerical solver parameters such as the upper limit of cluster size and cluster size sub-interval in the crystallization dynamics at low and high heating rates, both discrete and continuous forms of the Master rate equation were compared. The comparison showed that the upper limit of cluster sizes along with the number of subintervals has a significant effect on the crystallization dynamics for different heating rates with the use of the continuous Master rate equation. Moreover, it was found that crystallization curves calculated using the discrete form of the Master rate equation were less sensitive to increases in the maximum cluster size for clusters greater than 40 monomers. It was found that for more realistic simulations the discrete Master rate equation model is preferred to use in phase change modelling.

Attributing to the importance of viscosity on driving the crystallization rate, chapter 4 reviews the common models of viscosity dependence on temperature used in modelling phase change in the literature. This included a discussion of their validity and shortcomings highlighted in various measurements in the literature, and the large disparity in their measured critical parameters including the fragility index and glass transition temperature. As a result of this review, the more robust and widely accepted MYEGA viscosity model was chosen for this research programme and implemented in the Master rate equation. This model has physical grounding and can describe different viscosity behaviours over a wide temperature range, from the glass transition temperature to the melting temperature. To describe the behaviour of the viscosity at temperatures below the glass transition temperature, the Arrhenius model was used in the Master rate equation using parameters obtained from low temperature calorimetry experiment from literature, to complement the MYEGA model.

To study and understand the effects of the viscosity on crystallization dynamics, simulations were carried out with varying viscosity parameters within the range of published values at low (50 K/s) and ultra-high (40,000 K/s) heating rates. Those simulation showed that, with increasing heating rate, high fragility values ($m$ = 90) resulted in modest increases in crystallization temperature while lower values of fragility ($m$ = 23) reduced the crystallization rate and increased crystallization temperature. Moreover, the increase of the glass transition temperature made a corresponding shift in crystallization temperature towards higher values. Furthermore, at low heating rates, infinite temperature viscosity parameter has negligible effect on the crystallization dynamics while, at higher heating rates, smaller values of infinite temperature viscosity parameter increase the crystallization rate and final crystalline volume.

As previously indicated, recent measurements of Kissinger plots for the GST phase-change material obtained using ultrafast calorimetry were fitted to simplified models of crystallization (assuming growth dominated processes) and temperature dependence of viscosity to estimate the viscosity over a wide temperature range. The assumptions used in the simplified models were not fully justified, the extracted parameters were not validated against previous measurements, and the role of the glass transition temperature was totally ignored. Due to the practical computational times of the discrete Master rate equation solution, an iterative algorithm was developed in chapter 5 to estimate the values of the viscosity parameters using the more realistic MYEGA model, by comparing full transient crystallization simulations to the same published Kissinger plots from ultrafast DSC measurements. It is important to highlight that the developed iterative algorithm included both nucleation and growth processes, used the more physically realistic MYEGA model for viscosity and is able to extract both the fragility index and the glass transition temperature value at each of the heating rates between 50 K/s to 40,000 K/s used in the measurements. In

light of these findings, the new iterative algorithm raised a debate about the validity of the concept of assuming a fixed viscosity and kinetic behaviour to describe crystallization in phase-change material at different heating rates in DSC measurements, which was the assumption made in all previous fittings to Kissinger curves. In particular, the simulations of Kissinger curves and fittings to measurements indicated the strong coupling between the glass transition temperature and fragility index, and therefore any accurate measurement of fragility requires an accurate estimate of the glass transition and vice versa. Furthermore, the study highlighted the importance of the often ignored dependence of glass transition temperature on heating rate, which again must be taken into account to produce accurate estimates of fragility from Kissinger plots. For the first time, the newly developed iterative algorithm using the Master rate equation was able to produce estimates of the glass transition temperatures for GST as a function of heating rate, which were in close agreement to the values published in literature. The outcomes of the simulations and fittings indicate the importance of using accurate crystallization models for analysis of experimental measurements, and the validity of the Master rate equation approach for practical and realistic modelling of crystallization and analysis of kinetic measurements.

Due to the ability of the Master rate equation of modelling transient cluster formation of different sizes, chapter 6 focused on the theoretical investigation of cluster size distributions following pre-annealing and melt-quenching of the as-deposited amorphous GST. This is to understand the resulting cluster size distribution from the different thermal treatments of phase-change material in practical devices, and how this affects the crystallization dynamics of the amorphous starting phase following heating at very high heating rates. The simulations revealed that melt-quenching produces a very narrow distribution of cluster size distribution with few nano-clusters. Pre-annealing using ramped heating at low heating rates

to temperatures lower than the crystallization temperature on the other hand produced a narrow distribution of nano-clusters up to 20 monomers in sizes, a low density of larger clusters, and a sharp distribution of very large clusters. The simulated cluster size distributions were in good agreement with recent observations of formation of nano-clusters in sputtered and flash-evaporated GST using high resolution TEM. These distributions were then used as initial states embedded in the amorphous material, and followed by crystallization simulations using the Master rate equation at low (50 K/s) and high (40,000 K/s) heating rates, revealing crystallization curves with a reduction in crystallization time and temperature, and an increase in the initial crystalline volume fraction compared to the as-deposited initial state. This study was extended to include a hypothetical Gaussian model for the cluster size distribution in the initial amorphous state, with controlled mean and standard deviation for the initial monomer sizes (keeping the overall crystalline volume fraction constant at 5% in all cases). The subsequent crystallization simulations revealed a marked reduction in crystallization time and temperature (and hence increased crystallization rate) when there is an abundance of only small nano-cluster embedded in the amorphous phase. The simulated transient cluster size distributions for different cluster sizes showed that small clusters promote nucleation and growth of larger clusters and hence increase the crystallization rate, while large clusters tend to dissociate to help the formation of small clusters leading to crystallization curves that approach those produced from the as-deposited amorphous phase (which require longer times to nucleate and grow the small clusters). Thus the simulations show that fast crystallization favours the priming of the amorphous phase to produce a large concentration of small clusters (less than 20 monomers).

## 7.2 Future work

The developed Master rate equation approach is a valuable tool for studying the details of phase transitions in phase-change materials, as it models the transient attachment and detachment of monomers in the material at the nano-scale level thus simulating the dynamics of cluster size distributions and crystallization curves at practical computational times. At the same time it is flexible and robust to implement different heat sources, different thermodynamic and kinetic parameters of materials, and can take into account geometrical and surface effects to model heterogeneous (in addition to homogenous) nucleation.

Thus the numerical models developed in this work can be extended to study the crystallization dynamics in other technologically important phase-change material such as AIST, with growth dominated crystallization. The newly developed iterative algorithm may also be used with recently published calorimetry measurements on AIST at ultrafast heating rates [30] to study and extract the viscosity dependence on temperature for this material (which exhibits a cross-over from the strong to highly fragile behaviour with increasing temperature) and other important kinetic parameters which can be used for the design of fast and efficient phase-change devices and memories.

The modelling and simulation work carried out in this thesis focused on using ramped annealing at constant heating rate as the heat source, mainly to ensure that both nucleation and growth happen and can be traced with sufficient numerical resolutions, and for comparison with published work and kinetic calorimetry measurements. Practical phase-change devices, particularly optical and electronic memories, are normally excited using laser

and voltage pulses respectively with rise/fall times and pulse widths in the tens and hundreds of nanoseconds. Thermal modelling of the excited structures can be carried out through solution of the heat diffusion equation (which can include both electron and phonon contributions when using sub-nanosecond pulses [102] [103]). The more realistic computed transient temperatures can then be easily implemented in the Master rate equation model to enable study of the resulting transient cluster size distributions in practical devices and corresponding crystallization curves. This will also provide details about the stability of the amorphous phase particularly following the application of multiple, periodic pulses and used for investigations of the drift phenomenon (in electrical and optical properties) in phase-change material.

One of the useful extensions to the current research is the extension of the Master rate equation to model spatial variations in crystalline fraction. Simulating the spatial variation in crystallisation dynamics following a prescribed temperature distribution in finite structures is complex. One method of approaching this problem is to divide the simulation space into cells of specific shape and sufficient resolution to represent a practical number of monomers in the cell, and where the temperature can be considered uniform. Then the Master rate equation can be solved sequentially for each cell and according to the temperature in that cell, to provide a spatial distribution of the crystalline fraction in the simulated space. Additionally this would require the development of specific rules to govern the interaction between the cells where necessary.

The complete simulations of Kissinger curves and fitting to experimental measurements carried out in this work highlighted the strong correlation between the fragility index and

glass transition temperature, and the importance of considering the (often overlooked) dependence of the glass transition temperature on heating rate for analysis and interpretation of experimental measurements. The developed Master rate equation model and iterative algorithm in this work can be used to elucidate this coupling and the effect of including the temperature dependence of the glass transition temperature on crystallization dynamics and comparison to published experimental calorimetry and crystal growth measurements.

This thesis reviewed both mathematical forms of the Master rate equation, and derived the approximate continuous form from truncation of Taylor expansions of some of the terms in the original discrete rate equation. The error terms were identified and numerical simulations were carried out that highlighted the sensitivity of the continuous approximate form to simulations parameters and the resulting errors by comparison to the discrete form simulations. More detailed analyses of the continuous rate equation form can be carried out to estimate the order of their validity, quantify the error in the approximation, and therefore estimate the limits of its applicability.

# Appendices

## Research Papers

(1) **A. Aladool**, M. M. Aziz, and C. D. Wright, "Understanding the importance of the temperature dependence of viscosity on the crystallization dynamics in the Ge2Sb2Te5 phase-change material," J. Appl. Phys., vol. 224504, 2017.

(2) **A. Aladool**, M. M. Aziz, and C. D. Wright, "Understanding the effect of initial cluster size distribution on crystallization dynamics in phase-change materials", *manuscript in preparation.*

## Attended Conferences

(1) **A. S Younus**, M. M. Aziz, P. Ashwin and C. D. Wright, "Modelling the phase-change dynamic during ultrafast laser irradiation", European Phase Change and Ovonics Symposium (EPCOS), Amsterdam, Netherlands. September 2015 (Poster presentation).

(2) **A. S Younus**, M. M. Aziz, P. Ashwin and C. D. Wright, "The effect of the temperature dependence of viscosity on modelling crystallization dynamics in phase-change media using the Master equation", Global Conference on Applied Physics and Mathematics, Rome, Italy. July 2016 (Poster presentation).

(3) **A. S Younus**, M. M. Aziz, P. Ashwin and C. D. Wright, "The effect of the temperature dependence of viscosity on modelling crystallization dynamics in phase-change materials", European Phase Change and Ovonics Symposium (EPCOS), Amsterdam, Netherlands. September 2016 (Poster presentation).

JOURNAL OF APPLIED PHYSICS 121, 224504 (2017)

# Understanding the importance of the temperature dependence of viscosity on the crystallization dynamics in the $Ge_2Sb_2Te_5$ phase-change material

A. Aladool, M. M. Aziz, and C. D. Wright
*College of Engineering, Mathematics and Physical Sciences, University of Exeter, Exeter EX4 4QF, United Kingdom*

(Received 30 January 2017; accepted 29 May 2017; published online 14 June 2017)

The crystallization dynamics in the phase-change material $Ge_2Sb_2Te_5$ is modelled using the more detailed Master equation method over a wide range of heating rates commensurate with published ultrafast calorimetry experiments. Through the attachment and detachment of monomers, the Master rate equation naturally traces nucleation and growth of crystallites with temperature history to calculate the transient distribution of cluster sizes in the material. Both the attachment and detachment rates in this theory are strong functions of viscosity, and thus, the value of viscosity and its dependence on temperature significantly affect the crystallization process. In this paper, we use the physically realistic Mauro–Yue–Ellison–Gupta–Allan viscosity model in the Master equation approach to study the role of the viscosity model parameters on the crystallization dynamics in $Ge_2Sb_2Te_5$ under ramped annealing conditions with heating rates up to $4 \times 10^4$ K/s. Furthermore, due to the relatively low computational cost of the Master equation method compared to atomistic level computations, an iterative numerical approach was developed to fit theoretical Kissinger plots simulated with the Master equation system to experimental Kissinger plots from ultrafast calorimetry measurements at increasing heating rates. This provided a more rigorous method (incorporating both nucleation and growth processes) to extract the viscosity model parameters from the analysis of experimental data. The simulations and analysis revealed the strong coupling between the glass transition temperature and fragility index in the viscosity and crystallization models and highlighted the role of the dependence of the glass transition temperature on the heating rate for the accurate estimation of the fragility index of phase-change materials from the analysis of experimental measurements. *Published by AIP Publishing.*
[http://dx.doi.org/10.1063/1.4985282]

## I. INTRODUCTION

Modelling the crystallization dynamics of phase-change materials under fast annealing conditions is of importance to understand the requirements for achieving high data rates during the write and erase processes in optical and electronic memories.[1] While quenching from the melt and re-amporphization is a relatively fast process, crystallization from the amorphous phase remains the time limiting process in phase-change based memories.[2] The kinetic and thermodynamic parameters of the material, in addition to the viscosity dependence on temperature, directly affect the speed of crystallization of the phase-change material. Therefore, understanding the role of these parameters on the crystallization process through modelling and simulation is crucial for the development of modern, high-speed phase-change memory devices and technologies.

The crystallization process has been modelled using different approaches including the analytical and well-known model of Johnson-Mehl-Avrami-Kolmogorov (JMAK).[3,4] This model considers nucleation being random and uniform at constant (isothermal) temperature. However, these assumptions may not be applicable since crystallization in phase-change materials due to nucleation is not random nor uniform,[5] and the nucleation rate cannot be considered time independent for the entire crystallization process with temperature history. Nucleation and growth are separately considered in the classical nucleation and growth model.[6] This model only deals with crystal clusters exceeding the critical size[7] and therefore ignores transient subcritical cluster formation responsible for modelling the incubation time. Another approach for studying the crystallization process in phase-change materials at the fundamental level is ab-initio atomic scale modelling which depends on the density functional theory (for example, Ref. 8). Although this approach can provide deep insights into the crystallization behaviour in phase-change materials, these simulations are too computationally expensive for the analysis of experimental data or device level modelling.

One of the approaches for bridging the gap between the large-scale, simplified analytical models (such as the JMAK description) and the first-principle and numerically intensive atomistic modelling is the robust and physically realistic Master rate equation method considered in this work. Nucleation and growth in this model are described by the attachment and detachment of monomers,[5] yielding transient cluster size distributions in the subcritical and supercritical regimes under isothermal and non-isothermal annealing conditions.[9,11] This method has been successfully used to model crystallization in phase-change materials[10–12] and simulation of differential calorimetry for glasses[9] and offer relatively faster computation times compared to atomistic simulations for practical cluster sizes. The rates of attachment and detachment in the Master equation model, which control the

speed of crystallization, are functions of the temperature dependence of the viscosity, and hence, the simulations are sensitively characterized by the viscosity model.

A number of models have been developed to describe the viscosities of glasses in a broad range of chemical compositions and temperatures.[13] The Arrhenius viscosity model[14] is commonly used in investigations of crystallization dynamics in $Ge_2Sb_2Te_5$ (GST).[11,15] However, extracted viscosities for GST from ultrafast differential scanning calorimetry (DSC) measurements and growth rate measurements showed deviation from the Arrhenius temperature dependence, particularly demonstrating a fragile behaviour in the supercooled region.[16,17] Other non-Arrhenius models for viscosity in phase-change materials have been adopted including the Cohen and Grest viscosity model and the three-parameter models. The Cohen and Grest viscosity model has four adjustable parameters to fit measured viscosity data.[18] This model was used in Ref. 16 to extract the dependence of viscosity and crystal growth rates on temperature from ultrafast DSC measurements for GST. The fitting constants in this viscosity model are not related to physical parameters of viscosity (such as the fragility and glass transition temperature). It was also noted that the Cohen and Grest viscosity model over-estimated crystal growth rates in Ge-Sb alloys by 2–3 orders of magnitude compared to the three-parameter models[19] and was not able to provide accurate fitting to Kissinger plots at high heating rates for the AgInSbTe phase-change material.[20]

The three-parameter viscosity models include the well-known Vogel–Fulcher–Tammann (VFT) model,[21] the Avramov–Milchev (AM) model,[22] and the widely accepted Mauro–Yue–Ellison–Gupta–Allan (MYEGA) model.[23] The VFT model has three fitting parameters and was used to describe the temperature dependence of viscosity in GST (for example, Refs. 17 and 24). The more robust MYEGA viscosity model has physical foundation with three physical parameters including the glass transition temperature $T_g$, fragility $m$, and extrapolated infinite temperature viscosity $\eta_\infty$.[23] This model was successfully used to describe the temperature dependence of viscosity and crystal growth rates for AgInSbTe (AIST),[25,26] GeSb,[19] and GST.[27] The extended, five parameter generalised MYEGA model[28] was also used to describe the fragile-to-strong cross-over of viscosity in the AgInSbTe phase-change material (which is not apparent in GST).[20] This paper is therefore concerned with implementing the MYEGA model for the viscosity dependence on temperature in the Master equation system to simulate crystallization in GST at high heating rates.

The fragility index $m$ in the MYEGA viscosity model represents the slope of the viscosity in the Angell plot at the glass transition temperature and indicates the degree of deviation from the Arrhenius temperature dependence of viscosity. For the GST phase-change material, the fragility index has been extracted from fitting simplified (growth dominated) JMAK formulation with the VFT viscosity model to Kissinger plots measured using ultrafast differential scanning calorimetry (DSC), with a reported value of ~90.[16] Mechanical stress measurements on GST films at relatively low heating rates (assuming the Arrhenius temperature dependence of viscosity and a heating rate dependent $T_g$) indicated fragilities of 47 and 20 for pure and doped GST, respectively.[17] Higher values of fragility of 140 were also estimated from fitting to device level measurements of crystal growth rates as a function of temperature.[27] There is thus dispersion and uncertainty in the extracted values of fragility, but they all indicate the fragile nature of GST, which contributes to the high atomic mobility and fast crystallization of this phase-change material when heated at the relevant temperatures.

Published values of the glass transition temperature $T_g$ for GST also vary, with 373 K reported for thin (as-deposited) amorphous films using impedance, transmission, and heat capacity measurements.[29] This value is in agreement with a glass transition temperature of 384 K determined from the theory based on the enthalpy of atomization for GST[30] and was therefore adopted in the theoretical analysis and fitting to measured Kissinger plots in ultrafast DSC simulations in Ref. 16. However, DSC measurements of pre-annealed thin amorphous films of the phase-change material at relatively low heating rates (40 K/min) revealed higher glass transition temperatures within 10 K of the peak crystallization temperature (456 K for GST) and hence difficult to resolve from the main crystallization peak in the measurement.[31] The highest reported value of $T_g$ for GST was estimated from fitting the MYEGA model for the viscosity to crystal growth velocity measurements at the device level and was 472 K.[27] The infinite temperature viscosity parameter, $\eta_\infty$, can be extracted from Angell plots extrapolated to high temperatures and is typically in the range of $10^{-5}$–$10^{-3}$ (Pa s).[16]

It is clear from the brief overview of reported viscosity parameters above that there are uncertainties in the values of fragility and glass transition temperature for GST in the MYEGA model. This disparity in the estimated viscosity parameters may arise due to different types of samples (powder, flakes, and thin-films), preparation conditions, pre-annealing, heating rates, and more fundamentally the nature of the crystallization and viscosity models imposed for fitting to experimental data. An example is the large difference in the value of fragility $m > 100$ derived for AIST from fitting the MYEGA model to growth velocity measurements,[25] compared to the value of $m \sim 37$ derived for the same material using the generalised MYEGA model when accounting for the fragile-to-strong transition behaviour of the viscosity.[20] Furthermore, current methods of extraction of the viscosity parameters often rely on simple models of crystallization, such as the JMAK model with the constant nucleation rate and growth dominated crystallization which may not be appropriate for nucleation dominated materials such as GST. In this paper, we use the more detailed Master equation approach which includes both transient nucleation and growth processes with viscosity described by the MYEGA model to study the crystallization dynamics of GST over a wide range of heating rates. In particular, we investigate the role of the viscosity model and its parameters on the crystallization dynamics using Master equation simulations and use this model to simulate DSC measurements and full Kissinger plots. Due to its practical computational times, we also developed an iterative numerical algorithm

based on the physically realistic Master rate equation to estimate the values of the viscosity parameters for GST in comparison to published Kissinger plots from ultrafast DSC measurements. In this analysis, we particularly highlight and explore the effects of the dependence of glass transition temperature on the heating rate on the extracted fragility values and the strong correlation between the glass transition temperature and fragility index.

Section II of this paper will describe the theory of cluster formation thermodynamics in phase-change materials, leading to the mathematical formulation of the Master equation approach and the viscosity model used in the simulations. This is followed by the results and simulations section, illustrating the effects of the parameters of the MYEGA viscosity model on the crystallization dynamics in GST. The development of the iterative Master equation algorithm and comparison with published DSC measurements for GST at ultrafast heating rates is detailed in Section III, followed by discussion of the outcomes of this article and main conclusions.

## II. THEORY

### A. Cluster formation thermodynamics

The mechanism of attachment and detachment of monomers in the nucleation theory depends on the required work for the heterogeneous formation of clusters through attachment of monomers up to the theoretical cluster size, and then, they can grow rather than dissociate. The work for cluster formation, denoted by $W(n,T)$, is the sum of a surface free energy and a bulk free energy at certain temperature $T$ and is written as

$$W(n,T) = -K_1(T)n + K_2 n^{2/3}, \tag{1}$$

where $n$ is the number of monomers and $K_1$ is the difference in the bulk Gibbs free energy between the old and new phases, which may be calculated from[32]

$$K_1 = \sigma_0 \Delta H_f \left(\frac{T_m - T}{T_m}\right)\left[\frac{7T}{T_m + 6T}\right], \tag{2}$$

where $\sigma_0$ is the volume of a monomer (bonding molecule), $T_m$ is the melting temperature of the phase-change material, and $\Delta H_f$ is the enthalpy of fusion at the melting point. The difference in the surface energy between the two phases can be described by the interfacial energy coefficient $K_2$, which may be written as[5]

$$K_2 = a\sigma[\varphi(\theta_w)]^{\frac{2}{3}}, \tag{3}$$

where $a = (36\pi\sigma_0^2)^{\frac{1}{3}}$ is the surface area for spheres, $\sigma$ is the interfacial energy, and $\varphi(\theta_w)$ is the spherical cap geometrical factor to model the effects of heterogeneous nucleation with wetting angle $\theta_w$ (from the substrate surface)[5]

$$\varphi(\theta_w) = \frac{1}{4}(2 + \cos\theta_w)(1 - \cos\theta_w)^2, \tag{4}$$

where $0 < \theta_w \leq \pi$ to model homogeneous ($\theta_w \to \pi$) and heterogeneous ($\theta_w \to 0$) nucleation.

It can be seen from (2) that the sign of $K_1$ changes at $T = T_m$ and below the melting temperature $K_1 > 0$, indicating a maximum whose position is determined from

$$\frac{\partial W(n,T)}{\partial n} = 0, \tag{5}$$

yielding

$$n^* = \frac{8}{27}\left(\frac{K_1}{K_2}\right)^3. \tag{6}$$

This is the critical size when the crystal cluster is likely to continue to grow rather than dissociate. The cluster formation thermodynamics described in this section provide the driving force for crystallization in the Master rate equation formulation described next.

### B. The Master rate equation

The Master rate equation system is described here for completeness following the development by Kashchiev[5] consistently, which uses different attachment and detachment rates compared to previous work in Refs. 9 and 11. The dynamics of crystallization in phase-change materials is modelled by describing the transient evolution of the density of clusters of size $n$ monomers, $Z$, per unit volume with temperature $T$ in the Master equation

$$\begin{aligned}\frac{d}{dt}Z(n,t) = {} & f(n-1,t,T)Z(n-1,t) \\ & + g(n+1,t,T)Z(n+1,t) - f(n,t,T)Z(n,t) \\ & - g(n,t,T)Z(n,t), \quad n \geq 2,\end{aligned} \tag{7}$$

where $f(n,t,T)$ and $g(n,t,T)$ are the attachment and detachment rates respectively.[5] The detachment rate may be expressed in terms of the attachment rate following Zeldovich for ($n = 1,2,\ldots$):[33,34]

$$f(n,t,T)C(n,T) = g(n+1,t,T)C(n+1,T), \tag{8}$$

where $C(n,T)$ is the quasi-equilibrium cluster size distribution which can be expressed thermodynamically as[5]

$$C(n,T) = \exp\left(-W(n,T)/k_B T\right). \tag{9}$$

The attachment and detachment rates are given respectively by[5]

$$f(n,t,T) = Z_m \hat{f} n^{2/3} \exp\left(\frac{(W(n,T) - W(n+1,T))}{k_B T}\right), \tag{10}$$

$$g(n,t,T) = f(n-1,t,T)\frac{C(n-1,T)}{C(n,T)}, \tag{11}$$

where $k_B$ is the Boltzmann constant and $Z_m$ is the density of the remaining amorphous monomers, which is computed from

$$Z_m = Z_0 - \sum_{n=2}^{n_{max}} nZ(n,t), \tag{12}$$

where $Z_0$ is the total monomer density of the starting (amorphous) phase. Thus, the volume fraction of the crystallised material can be computed from (12) as

$$\chi = \sum_{n=2}^{n_{max}} nZ(n,t)/Z_0. \tag{13}$$

It is noted that the detachment rate in (11) is independent of the amount of free monomers $Z_m$. In (10) and (11), $\hat{f}$ is given by

$$\hat{f} = \frac{c\sigma_0^{2/3}(1-\cos\theta_w)}{2d_0\varphi(\theta_w)^{2/3}}D, \tag{14}$$

where $d_0$ is the diameter of a monomer, $c = (36\pi)^{1/3}$ is the shape factor for heterogeneous nucleation, and $D$ is the self-diffusion coefficient which may be described by the Stokes-Einstein equation

$$D = \frac{k_B T}{3\pi\lambda\eta(T)}. \tag{15}$$

In (15), $\lambda$ is the jump distance which is taken to be equal to the interatomic distance in GST (2.99 Å),[35] and $\eta(T)$ is the temperature dependant viscosity. Thus, as indicated in (10) and (11), both the attachment and detachment rates, respectively, and therefore crystallization dynamics, are strongly influenced by the functional dependence of viscosity on temperature.

### C. Viscosity model

In this section, both the Arrhenius and non-Arrhenius (MYEGA) models of the viscosity dependence on temperature are presented and used to derive the complete viscosity model from room temperature up to the melting point used in the subsequent Master equation simulations. In the Arrhenius model, the viscosity is described by

$$\eta(T) = K_\eta \exp\left[\frac{E_a}{k_B T}\right], \tag{16}$$

where $K_\eta$ is a prefactor and $E_a$ is the activation energy for viscous flow. This model has been previously employed in reaction rate modelling of crystallization in phase-change materials and yielded good agreement between simulations and measurements for isothermal annealing and at low heating rates.[9,11] Recent ultra-high heating rate DSC measurements, however, indicated the deviation of the viscosity from the Arrhenius behaviour for GST[16] and other phase-change materials including AIST[25,26] and GeSb.[19]

Therefore, in this work, we focus on the more robust and widely accepted viscosity model of Mauro-Yue-Ellison-Gupta-Allan (MYEGA).[23] This model has physical grounding and is able to describe different viscosity behaviours over a wide temperature range from $T_g$ (glass transition temperature) to $T_m$ (melting temperature) and is given by

$$\log_{10}\eta(T) = \log_{10}\eta_\infty + (12 - \log_{10}\eta_\infty)\frac{T_g}{T}\exp \times \left[\left(\frac{m}{(12-\log_{10}\eta_\infty)} - 1\right)\left(\frac{T_g}{T} - 1\right)\right], \tag{17}$$

for $T \geq T_g$. The three parameters in the MYEGA model are as follows: $\eta_\infty$ is the extrapolated infinite temperature viscosity, $T_g$ is the glass transition temperature at which the shear viscosity is equal to $10^{12}$ (Pa s),[36] and $m$ is the fragility index of the material defined as

$$m = \frac{\partial \log_{10}(\eta(T))}{\partial(T_g/T)}_{T=T_g}. \tag{18}$$

The fragility index is the slope of the viscosity curve at the glass transition temperature in the Angell plot and indicates the degree of deviation from the Arrhenius behaviour in the supercooled region.

The MYEGA model is also able to describe the viscosity of a wide class of phase-change materials and behaviours including the Arrhenius behaviour. This can be illustrated by taking the logarithm on both sides of (16) to yield

$$\log_{10}(\eta(T)) = \log_{10}K_\eta + \left[\frac{E_a\log_{10}(e)}{k_B T_g}\right] \times \frac{T_g}{T}. \tag{19}$$

By comparing (17) to (19), it can be readily shown that the MYEGA model can describe the Arrhenius temperature dependence provided that

$$\log_{10}K_\eta = \log_{10}\eta_\infty$$

and

$$12 - \log_{10}\eta_\infty = \left[\frac{E_a\log_{10}(e)}{k_B T_g}\right],$$

while the exponential term in (17) equates to

$$\exp\left[\left(\frac{m}{(12-\log_{10}\eta_\infty)} - 1\right)\left(\frac{T_g}{T} - 1\right)\right] = 1. \tag{20}$$

The above equalities show that through appropriate choice of the three parameters, the MYEGA model can describe the strong, Arrhenius temperature dependence of viscosity near the glass transition temperature for small fragilities where $m \to (12 - \log_{10}\eta_\infty)$.

For temperatures $T < T_g$, we have described the viscosity dependence on temperature using the Arrhenius model defined in (16), with the activation energy $E_a = 1.76 \pm 0.05$ eV measured by Kalb *et al.* for GST in Ref. 37. The prefactor $K_\eta$ in (16) in this case was derived here from the requirement that $\log_{10}\eta(T) = 12$ at $T = T_g$ to match the viscosity of the MYEGA model. Hence, the complete viscosity model derived in this work is given by

$$\log_{10}\eta(T) = \begin{cases} 12 + \log_{10}\left(\exp\left[\frac{E_a}{k_B}\left(\frac{1}{T} - \frac{1}{T_g}\right)\right]\right) & T < T_g \\ MYEGA & T \geq T_g. \end{cases} \tag{21}$$

Figure 1 illustrates the temperature dependence of viscosity calculated using the MYEGA model for different values of fragility. The viscosity model in (21) is used in the subsequent simulations in this paper.

## III. SIMULATION RESULTS

In this section, transient simulations of crystallization over a wide range of heating rates are carried out by solving the Master rate equation to determine the key parameters within the MYEGA viscosity model that affect the crystallization dynamics. Furthermore, an iterative numerical algorithm based on the Master equation method is developed to compare simulated and measured Kissinger plots from experimental calorimetry studies published in the literature so as to extract the viscosity model parameters and examine the role of the viscosity and crystallization models on the extracted values.

The system of coupled equations in (7) was solved numerically for the cluster size distribution $Z(n,t)$ using the *ode15s* solver in Matlab, with absolute and relative tolerances of $10^{-10}$ (to provide convergence to a stable and accurate solution with practical computation time). The solution tracks the formation and destruction of clusters of size $n \geq 2$ ($n=1$ representing the amorphous phase) with temperature history. The initial starting phase in all simulations was the amorphous phase with initial cluster size distribution $Z(n,0) \rightarrow 0$ ($10^{-11}$ clusters/m$^3$ used here). Starting from room temperature $T_0 = 300$ K, the numerical simulations were performed over increasing heating rates $\phi$ from 50 K/s up to 40 000 K/s according to $T = T_0 + \varphi t$ where $t$ is the time, to allow comparison with previously published ultrafast DSC measurements for GST.[16,19] The maximum number of equations solved in (7) (upper limit of cluster size) was 40, which is greater than the critical size of clusters over the temperature range (300 K to 635 K) used in this work, to allow accurate simulations of crystallization.[9] This was confirmed by carrying out simulations with increasing cluster sizes up to 1000 monomers at heating rates up to the 40 000 K/s, showing particularly negligible changes in the transient response and in peak crystallization temperatures with increasing cluster size (important in this work for accurate fitting to experimental Kissinger plots). The only noticeable difference was a 16% maximum increase in the steady-state crystalline volume fraction happening only at the highest heating rate as the maximum cluster size was increased from 40 to 1000 monomers. These simulations confirmed the validity of using a maximum cluster size of 40, which is larger than the maximum critical cluster size for the temperature range used in the simulations, enabling quick computational times and fitting to experimental measurements.

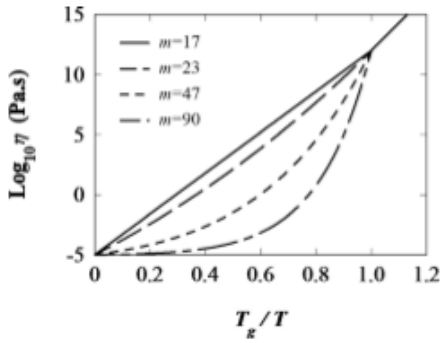


FIG. 1. Angell plot for the temperature dependence of calculated viscosity using the complete viscosity model described in (21) with parameter values: $\eta_\infty = 10^{-5}$ (Pa s), $T_g = 383$ K, and $E_\alpha = 1.76$ eV in the Arrhenius model for $T < T_g$.

The thermodynamic and material parameters used in the simulations are listed in Table I. The surface energy and glass transition temperatures were varied in the simulations within the range of reported values in the literature to investigate their effect (along with the fragility index) on the transient crystallization behaviour.

Figure 2(a) shows an example of the cluster size distribution from annealing at a heating rate of 50 K/s calculated from the solution of the Master equation using the parameters listed in Table I at different instances of time. This figure shows the formation and evolution of larger clusters during nucleation and growth following the initial amorphous phase. Figure 2(b) shows the distribution of cluster sizes at the final iteration in which the volume is fully crystallized.

### A. The effects of viscosity parameters on crystallization dynamics

The fragility index, the glass transition temperature, and the infinite temperature viscosity are the main parameters which describe the temperature dependence of viscosity in the MYEGA model and influence the rates of attachment and detachment of monomers (and therefore crystal nucleation and growth rates) in the Master rate equation. We will next study the effects of these parameters on the crystallization dynamics using the Master equation simulations, in particular, on the transient rate of crystallization and on the peak crystallization temperature $T_p$—defined here as

TABLE I. Thermodynamic and material parameters used for the numerical simulations.

| Parameter | Value | Unit |
|---|---|---|
| Volume of a monomer $\sigma_0$ | $2.9 \times 10^{-28}$[a] | m$^{-3}$ |
| Enthalpy of fusion $\Delta H_f$ | $6.18 \times 10^{8}$[a] | J/m$^3$ |
| Melting temperature $T_m$ | 889[b] | K |
| Specific surface energy $\sigma$ | 0.033–0.066[c] | J/m$^2$ |
| Wetting angle $\theta_w$ | 100[d] | Deg |
| Glass transition temperature $T_g$ | 383–472[e] | K |
| Infinite temperature viscosity $\eta_{\infty}$ | $1 \times 10^{-5}$[f] | (Pa s) |

[a]References 10 and 11.
[b]Reference 38.
[c]The surface energy for GST is within published values in Ref. 39.
[d]Reference 11; typical value for mostly homogeneous nucleation in powder samples[16] and includes a contribution of heterogeneous nucleation to account for potential surface crystallization in the experimental DSC samples that we are comparing with in this work.
[e]References 16, 27, 29, and 31.
[f]Extrapolated from Ref. 16 for temperatures $T \geq T_m$.

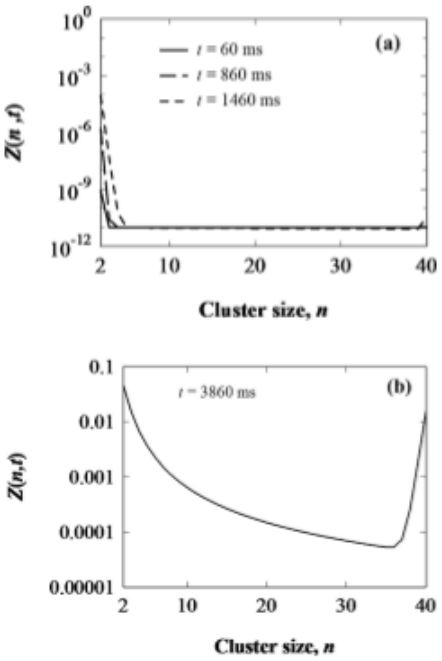


FIG. 2. Cluster size evolution with time calculated from the numerical solution of the Master equation for ramped annealing at a constant heating rate of 50 K/s. (a) Initial iterations. (b) Cluster size distribution at the final iteration. Viscosity model parameters used in the simulations include $m = 23$ and $T_g = 383$ K.

temperature at which the crystallization rate is maximum—at different heating rates.

Figure 3(a) shows the illustration of the effects of the fragility index on the crystalline volume fraction transformed, where low fragility values ($m = 23$) decrease the rate of crystallization and increase the peak crystallization temperature, leading to incomplete crystallization at high heating rates. This is attributed to the reduction in the diffusion coefficient (atomic mobility) in the rate equation with increasing viscosity, which increases the transient nucleation time for the clusters (time for the onset of steady-state nucleation in $Z$) as shown in Fig. 3(b) for relatively low heating rates (50 K/s) and in Fig. 3(c) for the highest heating rate (40 000 K/s). On the other hand, higher fragility values ($m = 90$) increase the atomic mobility in the supercooled region, therefore reducing the transient nucleation time and increasing the crystallization rates. This is illustrated by the sharp increase in the cluster size distributions for $n = 3$ in Figs. 3(b) and 3(c) around 1.7 s and 2 ms, respectively, marking the sharp drop in viscosity as the temperature reaches the glass transition temperature in the simulations. In this case (higher $m$), full crystallization is achieved even at relatively high heating rates with the modest increase in $T_p$ as indicated in Fig. 3(a). It can also be observed from Figs. 3(b) and 3(c) that the transient nucleation rate of clusters of different sizes is not uniform and changes with the heating rate. In general,

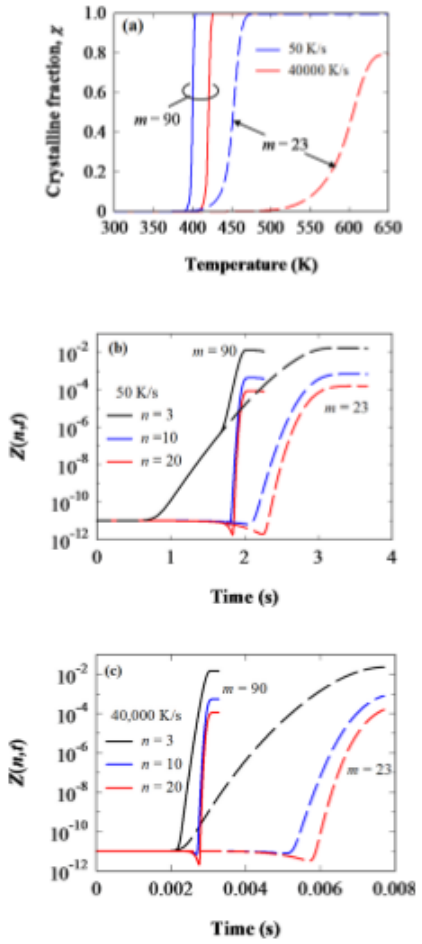


FIG. 3. (a) Calculated crystalline volume as a function of temperature during ramped anneals at different heating rates for two different fragility values: $m = 90$ (solid lines) and $m = 23$ (dashed lines). The calculated transient cluster densities for different cluster sizes at heating rates of (b) 50 K/s and (c) 40 000 K/s, showing non-uniform transient nucleation and the influence of the increasing fragility parameter on reducing the cluster nucleation time and increasing the crystallization speed. In these plots, the fragility values used in the calculations are $m = 90$ (solid line) and $m = 23$ (dashed line). Parameters used in the simulations include $T_g = 383$ K.

Fig. 3 illustrates the influence of the increasing fragility index on reducing the cluster nucleation time and increasing the crystallization speeds.

The glass transition temperature $T_g$ was next varied within the range of published values shown in Table I in the Master equation simulations. The calculated crystalline volume fractions are shown in Fig. 4(a) for a strong glass with $m = 23$ in the MYEGA model, illustrating an increase in $T_p$ followed by an increase in $T_p$ following the increase in $T_g$ (compare dashed lines versus solid lines), leading to incomplete crystallization and increased temperature difference

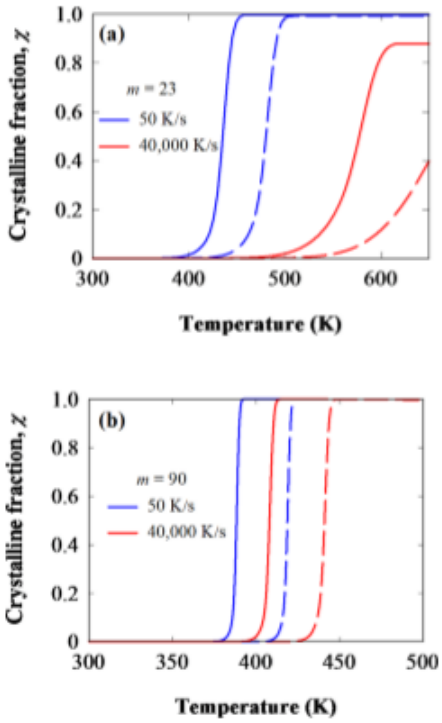


FIG. 4. Calculated crystalline volume fraction as a function of temperature during ramped anneals at different heating rates. Two different values of $T_g$ are used in the calculations: $T_g = 373$ K (solid line) and $T_g = 400$ K (dashed line) at different heating rates for (a) $m = 23$ and (b) $m = 90$.

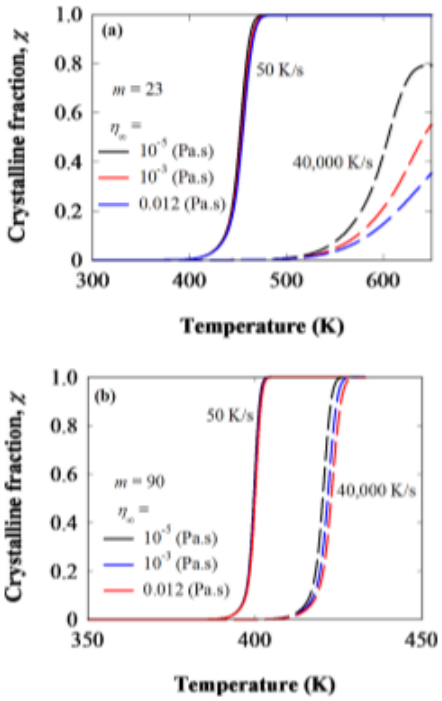


FIG. 5. Calculated crystalline volume fraction as a function of temperature during ramped anneals at different heating rates. Three different values of $\eta_\infty$ were used at the heating rates 50 K/s (dashed lines) and 40 000 K/s (solid lines). $T_g = 383$ K was used in the simulations for the fragilities: (a) $m = 23$ and (b) $m = 90$.

$T_p - T_g$ at high heating rates. The crystallization simulations in Fig. 4(b) also illustrate an increase in $T_p$ with increasing $T_g$ for a fragile material with $m = 90$, with the modest changes in the temperature $T_p - T_g$ with the increasing heating rate due to the high atomic mobility of the glass in this case.

The infinite temperature viscosity $\eta_\infty$ was varied within the range 0.012–$10^{-5}$ (Pa s)[16,27] in the Master equation simulations for the fragilities $m = 23$ and $m = 90$ and at different heating rates. It is expected that the influence of this parameter becomes important only at high temperatures near the melting point. As shown in Fig. 5(b), varying $\eta_\infty$ over this large range of values has a relatively small effect on the crystallization dynamics for high fragility values in the MYEGA model, where the high diffusivities increase the crystallization rate and lower $T_p$ well below the melting point $T_m$. For low fragility values, the influence of $\eta_\infty$ on the crystallization dynamics depends on the heating rate (which controls $T_p$). At low heating rates, $T_p$ is again well below $T_m$ and the value of $\eta_\infty$ has negligible effects on the crystallization dynamics as shown in Fig. 5(a) at 50 K/s. Increasing the heating rate increases $T_p$ to higher temperatures towards the melting point, where smaller values of $\eta_\infty$ increase the crystallization rate and final crystalline volume fraction as shown in Fig. 5(a). Since the simulations in this work occur within temperatures lower than the melting point for GST, a constant value of $\eta_\infty = 10^{-5}$ (Pa s) was employed in this work, allowing focus on the more important fragility index and glass transition temperature as variable parameters in the DSC simulations.

### B. Kissinger plots and comparison to DSC measurements

Differential scanning calorimetry (DSC) is a valuable tool to investigate crystallization dynamics and extract important kinetic and thermodynamic parameters of phase-change materials.[40] The peak crystallization temperature $T_p$ is determined from the peaks in the measured DSC traces at different heating rates $\phi$ and used to produce Kissinger plots[40] in which $\ln(\varphi/T_p^2)$ is plotted versus $1/T_p$ with the plot being typically a straight line (to describe an Arrhenius behaviour), enabling the estimation of the activation energy for the reaction.[41] The crystallization dynamics over a broad range of heating rates (50 K/s up to 40 000 K/s) have been measured using ultrafast DSC measurements for GST (see Fig. 7)[16,19] and for other phase-change materials (such as GeSb[19] and AIST[20]). A non-Arrhenius behaviour was observed in the Kissinger plots for GST in these measurements which cannot be described with a

single activation energy. The analysis of Kissinger plots is normally carried out using the JMAK theory assuming mainly growth dominated crystallization.[16,42]

Here, however, we instead use the Master equation approach that includes both nucleation and growth processes and is capable of simulating complete Kissinger plots from consecutive crystallization simulations at increasing heating rates. Typical crystallization simulations using the Master rate equation are presented in Fig. 6(a) at increasing heating rates, while Fig. 6(b) illustrates the time derivatives of the crystallization curves ($d\chi/dt$) to simulate DSC traces,[42] which enable the identification of the peak crystallization temperatures. Figure 6 shows a progressive increase in the peak crystallization temperature $T_p$ and a decrease in the slope of the crystallization curves at the transition temperatures with the increasing heating rate, which is normally observed experimentally as the shift in the peaks of the DSC traces and broadening of their distribution in differential calorimetry measurements. The calculated crystallization temperatures $T_p$ from the Master equation simulations at different heating rates in Fig. 6 can thus be used to produce complete theoretical Kissinger plots and compare to experimental measurements.

Due to the relatively low computational cost of solving the Master rate equation system and the ability to simulate both nucleation and growth, an iterative numerical approach has been developed to compare simulated and experimental Kissinger plots from ultrafast DSC measurements. This is to understand the crystallization process at high heating rates and enable the extraction of the important viscosity parameters from a more detailed theoretical approach. Preliminary focus will be on implementing the iterative algorithm to extract the fragility index parameter $m$ for the MYEGA viscosity model from ultrafast DSC experimental measurements reported for GST in Ref. 16. In this case, it is assumed that the glass transition temperature is constant (within the range of published values in Table I) for all the simulated heating rates, in accordance with the procedure used in the literature to analyse Kissinger plots.[16,19] The iterative algorithm proceeds by carrying out a complete crystallization simulation using ramped annealing at one heating rate from the solution of the Master equation system, using a starting value of $m = 17$ for the fragility. The simulated crystallization curve is then differentiated in time, and the computed peak temperature $T_p$ (corresponding to the maximum crystallization rate) is compared with the experimental value at the same heating rate (see Fig. 7),[16,19] and the absolute percentage error between the two temperatures is calculated. Repeated simulations at this

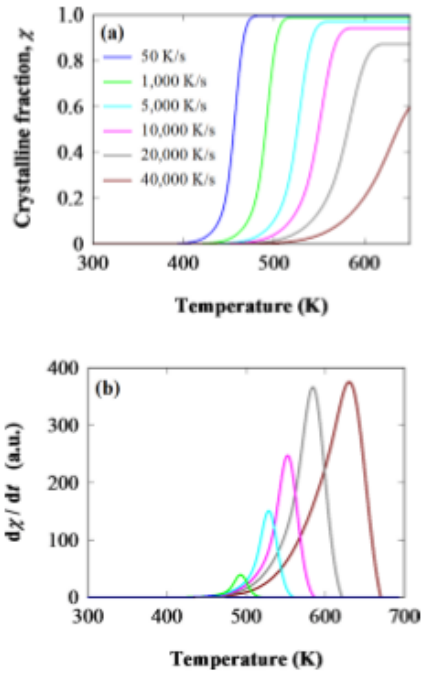


FIG. 6. (a) Calculated crystalline volume fraction as a function of temperature during ramped annealing at different heating rates. (b) Differentiated crystalline fraction curve [colour designation follows the legend of (a)]. The simulations parameters include $T_g = 383$ K and $m = 23$.

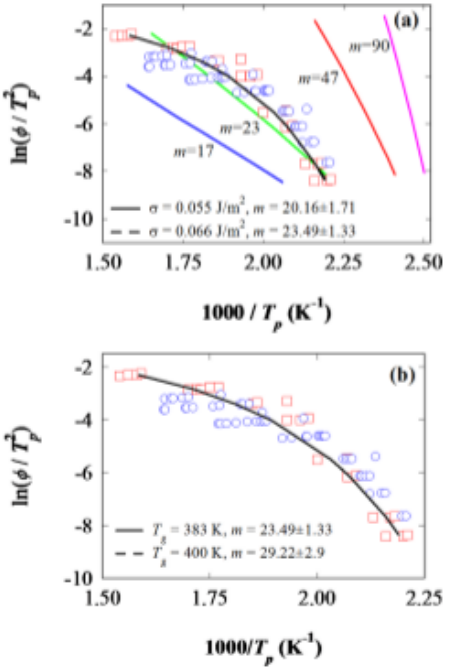


FIG. 7. Experimental Kissinger plots for GST using ultrafast DSC measurements from the study by Orava *et al.* (red squares)[16] and simulated plots using the iterative numerical algorithm based on the Master rate equation with the fragility index being the fitting parameter. All the fitting was carried out on the experimental data of Orava *et al.*[16] (Chen *et al.*[59] data—blue circles—shown for consistency). (a) Fitting taking into account the uncertainty in surface energy with $T_g = 383$ K and showing simulated Kissinger plots using four constant fragility values for comparison and (b) fitting for two glass transition temperature values with $\sigma = 0.066$ J/m$^2$. Simulation parameters are listed in Table I.

heating rate are then carried out to increment $m$ in each iteration until the absolute percentage error of the difference between the experimental and theoretical $T_p$ is less than 0.5%. This whole process is repeated at each heating rate to produce the theoretical Kissinger plot that closely fits the experimental curve as shown in Fig. 7 (solid and dashed black lines), and the extracted values of fragility that provide best agreement at each heating rate are recorded as shown in Table II as an example. Also shown in Fig. 7 for comparison are simulated Kissinger plots using four constant values of fragility (where $m = 17$ corresponds to the Arrhenius temperature dependence of viscosity).

To investigate the effects of the uncertainty in some of the modelling parameters, including the interfacial surface energy $\sigma$ and glass transition temperature $T_g$, on the extracted fragility values, these parameters were varied within the range of values listed in Table I in the iterative algorithm to produce the theoretical Kissinger plots shown in Fig. 7. It can be observed in Fig. 7(a) that increasing the interfacial energy $\sigma$ from 0.055 to 0.066 J/m$^2$ increases slightly the average extracted fragility values from $m \approx 20.16 \pm 1.7$ to $m \approx 23.49 \pm 1.3$, respectively. It can also be observed that increasing the glass transition temperature $T_g$ from 383 K to 400 K (within accepted values in the literature) also increases slightly the extracted fragility values from $m \approx 23.49 \pm 1.81$ to $m \approx 29.22 \pm 2.9$, respectively, as indicated in Fig. 7(b). In general, the effect of uncertainty in $\sigma$ and $T_g$ on the extracted fragility values is modest, and the average value of fragility extracted from the experimental measurements using the iterative algorithm is $m \sim 23$ (assuming constant $T_g$). Moreover, no clear trend was found in the variations of $m$ with the increasing heating rate in the iterative algorithm as indicated in Table II. This extracted value of fragility is lower than the value obtained from fitting using the JMAK model of $m \sim 90$ in Ref. 16. Exploration of the outcomes of the Master equation simulations and their interpretation in the light of published experimental measurements is discussed next.

## IV. DISCUSSION

The ability of the Master equation method to model transient crystallization including nucleation and growth and its low computational cost permitted the simulation of complete Kissinger plots in this work over a wide range of heating rates and the development of an iterative algorithm for the extraction of the important viscosity parameters from published experimental measurements. The discussion will now focus on the extracted fragility index in this work using the Master rate equation in relation to previously published values and the important role of the glass transition temperature and its dependence on the heating rate on the extracted fragility values.

TABLE II. Simulated Kissinger data and fitted fragility indices for $\sigma = 0.066$ J/m$^2$ and $T_g = 383$ K.

| Heating rate (K/s) | Measured $T_p$ (K) (Ref. 16) | Fitted $T_p$ (K) | Extracted fragility index $m$ |
|---|---|---|---|
| 50 | 456.3 | 456.8 | 21.99 |
| 100 | 462.3 | 463.0 | 23.18 |
| 500 | 481 | 481.7 | 24.78 |
| 1000 | 491.5 | 492.5 | 25.04 |
| 5000 | 527.1 | 528.1 | 24.63 |
| 10 000 | 550.5 | 551.8 | 23.92 |
| 20 000 | 582.7 | 584.0 | 22.95 |
| 40 000 | 629.5 | 631.1 | 21.42 |

Extracted values of the fragility index for GST in the literature varied considerably from 20 to 140. This variation in reported values may be attributed to several factors such as different sample and substrate structures (powder, thin-films, and flakes), sample preparation conditions, measurement technique (DSC, mechanical stress, and crystal growth velocity), pre-annealing conditions, doping, and heating and cooling rates. An equally important factor that affects the extracted values from measurements is the crystallization and viscosity models employed in the fitting and their parameters. The average fragility value of $m \sim 23$ derived in this work from fitting to the ultrafast DSC measurements is lower than reported values for GST ($m \sim 90$ in Ref. 16). This value was computed using a more physically realistic crystallization model which incorporates both transient nucleation and growth processes. The JMAK model, which assumes stationary nucleation and growth dominated crystallization, was used to extract the fragility values for GST in Ref. 16, which is commonly classified as a nucleation dominated material.[40] Moreover, in using the JMAK model for fitting to the experimental Kissinger curves in the literature, both the number of pre-existing nuclei and temperature dependant growth rate were combined into a single fitting kinetic coefficient, and the influence of each of these factors acting independently on the fitting process or on the computed fitted parameters was not clarified. Furthermore, the more physically realistic MYEGA model for the viscosity dependence on temperature was implemented here in the Master equation simulations, which has been shown to produce different results from the Cohen and Grest model employed in Ref. 16 to fit to experimental Kissinger curves and extract the fragility index.

In further exploring the potential causes for the difference between the extracted fragility values in this work and from the literature, it is fundamentally important to emphasise that the iterative algorithm used here produced complete transient crystallization simulations and extracted a separate fragility value at *each* heating rate. This is unlike DSC simulations employing the JMAK equation where a single fragility index was extracted over the whole range of heating rates (using a fixed value for $T_g$). This raises the important question of the validity of assuming a fixed viscosity and kinetic behaviour to describe crystallization in the phase-change material at different heating rates. In particular, it has been shown that the glass transition temperature, due to its kinetic nature, is sensitive to the heating rate and increases with the increasing heating rate in amorphous GeTe alloys,[43] Chalcogenide glasses,[44] and the GST phase-change material.[17,37] At relatively low heating rates, the dependence of the glass transition temperature on the heating rate in GST was described by the Moynihan relation $dln(\phi)/d(1/T_g) \approx -E/k_B$,[45] with a relaxation activation energy $E$ corresponding to the activation energy for shear viscous flow.[17]

To elucidate the effect of the dependence of the glass transition temperature on the heating rate in the Master equation simulations, $T_g$ was allowed to vary in the iterative fitting algorithm to the experimental Kissinger plots in Fig. 7 while assuming a constant value for the fragility ($m = 47$ here taken for pure GST from mechanical stress measurements).[17] Figure 8(a) illustrates the extracted values of $T_g$ from the iterative algorithm required to achieve the closest fit to the experimental data (within 0.5% absolute difference error). This figure shows the clear trend of increasing $T_g$ from 416 K to 488 K when $m = 47$ with the increase in the heating rate in the experiment from 50 K/s to 40 000 K/s, which is within the range of reported values for $T_g$ in the literature for GST as indicated in Table I. Moreover, the difference between the experimental peak crystallization temperature and fitted glass transition temperature, $T_p$–$T_g$ (reflecting the degree of mobility in the supercooled region), in Fig. 8(b) is approximately 40 K at low heating rates, in agreement with the DSC measurements for GST at low heating rates in Ref. 31. Increasing the fragility in the iterative algorithm to $m = 90$ increases the diffusivity and crystallization rate, therefore reducing the peak crystallization temperature in the simulations. This requires further increases in $T_g$ with the increasing heating rate in the fitting algorithm to achieve the closest fit to the experimental Kissinger data in Fig. 7, as indicated in Fig. 8(a). Furthermore, the sharp drop

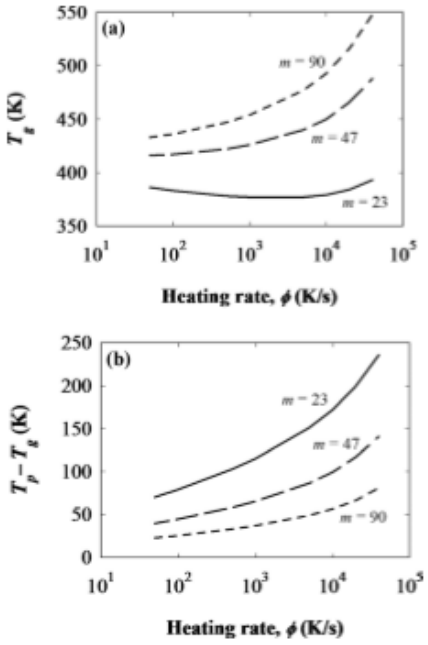


FIG. 8. (a) The glass transition temperature as a function of the heating rate determined from fitting the Master rate equation to experimental Kissinger plots, assuming constant values for the fragility. (b) The computed difference between the experimental peak crystallization temperature and derived glass transition temperature from (a). The glass transition temperatures and temperature differences for low fragility at $m = 23$ are shown for comparison.

of the viscosity with temperature near $T_g$ for $m = 90$ reduces the temperature difference $T_p$–$T_g$ as indicated in Fig. 8(b), which at low heating rates is ~22 K (again in agreement with Ref. 31). The increase in fitted values for $T_g$ for $m = 90$ at high heating rates go beyond reported values for GST in the literature.

In the above simulations and fittings, the representative value of $m = 47$ for the fragility index (from Ref. 17) produced values of $T_g$ that are in general agreement with reported values in the literature for GST. This agreement may suggest that this lower value of fragility is more reasonable than larger values found in the literature based on a constant $T_g$. However, this fragility value ($m = 47$) remains to be an assumption which can still be further refined to produce a modified range of values of $T_g$ with the increasing heating rate, particularly in the absence of experimental measurements or theory that confirms the dependence of $T_g$ on the heating rate for GST. Thus, the Master rate equation simulations and fittings highlight the important observations that

(a) the fragility index and glass transition parameters in the viscosity and crystallization simulations are coupled, and evaluation or extraction of one from experimental measurements requires that the other is available from the experiment or theory, and thus
(b) the accurate estimation of the fragility index from DSC measurements and Kissinger plots require information on the dependence of the glass transition temperature on the heating rate.

The simulations carried out in this work assumed the applicability of the Stokes-Einstein equation in (15) to describe the relationship between the diffusion coefficient and viscosity. Deviation from the form in the form $D \propto 1/\eta^{\zeta}$ where $\zeta < 1$ for temperatures down to $T_g$ was indicated using molecular dynamic simulations for the GeTe compound (not GST) in Ref. 46. This decoupling was also suggested and introduced in Ref. 16 for GST, however, mainly to overcome the inability of the Cohen and Grest viscosity model used in the analysis of Kissinger data to correctly describe the viscosity behaviour at $T_g$ (with the value of $10^{12}$ Pa s). This limitation was highlighted in Refs. 25 and 20 for AIST (and indicated that the more physically realistic MYEGA models for viscosity can alternatively provide accurate analysis of DSC measurements without the need for decoupling) and Ref. 19 for GeSb. Moreover, fittings to device level measurements in Ref. 27 found no sufficient evidence for the need for this decoupling for GST. There is thus currently neither concrete evidence that confirms the breakdown of the Stokes-Einstein equation for GST nor confirmed values for the decoupling factor in the literature. Evaluation of this decoupling is also made difficult by the disparity of reported values of $T_g$ and fragility index for GST. Our focus here is on studying the fundamental effects of more physically realistic nucleation-growth and viscosity models and the variation in the glass transition temperature with the heating rate to explain the very good agreement that we obtained with DSC measurements at ultrafast heating rates and the subsequent alternative fitted values of fragility indices.

The Master rate equation simulations and analysis of previously published ultrafast DSC measurements carried out in this work clarified the effects of the glass transition temperature and fragility index on the crystallization dynamics in phase-change materials. More importantly, this work highlighted the fundamental need to measure and understand the heating rate dependence of the glass transition temperature for the correct analysis of DSC measurements and estimation of the viscosity parameters necessary for modelling and characterising the crystallization dynamics in phase-change materials. This dependence will also have an impact on the estimation of crystal growth rates from DSC measurements for phase-change materials (since the growth velocity for interface controlled growth depends on viscosity).[6] Alternatively and if the fragility index is known for the phase-change material, then the iterative algorithm developed in this work can potentially be used to estimate the glass transition temperature and its dependence on the heating rate from DSC measurements.

## V. CONCLUSIONS

The crystallization dynamics in $Ge_2Sb_2Te_5$ were modelled using the Master rate equation approach which includes both nucleation and growth processes, under ramped annealing with heating rates up to $4 \times 10^4$ K/s. The temperature dependence of viscosity was implemented in this numerical approach using the physically founded MYEGA model. The influence of the viscosity model parameters including the fragility index, glass transition temperature, and infinite temperature viscosity on the crystallization dynamics was investigated for different heating rates. The relatively low computational cost of solving the Master rate equation for a practical system enabled the use of a more rigorous crystallization model for the analysis of previously published ultrafast DSC measurements of the $Ge_2Sb_2Te_5$ phase-change material and the development of an iterative numerical algorithm to extract the viscosity parameters from the measurements. In particular, we have taken into account the dependence of the glass transition temperature on the heating rate in the analysis of the experimental measurements and demonstrated its impact on the extracted fragility values. The outcomes of this theoretical investigation highlighted the coupling between the fragility index and glass transition temperature in the viscosity and crystallization models and the need for the experimental or theoretical determination of the dependence of glass transition temperature on the heating rate for the accurate estimation of the viscosity parameters from experimental measurements. This enables the accurate modelling and characterisation of phase-change materials and provides deeper understanding of the crystallization dynamics necessary for the development of high data rate phase-change memories and devices.

## ACKNOWLEDGMENTS

The authors would like to acknowledge the financial support from the Ministry of Higher Education of Iraq for the Ph.D. scholarship of Mr. Aladool.

[1]*Phase-Change Materials: Science and Applications*, edited by S. Raoux and M. Wuttig (Springer Science & Business Media, 2010).
[2]P. K. Khulbe, E. M. Wright, and M. Mansuripur, J. Appl. Phys. **88**, 3926 (2000).
[3]W. A. Johnson and R. F. Mehl, Trans. AIME **135**, 416 (1939).
[4]M. Avrami, J. Chem. Phys. **7**, 1103 (1939).
[5]D. Kashchiev, *Nucleation: Basic theory and applications, Part 2: Kinetics of Nucleation* (Butterworth-Heinemann, Oxford, 2000), p. 113.
[6]J. W. Christian, *The Theory of Transformations in Metals and Alloys: Part I* (Elsevier Science Ltd., Oxford, 2002).
[7]S. Raoux, W. Welnic, and D. Ielmini, Chem. Rev. **110**, 240 (2010).
[8]M. Terao, T. Morikawa, and T. Ohta, Jpn. J. Appl. Phys. **48**, 80001 (2009).
[9]K. F. Kelton, J. Non-Cryst. Solids **163**, 283–296 (1993).
[10]K. B. Blyuss, P. Ashwin, A. P. Bassom, and C. D. Wright, Phys. Rev. E - Stat., Nonlinear, Soft Matter Phys. **72**(1), 011607 (2005).
[11]S. Senkader and C. D. Wright, J. Appl. Phys. **95**, 504 (2004).
[12]C. D. Wright, K. Blyuss, and P. Ashwin, Appl. Phys. Lett. **90**, 063113 (2007).
[13]A. Kondratiev and A. Khvan, J. Non-Cryst. Solids **432**, 366 (2016).
[14]J. de Guzman, An. R. Soc. Esp. Fis. Quim. **11**, 353 (1913).
[15]A. Redaelli, A. Pirovano, A. venuti, and A. L. Lacaita, J. Appl. Phys. **103**, 111101 (2008).
[16]J. Orava, L. Greer, B. Gholipour, D. Hewak, and C. Smith, Nat. Mater. **11**, 279 (2012).
[17]J.-Y. Cho, D. Kim, Y.-J. Park, T.-Y. Yang, and Y.-Y. Lee, Acta Mater. **94**, 143 (2015).
[18]M. H. Cohen and G. Grest, Phys. Rev. B. **20**, 1077 (1979).
[19]B. Chen, J. Momand, P. Vermeulen, and B. J. Kooi, Cryst. Growth Des. **16**, 242 (2016).
[20]J. Orava, D. Hewak, and A. L. Greer, Adv. Funct. Mater. **25**, 4851 (2015).
[21]G. W. Scherer, J. Am. Ceram. Soc. **75**, 1060 (1992).
[22]I. Avramov and A. Milchev, J. Non-Cryst. Solids **104**, 253 (1988).
[23]J. C. Mauro, Y. Yue, A. J. Ellison, P. K. Gupta, and D. C. Allan, Proc. Natl. Acad. Sci. U.S.A. **106**, 19780 (2009).
[24]L. Battezatti and A. L. Greer, Acta Metall. **37**, 1791 (1989).
[25]M. Salinga, E. Carria, A. Kaldenbach, M. Bornhofft, J. Benke, J. Mayer, and M. Wuttig, Nat. Commun. **4**, 2371 (2013).
[26]P. Zalden, A. von Hoegen, P. Landreman, M. Wuttig, and A. M. Lindenberg, Chem. Mater. **27**, 5641 (2015).
[27]A. Sebastian, M. Le Gallo, and D. Krebs, Nat. Commun. **5**, 4314 (2014).
[28]C. Zhang, L. Hu, Y. Yue, and J. C. Mauro, J. Chem. Phys. **133**, 014508 (2010).
[29]E. Morales-Sanchez, E. Prokhorov, A. Mendoza-Galvan, and J. Gonzalez-Hernandez, J. Appl. Phys. **91**, 697 (2002).
[30]M. Lankhorst, J. Non-Cryst. Solids **297**, 210 (2002).
[31]J. Kalb, M. Wuttig, and F. Spaepen, J. Mater. Res. **22**, 748 (2007).
[32]H. B. Singh and A. Holz, Solid State Commun. **45**, 985 (1983).
[33]J. B. Zeldovich, Acta Physicochim. USSR **18**, 1 (1943).
[34]D. Kashchiev, Surf. Sci. **18**, 293 (1969).
[35]T. Nonaka, G. Ohbayashi, Y. Toriumi, Y. Mori, and H. Hashimoto, Thin Solid Films **370**, 258 (2000).
[36]Y. Yue, J. Non-Cryst. Solids **354**, 1112 (2008).
[37]J. Kalb, F. Spaepen, T. L. Pedersen, and M. Wuttig, J. Appl. Phys. **94**, 4908 (2003).
[38]N. Yamada, E. Ohno, K. Nishiuchi, N. Akahira, and M. Takao, J. Appl. Phys. **69**, 2849 (1991).
[39]K. Kohary and C. D. Wright, Phys. Status Solidi B **250**, 944 (2013).
[40]H. E. Kissinger, Anal. Chem. **29**, 1702 (1957).
[41]I. Friedrich, V. Weidenhof, W. Njoroge, P. Franz, and M. Wutting, J. Appl. Phys. **87**, 4130 (2000).
[42]A. L. Greer, Acta Metall. **30**, 171 (1982).
[43]I. Kaban, E. Dost, and W. Hoyer, J. Alloys Compd. **379**, 166 (2004).
[44]J. M. Saiter, J. Ledru, A. Hamou, and A. Zumailan, Mater. Lett. **33**, 91 (1997).
[45]F. S. Howell, R. A. Bose, P. B. Macedo, and C. T. Moynihan, J. Phys. Chem. **78**, 639 (1974).
[46]G. C. Sosso, J. Behler, and M. Bernasconi, Phys. Status Solidi B **249**, 1880 (2012).

# Bibliography


[1] C. Lam, "Cell Design Considerations for Phase Change Memory as a Universal Memory," in *2008 International Symposium on VLSI Technology, Systems and Applications (VLSI-TSA)*, 2008, pp. 132–133.

[2] A. Pavlov and M. Sachdev, *CMOS SRAM Circuit Design and Parametric Test in Nano-Scaled Technologies*, vol. 40. Dordrecht: Springer Netherlands, 2008.

[3] "2013 ITRS - International Technology Roadmap for Semiconductors." [Online]. Available: http://www.itrs2.net/itrs-reports.html. [Accessed: 30-Jan-2015].

[4] A. V Kolobov and J. Tominaga, *Chalcogenides*, vol. 164. Berlin, Heidelberg: Springer Berlin Heidelberg, 2012.

[5] E. Hamada, Y. Takagishi, T. Yoshizawa, T. Fujii, R. Negishi, and T. Nakajima, "Ten-Year Overview and Future Prospects of Write-Once Organic Recordable Media," *Jpn. J. Appl. Phys.*, vol. 39, no. 2S, p. 785, 2000.

[6] "IBM scientists demonstrate computer memory breakthrough." [Online]. Available: https://www.zurich.ibm.com/news/11/pcm.html. [Accessed: 17-Mar-2015].

[7] H.-S. P. Wong, S. Raoux, S. Kim, J. Liang, J. P. Reifenberg, B. Rajendran, M. Asheghi, and K. E. Goodson, "Phase Change Memory," *Proc. IEEE*, vol. 98, no. 12, pp. 2201–2227, Dec. 2010.

[8] F. Xiong, A. D. Liao, D. Estrada, and E. Pop, "Low-Power Switching of Phase-Change Materials with Carbon Nanotube Electrodes," *Science (80-. ).*, vol. 332, no. 6029, pp.

568–570, Apr. 2011.

[9] H. Hayat, K. Kohary, and C. D. Wright, “Can conventional phase-change memory devices be scaled down to single-nanometre dimensions?,” *Nanotechnology*, vol. 28, no. 3, p. 35202, Jan. 2017.

[10] D. Loke, T. H. Lee, W. J. Wang, L. P. Shi, R. Zhao, Y. C. Yeo, T. C. Chong, and S. R. Elliott, “Breaking the Speed Limits of Phase-Change Memory,” *Science (80-. ).*, vol. 336, no. 6088, pp. 1566–1569, Jun. 2012.

[11] T. Nirschl, J. B. Philipp, T. D. Happ, G. W. Burr, B. Rajendran, M.-H. Lee, A. Schrott, M. Yang, M. Breitwisch, C.-F. Chen, E. Joseph, M. Lamorey, R. Cheek, S.-H. Chen, S. Zaidi, S. Raoux, Y. C. Chen, Y. Zhu, R. Bergmann, H.-L. Lung, and C. Lam, “Write Strategies for 2 and 4-bit Multi-Level Phase-Change Memory,” in *2007 IEEE International Electron Devices Meeting*, 2007, pp. 461–464.

[12] C.-F. Chen, A. Schrott, M. H. Lee, S. Raoux, Y. H. Shih, M. Breitwisch, F. H. Baumann, E. K. Lai, T. M. Shaw, P. Flaitz, R. Cheek, E. A. Joseph, S. H. Chen, B. Rajendran, H. L. Lung, and C. Lam, “Endurance Improvement of Ge2Sb2Te5-Based Phase Change Memory,” in *2009 IEEE International Memory Workshop*, 2009, pp. 1–2.

[13] C. D. Wright, “Phase-change devices: Crystal-clear neuronal computing,” *Nat. Nanotechnol.*, vol. 11, no. 8, pp. 655–656, May 2016.

[14] S. G.-C. Carrillo, G. R. Nash, H. Hayat, M. J. Cryan, M. Klemm, H. Bhaskaran, and C. D. Wright, “Design of practicable phase-change metadevices for near-infrared absorber and modulator applications,” *Opt. Express*, vol. 24, no. 12, p. 13563, Jun. 2016.

[15] M. Wuttig and N. Yamada, “Phase-change materials for rewriteable data storage,” *Nat. Mater.*, vol. 6, no. 11, pp. 824–832, Nov. 2007.

[16] S. Raoux, F. Xiong, M. Wuttig, and E. Pop, “Phase change materials and phase change memory,” *MRS Bull.*, vol. 39, no. August, pp. 703–710, 2014.

[17] D.-H. Kim, F. Merget, M. Först, and H. Kurz, “Three-dimensional simulation model of switching dynamics in phase change random access memory cells,” *J. Appl. Phys.*, vol. 101, no. 6, p. 64512, Mar. 2007.

[18] C. D. Wright, L. Wang, P. Shah, M. M. Aziz, E. Varesi, R. Bez, M. Moroni, and F. Cazzaniga, “The Design of Rewritable Ultrahigh Density Scanning-Probe Phase-Change Memories,” *IEEE Trans. Nanotechnol.*, vol. 10, no. 4, pp. 900–912, Jul. 2011.

[19] U. Russo, D. Ielmini, and A. L. Lacaita, “Analytical Modeling of Chalcogenide Crystallization for PCM Data-Retention Extrapolation,” *IEEE Trans. Electron Devices*, vol. 54, no. 10, pp. 2769–2777, Oct. 2007.

[20] S. Raoux, W. Wełnic, and D. Ielmini, “Phase Change Materials and Their Application to Nonvolatile Memories,” *Chem. Rev.*, vol. 110, no. 1, pp. 240–267, Jan. 2010.

[21] S. Raoux and M. Wuttig, Eds., *Phase Change Materials*. Boston, MA: Springer US, 2009.

[22] J. Kalb, F. Spaepen, and M. Wuttig, “Atomic force microscopy measurements of crystal nucleation and growth rates in thin films of amorphous Te alloys,” *Appl. Phys. Lett.*, vol. 84, no. 25, pp. 5240–5242, Jun. 2004.

[23] J. A. Kalb, “Crystallization kinetics in antimony and tellurium alloys used for phase change recording,” PhD Thesis, University in Aachen, 2001.

[24] Y. Choi, M. Jung, and Y.-K. Lee, “Effect of Heating Rate on the Activation Energy for Crystallization of Amorphous Ge[sub 2]Sb[sub 2]Te[sub 5] Thin Film,” *Electrochem. Solid-State Lett.*, vol. 12, no. May, p. F17, 2009.

[25] T. Wagner, J. Orava, J. Prikryl, T. Kohoutek, M. Bartos, and M. Frumar, “Medium-term thermal stability of amorphous Ge2Sb2Te5 flash-evaporated thin films with regards to change in structure and optical properties,” *Thin Solid Films*, vol. 517, no. 16, pp. 4694–4697, Jun. 2009.

[26] I. Friedrich, V. Weidenhof, W. Njoroge, P. Franz, and M. Wuttig, “Structural transformations of Ge2Sb2Te5 films studied by electrical resistance measurements,” *J. Appl. Phys.*, vol. 87, no. 9, pp. 4130–4134, May 2000.

[27] R. M. R. Wellen and E. L. Canedo, “On the Kissinger equation and the estimate of activation energies for non-isothermal cold crystallization of PET,” *Polym. Test.*, vol. 40, pp. 33–38, Dec. 2014.

[28] J. Orava, a. L. L. Greer, B. Gholipour, D. W. W. Hewak, and C. E. E. Smith, “Characterization of supercooled liquid Ge2Sb2Te5 and its crystallization by ultrafast-heating calorimetry,” *Nat. Mater.*, vol. 11, no. 4, pp. 279–283, Mar. 2012.

[29] B. Chen, J. Momand, P. A. Vermeulen, and B. J. Kooi, “Crystallization Kinetics of Supercooled Liquid Ge–Sb Based on Ultrafast Calorimetry,” *Cryst. Growth Des.*, vol. 16, no. 1, pp. 242–248, Jan. 2016.

[30] J. Orava, D. W. Hewak, and a. L. Greer, “Fragile-to-Strong Crossover in Supercooled Liquid Ag-In-Sb-Te Studied by Ultrafast Calorimetry,” *Adv. Funct. Mater.*, vol. 25, no. 30, pp. 4851–4858, Aug. 2015.

[31] G. C. Sosso, J. Behler, and M. Bernasconi, “Breakdown of Stokes-Einstein relation in

the supercooled liquid state of phase change materials," *Phys. Status Solidi*, vol. 249, no. 10, pp. 1880–1885, 2012.

[32] S. Senkader and C. D. Wright, "Models for phase-change of Ge2Sb2Te5 in optical and electrical memory devices," *J. Appl. Phys.*, vol. 95, no. 2, pp. 504–511, Jan. 2004.

[33] U. Russo, D. Ielmini, A. Redaelli, and A. L. Lacaita, "Intrinsic Data Retention in Nanoscaled Phase-Change Memories—Part I: Monte Carlo Model for Crystallization and Percolation," *IEEE Trans. Electron Devices*, vol. 53, no. 12, pp. 3032–3039, Dec. 2006.

[34] P. K. Khulbe, E. M. Wright, and M. Mansuripur, "Crystallization behavior of as-deposited, melt quenched, and primed amorphous states of Ge[sub 2]Sb[sub 2.3]Te[sub 5] films," *J. Appl. Phys.*, vol. 88, no. 7, p. 3926, 2000.

[35] B.-S. Lee, R. M. Shelby, S. Raoux, C. T. Retter, G. W. Burr, S. N. Bogle, K. Darmawikarta, S. G. Bishop, and J. R. Abelson, "Nanoscale nuclei in phase change materials: Origin of different crystallization mechanisms of Ge 2 Sb 2 Te 5 and AgInSbTe," *J. Appl. Phys.*, vol. 115, no. 6, p. 63506, Feb. 2014.

[36] T. H. Lee and S. R. Elliott, "Ab Initio Computer Simulation of the Early Stages of Crystallization: Application to Ge 2 Sb 2 Te 5 Phase-Change Materials," *Phys. Rev. Lett.*, vol. 107, no. 14, p. 145702, Sep. 2011.

[37] K. Kohary, A. S. H. Marmier, and C. D. Wright, "Ab initio determination of the elastic properties of cubic Ge1Sb2Te4," *MRS Proc.*, vol. 1431, p. mrss12-1431-f05-01, Jan. 2012.

[38] J. C. Mauro, Y. Yue, A. J. Ellison, P. K. Gupta, and D. C. Allan, "Viscosity of glass-forming liquids," *Proc. Natl. Acad. Sci.*, vol. 106, no. 47, pp. 19780–19784, Nov.

2009.

[39] A. Aladool, M. M. Aziz, and C. D. Wright, “Understanding the importance of the temperature dependence of viscosity on the crystallization dynamics in the Ge 2 Sb 2 Te 5 phase-change material,” *J. Appl. Phys.*, vol. 121, no. 22, p. 224504, Jun. 2017.

[40] A. N. Kolmogorov, “On the statistical theory of the crystallization of metals,” *Bull. Acad. Sci. USSR, Math. Ser*, vol. 1, pp. 355–359, 1937.

[41] M. Avrami, “Kinetics of Phase Change. I General Theory,” *J. Chem. Phys.*, vol. 7, no. 12, pp. 1103–1112, Dec. 1939.

[42] W. A. Johnson and R. F. Mehl, “Reaction Kinetics in Processes of Nucleation and Growth,” *Trans. Am. Inst. Min. Metall. Eng.*, vol. 135, pp. 416–442, 1939.

[43] D. Kashchiev, *Nucleation: Basic theory and applications*. Butterworth-Heinemann, 2000.

[44] V. Weidenhof, I. Friedrich, S. Ziegler, and M. Wuttig, “Laser induced crystallization of amorphous Ge2Sb2Te5 films,” *J. Appl. Phys.*, vol. 89, no. 6, pp. 3168–3176, Mar. 2001.

[45] T. H. Jeong, M. R. Kim, H. Seo, S. J. Kim, and S. Y. Kim, “Crystallization behavior of sputter-deposited amorphous Ge2Sb2Te5 thin films,” *J. Appl. Phys.*, vol. 86, no. 2, pp. 774–778, Jul. 1999.

[46] D. Turnbull and J. C. Fisher, “Rate of Nucleation in Condensed Systems,” *J. Chem. Phys.*, vol. 17, no. 1, pp. 71–73, Jan. 1949.

[47] J. A. Kalb, “Crystallization kinetics in antimony and tellurium alloys used for phase change recording,” *Dr. Diss. RWTH Aachen, Ger.*, 2006.

[48] E. R. Meinders, H. J. Borg, M. H. R. Lankhorst, J. Hellmig, and a. V. Mijiritskii, "Numerical simulation of mark formation in dual-stack phase-change recording," *J. Appl. Phys.*, vol. 91, no. 12, p. 9794, 2002.

[49] E. K. U. Gross and R. M. Dreizler, *Density functional theory*, vol. 337. Springer Science & Business Media, 2013.

[50] W. Zhang, V. L. Deringer, R. Dronskowski, R. Mazzarello, E. Ma, and M. Wuttig, "Density-functional theory guided advances in phase-change materials and memories," *MRS Bull.*, vol. 40, no. 10, pp. 856–869, Oct. 2015.

[51] R. M. Martin, *Electronic structure: basic theory and practical methods*. Cambridge University Press, 2004.

[52] D. Frenkel and B. Smit, *Understanding molecular simulation: from algorithms to applications*, Second Ed., vol. 1. Academic Press, 2001.

[53] J. Hegedüs and S. R. Elliott, "Microscopic origin of the fast crystallization ability of Ge–Sb–Te phase-change memory materials," *Nat. Mater.*, vol. 7, no. 5, pp. 399–405, May 2008.

[54] K. F. Kelton, a. L. Greer, and C. V. Thompson, "Transient nucleation in condensed systems," *J. Chem. Phys.*, vol. 79, no. 12, pp. 6261–6276, Dec. 1983.

[55] K. F. Kelton and A. L. Greer, "Transient nucleation effects in glass formation," *J. Non. Cryst. Solids*, vol. 79, no. 3, pp. 295–309, Feb. 1986.

[56] K. F. Kelton, "Numerical model for isothermal and non-isothermal crystallization of liquids and glasses," *J. Non. Cryst. Solids*, vol. 163, no. 3, pp. 283–296, Dec. 1993.

[57] K. F. Kelton, "Analysis of crystallization kinetics," *Mater. Sci. Eng. A*, vol. 226–228,

pp. 142–150, Jun. 1997.

[58] C. D. Wright, K. Blyuss, and P. Ashwin, “Master-equation approach to understanding multistate phase-change memories and processors,” *Appl. Phys. Lett.*, vol. 90, no. 6, p. 63113, Feb. 2007.

[59] G. W. Burr, P. Tchoulfian, T. Topuria, C. Nyffeler, K. Virwani, A. Padilla, R. M. Shelby, M. Eskandari, B. Jackson, and B.-S. Lee, “Observation and modeling of polycrystalline grain formation in Ge 2 Sb 2 Te 5,” *J. Appl. Phys.*, vol. 111, no. 10, p. 104308, May 2012.

[60] J. A. Vázquez Diosdado, P. Ashwin, K. I. Kohary, and C. D. Wright, “Threshold switching via electric field induced crystallization in phase-change memory devices,” *Appl. Phys. Lett.*, vol. 100, no. 25, p. 253105, Jun. 2012.

[61] H. Hayat, “A study of the scaling and advanced functionality potential of phase change memory devices,” PhD thesis, University of Exeter, 2016.

[62] J. B. Zeldovich, “On the theory of new phase formation: cavitation,” *Acta Physicochim. URSS*, vol. 18, pp. 1–22, 1943.

[63] D. Kashchiev, “The kinetic approach to nucleation,” *Cryst. Res. Technol.*, vol. 19, no. 11, pp. 1413–1423, 1984.

[64] D. Kashchiev, “Nucleation at variable supersaturation,” *Surf. Sci.*, vol. 18, no. 2, pp. 293–297, Dec. 1969.

[65] H. B. Singh and A. Holz, “Stability limit of supercooled liquids,” *Solid State Commun.*, vol. 45, no. 11, pp. 985–988, Mar. 1983.

[66] T. Nonaka, G. Ohbayashi, Y. Toriumi, Y. Mori, and H. Hashimoto, “Crystal structure

of GeTe and Ge2Sb2Te5 meta-stable phase," *Thin Solid Films*, vol. 370, no. 1–2, pp. 258–261, Jul. 2000.

[67] L. F. Shampine, I. Gladwell, and S. Thompson, *Solving ODEs with MATLAB*. Cambridge University Press, 2003.

[68] T. P. L. Pedersen, J. Kalb, W. K. Njoroge, D. Wamwangi, M. Wuttig, and F. Spaepen, "Mechanical stresses upon crystallization in phase change materials," *Appl. Phys. Lett.*, vol. 79, no. 22, pp. 3597–3599, Nov. 2001.

[69] K. B. Blyuss, P. Ashwin, a. P. Bassom, and C. D. Wright, "Master-equation approach to the study of phase-change processes in data storage media," *Phys. Rev. E*, vol. 72, no. 1, p. 11607, Jul. 2005.

[70] B. Shizgal and J. C. Barrett, "Time dependent nucleation," *J. Chem. Phys.*, vol. 91, no. 10, pp. 6505–6518, Nov. 1989.

[71] C. F. Clement and M. H. Wood, "Moment and Fokker-Planck Equations for the Growth and Decay of Small Objects," *Proc. R. Soc. A Math. Phys. Eng. Sci.*, vol. 371, no. 1747, pp. 553–567, Aug. 1980.

[72] R. L. Burden and J. D. Faires, *Numerical Analysis*, 9th ed. Brooks Cole.

[73] A. Sebastian, M. Le Gallo, and D. Krebs, "Crystal growth within a phase change memory cell," *Nat. Commun.*, vol. 5, pp. 1–9, Jul. 2014.

[74] E. Morales-Sánchez, E. F. Prokhorov, A. Mendoza-Galván, and J. González-Hernández, "Determination of the glass transition and nucleation temperatures in Ge2Sb2Te5 sputtered films," *J. Appl. Phys.*, vol. 91, no. 2, pp. 697–702, Jan. 2002.

[75] J. A. Kalb, M. Wuttig, and F. Spaepen, "Calorimetric measurements of structural

relaxation and glass transition temperatures in sputtered films of amorphous Te alloys used for phase change recording," *J. Mater. Res.*, vol. 22, no. 3, pp. 748–754, Mar. 2007.

[76] N. Yamada, E. Ohno, K. Nishiuchi, N. Akahira, and M. Takao, "Rapid-phase transitions of GeTe-Sb 2 Te 3 pseudobinary amorphous thin films for an optical disk memory," *J. Appl. Phys.*, vol. 69, no. 5, pp. 2849–2856, Mar. 1991.

[77] K. Kohary and C. D. Wright, "Electric field induced crystallization in phase-change materials for memory applications," *Appl. Phys. Lett.*, vol. 98, no. 22, p. 223102, 2011.

[78] J.-Y. Cho, D. Kim, Y.-J. Park, T.-Y. Yang, Y. Lee, and Y.-C. Joo, "The phase-change kinetics of amorphous Ge2Sb2Te5 and device characteristics investigated by thin-film mechanics," *Acta Mater.*, vol. 94, pp. 143–151, Aug. 2015.

[79] A. Kondratiev and A. V. Khvan, "Analysis of viscosity equations relevant to silicate melts and glasses," *J. Non. Cryst. Solids*, vol. 432, pp. 366–383, Jan. 2016.

[80] J. de Guzman, "Relation between fluidity and heat of fusion," *An. la Real Soc. Esp. Fis. y Quim.*, vol. 11, p. 353−362, 1913.

[81] A. Redaelli, A. Pirovano, A. Benvenuti, and A. L. Lacaita, "Threshold switching and phase transition numerical models for phase change memory simulations," *J. Appl. Phys.*, vol. 103, no. 11, p. 111101, Jun. 2008.

[82] M. H. Cohen and G. S. Grest, "Liquid-glass transition, a free-volume approach," *Phys. Rev. B*, vol. 20, no. 3, pp. 1077–1098, Aug. 1979.

[83] G. W. Scherer, "Editorial Comments on a Paper by Gordon S. Fulcher," *J. Am. Ceram. Soc.*, vol. 75, no. 5, pp. 1060–1062, May 1992.

[84] I. Avramov and A. Milchev, “Effect of disorder on diffusion and viscosity in condensed systems,” *J. Non. Cryst. Solids*, vol. 104, no. 2–3, pp. 253–260, Sep. 1988.

[85] L. Battezzati and A. L. Greer, “The viscosity of liquid metals and alloys,” *Acta Metall.*, vol. 37, no. 7, pp. 1791–1802, Jul. 1989.

[86] M. Salinga, E. Carria, A. Kaldenbach, M. Bornhöfft, J. Benke, J. Mayer, and M. Wuttig, “Measurement of crystal growth velocity in a melt-quenched phase-change material,” *Nat. Commun.*, vol. 4, p. 2371, Aug. 2013.

[87] P. Zalden, A. von Hoegen, P. Landreman, M. Wuttig, and A. M. Lindenberg, “How Supercooled Liquid Phase-Change Materials Crystallize: Snapshots after Femtosecond Optical Excitation,” *Chem. Mater.*, vol. 27, no. 16, pp. 5641–5646, Aug. 2015.

[88] C. Zhang, L. Hu, Y. Yue, and J. C. Mauro, “Fragile-to-strong transition in metallic glass-forming liquids,” *J. Chem. Phys.*, vol. 133, no. 1, p. 14508, Jul. 2010.

[89] M. H. . Lankhorst, “Modelling glass transition temperatures of chalcogenide glasses. Applied to phase-change optical recording materials,” *J. Non. Cryst. Solids*, vol. 297, no. 2–3, pp. 210–219, Feb. 2002.

[90] Y.-Z. Yue, “Characteristic temperatures of enthalpy relaxation in glass,” *J. Non. Cryst. Solids*, vol. 354, no. 12–13, pp. 1112–1118, Feb. 2008.

[91] J. Kalb, F. Spaepen, T. P. Leervad Pedersen, and M. Wuttig, “Viscosity and elastic constants of thin films of amorphous Te alloys used for optical data storage,” *J. Appl. Phys.*, vol. 94, no. 8, p. 4908, 2003.

[92] H. E. Kissinger, “Reaction Kinetics in Differential Thermal Analysis,” *Anal. Chem.*, vol. 29, no. 11, pp. 1702–1706, Nov. 1957.

[93] A. L. Greer, “Crystallisation kinetics of Fe80B20 glass,” *Acta Metall.*, vol. 30, no. 1, pp. 171–192, Jan. 1982.

[94] K. Kohary and C. D. Wright, “Modelling the phase-transition in phase-change materials,” *Phys. status solidi*, vol. 250, no. 5, pp. 944–948, May 2013.

[95] I. Kaban, E. Dost, and W. Hoyer, “Thermodynamic and structural investigations of heat-treated amorphous Ge–Te alloys,” *J. Alloys Compd.*, vol. 379, no. 1–2, pp. 166–170, Oct. 2004.

[96] J. M. Saiter, J. Ledru, A. Hamou, and A. Zumailan, “Dependence of the glass transition temperature on the heating rate and structure of chalcogenide glasses,” *Mater. Lett.*, vol. 33, no. 1–2, pp. 91–96, Nov. 1997.

[97] F. S. Howell, R. A. Bose, P. B. Macedo, and C. T. Moynihan, “Electrical relaxation in a glass-forming molten salt,” *J. Phys. Chem.*, vol. 78, no. 6, pp. 639–648, Mar. 1974.

[98] J. W. Christian, *The theory of transformations in metals and alloys*. Pergamon, 2002.

[99] S. Raoux, R. Shelby, B. Munoz, M. Hitzbleck, D. Krebs, M. Salinga, M. Woda, M. Austgen, K. M. Chung, and M. Wuttig, “Crystallization times of as-deposited and melt-quenched amorphous phase change materials,” *Eur. Phase Chang. Ovonic Sci. Symp., Prague*, no. May 2016, pp. 40–47, 2008.

[100] M. Frumar, T. Kohoutek, J. Prikryl, J. Orava, and T. Wagner, “On the atomic structure of thin amorphous Ge-Sb-Te films,” *Phys. status solidi*, vol. 246, no. 8, pp. 1871–1874, Aug. 2009.

[101] B. J. Kooi, W. M. G. Groot, and J. T. M. De Hosson, “In situ transmission electron microscopy study of the crystallization of Ge2Sb2Te5,” *J. Appl. Phys.*, vol. 95, no. 3,

pp. 924–932, Feb. 2004.

[102] S. I. Anisimov, B. L. Kapeliovich, and T. L. Perelman, “Electron emission from metal surfaces exposed to ultrashort laser pulses,” *L. D. Landau Inst. Theor. Physics, USSR Acad. Sci.*, vol. 66, pp. 776–781, 1974.

[103] M. A. Al-Nimr, “Heat transfer mechanisms during short-duration laser heating of thin metal films,” *Int. J. Thermophys.*, vol. 18, no. 5, pp. 1257–1268, Sep. 1997.